

**Subcellular labelling of myelin protein (PLP and  
DM20) in the central nervous system**

**Maj-Lis Christina McCulloch**

**A thesis submitted for the degree of**

**Master of Science**

**in the**

**Faculty of Veterinary Medicine**

**Division of Cell Science**

**of the**

**University of Glasgow**

**©September 2008**

To my loving family.  
Husband James  
and  
Children Cameron and Michael  
Och till min älskade mor Gulli  
Aspegren  
Jag kommer snart hem

## **Declaration**

I hereby declare that the work within this thesis is original and entirely of my own composition unless otherwise stated. Work by other researchers is quoted and given due acknowledgement in the text. No part of this work has been submitted for a degree elsewhere.

## Acknowledgements

My sincere thanks to Dr. Christine E. Thomson who was my initial supervisor and pivotal in initiating these studies. I am very grateful for the scientific support and encouragement that she also provided. Further thanks to Professor Thomas J. Anderson who latterly assumed my supervision and aided completion of this thesis.

I would like to thank especially Dr. Julia M. Edgar for reading the thesis and offering scientific criticism. She also provided me with information on the subject of CNP and microglia as well as advice on photographs. The friendship and discussions (sometimes heated) that we shared were invaluable. I thank also Professor Ian R. Griffiths whom I have been privileged to work alongside for almost 30 years. His scientific knowledge and integrity were invaluable and he provided pertinent suggestions. He also kindly provided some of the photographs for the introduction of the thesis.

My gratitude goes to Professor David Maxwell and technician Mr Robert Kerr for kindly providing advice and instruction in immunogold procedures and for donating antibodies as acknowledged. I would also like to acknowledge Tom J. Deerinck who pioneered the EITC/photo-oxidation technique which is a big part of my thesis. He showed me around his laboratory in UCSD, offered technical advice and support which was very much appreciated.

Dr. Mark McLaughlin, my fellow MSc student Jennifer A. Barrie and Mrs. Marie Ward has been a source of friendship, technical support, and academic assistance throughout my studies for which I am extremely grateful. Past and present members of the group also have my gratitude for providing a cheerful and friendly but still productive environment.

My sincere thanks go to Miss Audrey Kerr for bringing my typing and layout up to professional standards.

I would also like to thank the Faculty of Veterinary Medicine for their support in staff development.

Last but not least I would like to thank my husband for supplying verbs (when needed) and for proof reading and my children for allowing me to “hog” the computer at inopportune times.

## Abstract

The *Plp1* gene encodes the two proteins DM20 and PLP. Ultrastructural techniques will provide the best resolution to establish the sub-cellular localisation of the two myelin protein isoforms encoded by the *Plp1* gene in mice and thus provide insight into the functions for the two isoforms. The gene is expressed primarily by oligodendroglia of the central nervous system (CNS), with some expression (primarily of DM20) in the Schwann cells of the peripheral nervous system. In the CNS, the DM20 isoform is expressed initially prior to myelin initiation and expression maintained throughout life. The function of DM20 is unknown. The expression of the PLP isoform appears to be related to myelination and have a structural role in compact myelin. The objective was to establish an immunolocalisation technique which would allow the hypothesis to be tested that DM20 is expressed in non-compacted regions of the myelinating oligodendrocyte, whilst PLP expression is confined to the compact myelin sheath. In order to differentially label PLP and DM20 at the paranodal region of myelinated axons, two different immunological techniques suitable for subcellular localisation were investigated.

The photo-oxidation technique was applied to both cerebellar and cervical spinal cord vibratome sections. A brominated eosin conjugated secondary antibody was created and used to label a primary antibody against PLP and DM20. The photo-oxidation technique, a pre-embedding immunostaining, generated a very fine reaction product that was excellent at light microscopic resolution but only visible at electron microscopic resolution in sections that were not contrast stained.

The immunogold technique was applied to sections from ventral columns in cervical spinal cord which has a dense population of medium to large myelinated axons. Assessments were made using anti-PLP antibodies in mature animals (with PLP at its peak of production and the myelin compacted and well established) and in young animals (with PLP in its beginning of production and less compacted). The immunogold technique, a post-embedding immuno-staining, produced a well-defined electron dense particle that was easily visualised in the EM. The technique proved insufficient to

differentiate two different PLP antibodies, one labelling both isoforms (i.e. PLP and DM20) and the other specifically labelling only PLP. A substantially higher level of labelling was achieved, uniquely using the freeze substitution method of tissue preservation; however quantitative analysis could not be carried out because preservation was inconsistent both within the same tissue and from sample to sample.

## List of Figures

<b>Figure 1.1</b>	Electron micrograph of a neuron (Purkinje cell) from the cerebellar grey matter of an adult mouse	3
<b>Figure 1.2</b>	Electron micrograph of an astrocyte from the optic nerve of an adult mouse	6
<b>Figure 1.3</b>	Oligodendrocyte ultrastructure	9
<b>Figure 1.4</b>	Schematic model of myelin proteolipid protein (PLP) based on the predicted tertiary structure developed by Popot, (1991)	15
<b>Figure 1.5</b>	Transverse sections of myelinated axons from the spinal cord ventral columns of an adult mouse	21
<b>Figure 1.6</b>	Electron micrograph of longitudinally sectioned myelinated axons from the optic nerve of an adult mouse	22
<b>Figure 3.1</b>	Electron micrographs of myelinated axons, in the spinal cord ventral columns from adult mice, showing the influence of glutaraldehyde concentration	47
<b>Figure 3.2</b>	SDS-PAGE acrylamide gel to confirm successful conjugation of EITC to rabbit IgG and comparison to FITC	49
<b>Figure 3.3</b>	Cultured oligodendrocytes immunostained with a PLP/DM20 primary antibody to determine secondary antibody concentration for optimal fluorescence	50
<b>Figure 3.4</b>	Fluorescent images of myelinated axons in cerebellar folia to confirm appropriateness of titres	51

<b>Figure 3.5a</b>	Light microscopy images of cerebellar folium, showing photo-oxidised area restricted by objective aperture size	53
<b>Figure 3.5b</b>	Light microscopy images as in figure 3.5a (at higher magnification) highlighting labelled cell nuclei	54
<b>Figure 3.6</b>	Successful photo-oxidation of myelin at LM resolution	55
<b>Figure 3.7</b>	Astrocytes and myelinated axons in cerebellar folium labelled with anti-GFAP or anti-PLP antibodies and stained with an avidin-biotin complex (ABC) at LM resolution	58
<b>Figure 3.8</b>	Astrocytes in cerebellar folium, labelled with anti-GFAP and stained with an avidin-biotin complex (ABC) at EM resolution	59
<b>Figure 3.9</b>	Electron micrograph of myelinated axons in cerebellar white matter from an adult mouse after photo-oxidation of EITC in the presence of DAB using a PLP/DM20 antibody	61
<b>Figure 3.10</b>	Electron micrograph of myelinated axons in cerebellar white matter from an adult mouse after photo-oxidation of EITC in the presence of DAB using a GFAP antibody and a variant PLP/DM20 antibody	62
<b>Figure 3.11</b>	Comparison of two different immunocytochemical reaction products	64
<b>Figure 3.12</b>	Influence of grid type on immunogold labelling	66
<b>Figure 3.13</b>	EM micrographs of spinal cord sections, stained with immunogold, and used as positive and negative controls for the antibody PLP 226	68
<b>Figure 3.14</b>	Electron micrographs of myelinated axons (Ax) in spinal cord ventral columns displaying the impact of various fixatives	70

<b>Figure 3.15</b>	Immunogold labelling associated with myelin disruption	71
<b>Figure 3.16</b>	Freeze substitution increased specific immunogold labelling	72
<b>Figure 3.17</b>	Influence of gold particle size on immunolabelling	74
<b>Figure 3.18</b>	Confirmation of immunogold labelling using knockout mice	
<b>Figure 3.19</b>	Comparison of immunogold labelling of myelin in young and mature animals	76
<b>Figure 3.20</b>	Electron micrographs of myelinated axons in spinal cord ventral columns, oblique orientation, displaying level of immunogold labelling	78
<b>Figure 3.21</b>	Electron micrograph of paranodal loops at the node of Ranvier displaying level of immunogold labelling in young animals	79

## List of Tables

Table 1 :	Optimisation of Photo-oxidation : Factors varied	56
Table 2 :	Evaluation of Immunogold Labelling : Fixation	80
Table 3 :	Evaluation of Immunogold Labelling : Freeze Substitution	81

## List of Abbreviations:

Ab	-	Antibody
ABC	-	Avidin-biotin Complex
BSA	-	Bovine Serum Albumin
cDNA	-	complementary Deoxyribonucleic acid
CNS	-	Central Nervous System
CNP	-	2',3' Cyclic Nucleotide 3' Phosphodiesterase
COSHH	-	Control Of Substances Hazardous to Health
CSF	-	Cerebrospinal Fluid
DAB	-	Diaminobenzidine
DAPI	-	4,6-diamino-2-phenyl-indole
dH <sub>2</sub> O	-	distilled water
DM20	-	DM20 (the origin of the nomenclature is obscure)
DMSO	-	Dimethylsulfoxide
DPX	-	mounting media
E	-	Embryonic day
EITC	-	Eosin 5 – isothiocyanate
EM	-	Electron microscope
ER	-	Endoplasmic reticulum
FITC	-	Fluorescein-isothiocyanate
FM	-	Fluorescence microscope
FRIL	-	Freeze fracture Immunogold Labelling
GABA	-	Gamma-aminobutyric acid
GalC	-	Galactocerebroside
GFAP	-	Glial Fibrillary Acidic Protein
IG	-	Immunogold
IgG	-	Immunoglobulin G
kDa	-	kiloDalton
kb	-	kilobase pair
LM	-	Light microscope
M	-	Molar
MAG	-	Myelin-Associated Glycoprotein
L-MAG	-	Large- Myelin-Associated Glycoprotein
S-MAG	-	Small- Myelin-Associated Glycoprotein
MBP	-	Myelin Basic Protein
µm	-	micrometer
ml	-	millilitre
mm	-	millimeter
mM	-	milliMolar
min	-	minute
mRNA	-	messenger Ribonucleic Acid
mt	-	Microtubules
MW	-	Molecular Weight
MWCO	-	Molecular Weight Cut Off
NaCl	-	sodium chloride
NaOH	-	sodium hydroxide
nf	-	neurofilaments
NGS	-	Normal Goat Serum
Ni	-	Nickel

nm	-	nanometer
<sup>1</sup> O <sub>2</sub>	-	singlet oxygen molecule
OLG	-	Oligodendrocyte
OsO <sub>4</sub>	-	Osmiumtetroxide
P	-	Postnatal day
PAP	-	Peroxidase-anti-peroxidase
PB	-	Phosphate Buffer
PBS	-	Phosphate Buffered Saline
PBST	-	Phosphate Buffered Saline with Triton X-100
PLP	-	Proteolipid protein
<i>Plp</i>	-	gene expressing proteolipid protein
PNS	-	Peripheral Nervous System
PO	-	Photo-oxidation
PVP	-	Polyvinalpyrrolidone
RT	-	Room Temperature
SDS	-	Sodium Dodecyl Sulphate
SDS-PAGE	-	Sodium Dodecyl Sulphate-Polyacrylamide gel
SIG	-	Silver intesified Immuno Gold
TBST	-	Tris Buffered Saline with Triton X-100
TMEV	-	Theilers Murine Encephalomyelitis Virus
Å	-	Ångström

# Table of Contents

<b>CHAPTER 1 INTRODUCTION</b>	<b>1</b>
1.1 BACKGROUND AND LITERATURE REVIEW	1
1.2 NEURONS	2
1.3 ASTROCYTES	4
1.4 OLIGODENDROCYTES	7
1.4.1 Biochemistry of Myelin	8
1.4.1.1 Lipids	10
1.4.1.2 Proteins	11
1.4.2 Protein Trafficking	16
1.5 MICROGLIA	16
1.6 EPENDYMAL CELLS	17
1.7 ULTRASTRUCTURE	18
1.7.1 Ultrastructural anatomy of myelinated fibres	19
1.7.1.1 Axon	19
1.7.1.2 Myelin	20
1.7.2 Ultrastructural immunohistochemical techniques	20
1.7.2.1 Immunogold	23
1.7.2.2 PAP and ABC	23
1.7.2.3 Ultracryosectioning	24
1.7.2.4 Photo-oxidation	24
1.8 AIM OF STUDY	25
<b>CHAPTER 2 MATERIALS AND METHODS</b>	<b>27</b>
2.1 GENERAL TISSUE PREPARATION	27
2.1.1 Tissue Source	27
2.1.2 Fixation	27
2.1.3 Dissection	27
2.1.4 Cell Culture	28
2.1.4.1 Staining Protocol	28
2.1.5 Cryostat Sections	29
2.1.6 Antibodies	29
2.1.7 EM Preparation	30

2.1.8	General Imaging	31
	2.1.8.1 Fluorescence Microscopy	31
	2.1.8.2 Electron Microscopy	32
	2.1.8.3 Image Capture	32
2.2	PHOTO-OXIDATION	32
2.2.1	Animal Source and Tissue Preparation	32
	2.2.1.1 Fixation	32
	2.2.1.2 Vibratome sectioning	33
2.2.2	Immunohistochemistry	34
	2.2.2.1 Primary antibody concentration	34
	2.2.2.2 Secondary antibodies concentration	34
2.2.3	Photo-oxidation Protocol	36
	2.2.3.1 Materials	36
	2.2.3.2 Photo-oxidation	36
	2.2.3.3 Propidium Iodide	37
2.2.4	EM Preparation	37
2.3	PAP and ABC	38
2.3.1	PAP Staining	38
2.3.2	ABC Staining for EM	39
2.4	IMMUNOGOLD	40
2.4.1	Tissue Preparation	40
	2.4.1.1 Animal source	40
	2.4.1.2 Fixation	41
2.4.2	EM Preparation	41
2.4.3	Immunocytochemistry	42
	2.4.3.1 Primary antibodies	42
	2.4.3.2 Secondary antibodies	42
2.4.4	Immunogold Labelling	42
	2.4.4.1 Pre-embedding immunogold	42
	2.4.4.2 Post-embedding immunogold	43
2.5	FREEZE SUBSTITUTION	44
2.5.1	Animal Source	44
2.5.2	Protocol	44

<b>CHAPTER 3 RESULTS</b>	45
3.1 CRITERIA FOR SUCCESSFUL LABELLING	45
3.2 PHOTO-OXIDATION	45
3.2.1 Fixation	46
3.2.2 Conjugation of Eosin	46
3.2.3 Titre	48
3.2.4 Photo-Oxidation	48
3.2.5 Immunohistochemistry	57
3.3 EVALUATION OF IMMUNOGOLD TECHNIQUES	63
3.3.1 Pre- and Post-Embedding Techniques	63
3.3.2 Improving quality and specificity of immunogold labelling	65
3.3.3 Immunolabelling of PLP	73
<b>CHAPTER 4 DISCUSSION</b>	82
<b>CHAPTER 5 APPENDICES</b>	91
5.1 GENERAL SOLUTIONS	91
5.1.1 Phosphate Buffered Saline (PBS)	91
5.1.2 Karnovsky's Modified Fixative	91
5.1.3 DV Buffer	91
5.1.4 Isotonic Cacodylate Buffer	92
5.1.5 Araldite Resin	92
5.1.6 Methylene Blue / Azure II	92
5.1.7 Reynold's Lead Citrate	92
5.2 SOLUTIONS FOR PHOTO-OXIDATION	93
5.2.1 Photo-Oxidation Buffer	93
5.2.2 SDS-PAGE	93
5.2.3 Polyethyleneamine coated Petridishes	94
5.2.4 Durcupan Resin	94

5.3	SOLUTIONS FOR IMMUNOGOLD	95
5.3.1	Phosphate Buffer (PB)	95
5.3.2	Maleate Buffer	95
5.3.3	Formvar Coated Grids	95
5.3.4	Phosphate Buffered Saline with Triton-X 100 (PBST)	96
5.3.5	Tris Buffered Saline with Triton-X 100 (TBST)	96
	<b>REFERENCES</b>	<b>97</b>

# **CHAPTER 1 INTRODUCTION**

## **1.1 BACKGROUND AND LITERATURE REVIEW**

A knowledge of neuroanatomy and an understanding of intracellular and extracellular relationships is of vital importance when undertaking any electron microscopic study of the central nervous system. Equally, awareness of the functions of different cells and their components forms a basis from which to elucidate findings on a subcellular level. Although both these areas are being vigorously investigated and are constantly changing, the basic facts have remained remarkably unchanged.

The nervous system is functionally divided into a somatic and an autonomic system where the somatic system regulates conscious processes e.g. activities of skeletal musculature and the autonomic system regulates activities of inner organs, smooth muscle and glands. Anatomically, the nervous system is divided into the central and peripheral nervous system (CNS and PNS). The CNS consists of the brain and spinal cord and the PNS consists of ganglia and nerves spread throughout the body.

The CNS is a complex heterogeneous organ sequestered from the rest of the body by the blood brain barrier. It is also protected by a triple layer of membranes called the meninges. The outermost membrane is the dura mater, next is the arachnoid and innermost, the pia mater loosely covers the surface of the CNS. The dura mater is derived from the mesoderm; the arachnoid and pia mater are derived from the ectoderm and are together called the leptomeninges. Circulating throughout the ventricular and sub-arachnoid space is cerebrospinal fluid (CSF), which protects the CNS from mechanical trauma and maintains the ventricular pressure.

Macroscopically, the CNS is intricately folded around five ventricles and in the forebrain reveals a rim of gray matter, the cortex, overlying an inner white matter which is interspersed with islands of more gray matter. This situation is reversed in brain stem and spinal cord where the dorsal and ventral horns with the central canal in the centre form an

H shaped configuration of gray matter surrounded by white matter. The white matter contains myelinated nerve fibres where the lipid component of the myelin is responsible for its whiteness. The gray matter consists mainly of nerve cell bodies and glia.

The major components of the CNS and their interrelationships have extensively been investigated and recorded. Briefly, on the microscopic level, the pia-astroglia (glia limitans) provides the barrier between the exterior and the CNS parenchyma. The neurons and its processes together with astrocytes, oligodendrocytes and microglia interspersed with blood vessels forms the parenchyma (for an excellent introduction to cellular morphology in the CNS, see Raine, 1994).

## **1.2 NEURONS**

The neuron consists of a cell body (perikaryon) with one or more cytoplasmic processes. The large variety of neurons can be subdivided by size, ranging from the small cerebellar granule cells with a perikaryal diameter of 5 to 8  $\mu\text{m}$  to the larger pear shaped Purkinje cells and the star shaped anterior horn cells both of which can reach diameter of up to 80  $\mu\text{m}$  in humans. The size and shape of the neurones were initially established as early as 1839 by Purkinje and further explored by Deiters, Ramón y Cajal and Golgi in the late nineteenth century and early twentieth century (see Raine, 1994 for a historical perspective).

The shape of the neurons varies greatly and is largely dependent on the amount and arrangement of its processes. Morphologically, neurons are sub-classified into unipolar, bipolar and multipolar. There are two types of perikaryal processes, axons or dendrites. Dendrites are usually short branching processes whereas axons are long and unbranched except at the terminals.

The cytoarchitectural features of the perikaryon reveal a large spherical shaped nucleus, usually situated centrally, well developed rough endoplasmic reticulum (ER), prominent Golgi apparatus and abundant mitochondria (Fig.1.1). Lysosomes, peroxisomes and multivesicular bodies are frequently visible.

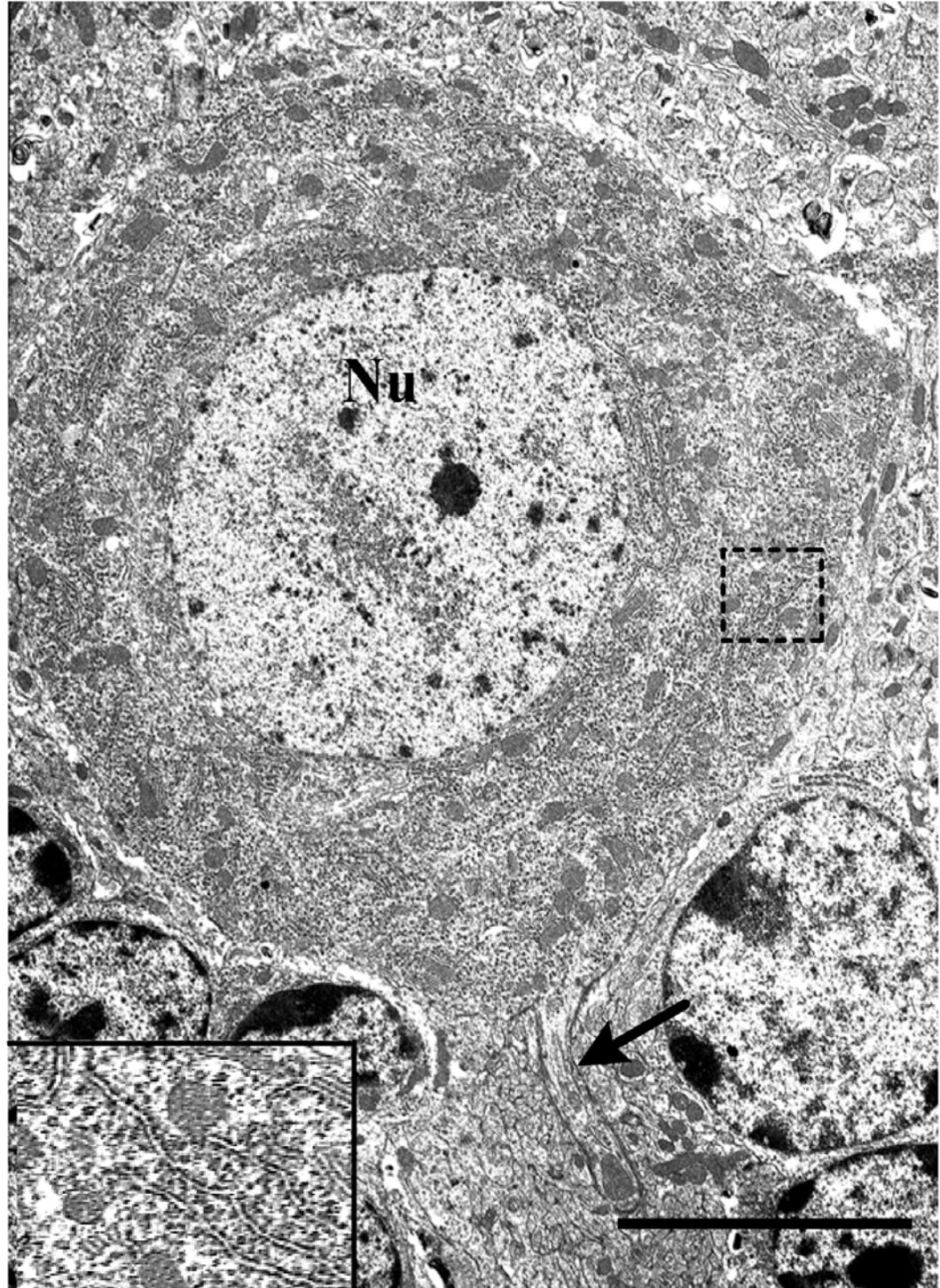


**FIGURE 1.1** Electron micrograph of a neuron (Purkinje cell), flanked by basket cells, from the cerebellar grey matter of an adult mouse. The nucleus (Nu) has a central orientation in the cellbody. Note the rich organelle filled cytoplasm with well developed rough endoplasmic reticulum, abundant mitochondria, as well as the striking basophilic Nissl substance (see enlarged inset). Part of the axon hillock can be seen at the bottom of the picture (arrow) with organelles aligning in a longitudinal fashion (McCulloch, unpublished observation). Scale bar = 5 $\mu$ m.

A characteristic feature for nerve cells is the abundant basophilic Nissl substance. It consists of tightly packed membranes and sacs from the ER with ribosomes both attached and freely interspersed, sometimes clumped together, so called polyribosomes. The organization of Nissl bodies in the perikaryal cytoplasm and dendrites is varied and often form a characteristic pattern, which is used as a criterion for neuron identification. The Nissl substance is however missing in axons and the axon hillock (the area where the axon emerges from the perikaryon).

The neuronal cytoskeleton consists of neurofilaments, microtubules and intermediate filaments. These are arranged in many directions in the perikaryon but are aligned longitudinally in the axon and dendrites

Axons are the elongated processes of the neurons that pass information from the perikaryon to other cells. The most prominent and consistent feature of large axons is neurofilaments that run parallel to the long axis of the axon. The  $\sim 100 \text{ \AA}$  neurofilaments are less common in small axons where microtubules, a larger cylindrical  $200 - 250 \text{ \AA}$  structure, are more frequent. Neurofilaments play a major role in determining the shape and diameter of the axons while microtubules are involved in axonal transport.

### **1.3 ASTROCYTES**

The nervous tissue consists not only of neurones and their processes but also of glial cells which surrounds them throughout the nervous system. It was Virchow who in 1846 first discovered a non-nervous component, which he called neuroglia from the Greek words meaning “nerve” and “glue” but it was not until the early twentieth century when the Spanish histologists Ramon y Cajal and del Rio Hortega who, with their metallic impregnation techniques, established and classified the neuroglia as distinct cells (for a historical perspective see Privat et al, 1995).

Today three groups of glia are recognised:

1. macroglia, which consists of astrocytes and oligodendrocytes. The macroglia originate from ectodermal stem cells called spongioblasts.
2. microglia, of mesodermal origin.
3. ependymal cells, also of ectodermal spongioblasts.

Glial cells retain their ability to divide throughout their life and possess no synaptic contacts.

Astrocytes are traditionally subdivided into protoplasmic and fibrous astrocytes (Mugnani and Walberg, 1964) though there are a large variety of transitional cells differing in location, function and to some extent morphology. Radial cells (e.g. Bergmann glia and Müller glia) are considered by some a distinct group (Privat et al, 1995). There is also growing evidence that protoplasmic and fibrous astrocytes are derived from different progenitors; Raff et al (1983) suggested that fibrous astrocytes were derived from the same progenitor as oligodendrocytes. Both types of astrocyte contain all normal organelles found in eukaryotic cells, but are sparser than in other glia. The most prominent cytoplasmic components of the astrocyte are filaments 9 nm in diameter, which occur in the perikarya and extend into the processes (Fig.1.2). These filaments closely resemble intermediate filaments found in neurons, however their dimensions are smaller and they regularly appear as closely packed bundles. Protoplasmic astrocytes range in size from 10 to 40  $\mu\text{m}$  and are located mostly in grey matter, frequently abutting capillaries. They have a clearer cytoplasm than fibrous astrocytes. Characteristic for both types is a large, ovoid nucleus with homogenous chromatin except for a narrow denser rim and one or two poorly defined nucleoli. Fibrous astrocytes are located in white matter, with twig-like processes composed of a large number of 9 nm filaments arranged in bundles. The filaments within these cell processes can be distinguished from neurofilaments by their close packing and the absence of side arms. Desmosomes and gap junctions occur between adjacent astrocytic processes. After trauma, astrocytes proliferate, swell, and accumulate glycogen and filaments. If gliosis is total, all other elements are lost and a glial scar will form. Astrocytes have the ability to become macrophages in some diseases and astrocytes are probably the most disease-resistant component in the CNS because very few diseases (alcoholism is one exception) cause depletion of astrocytes (Raine, 1994).

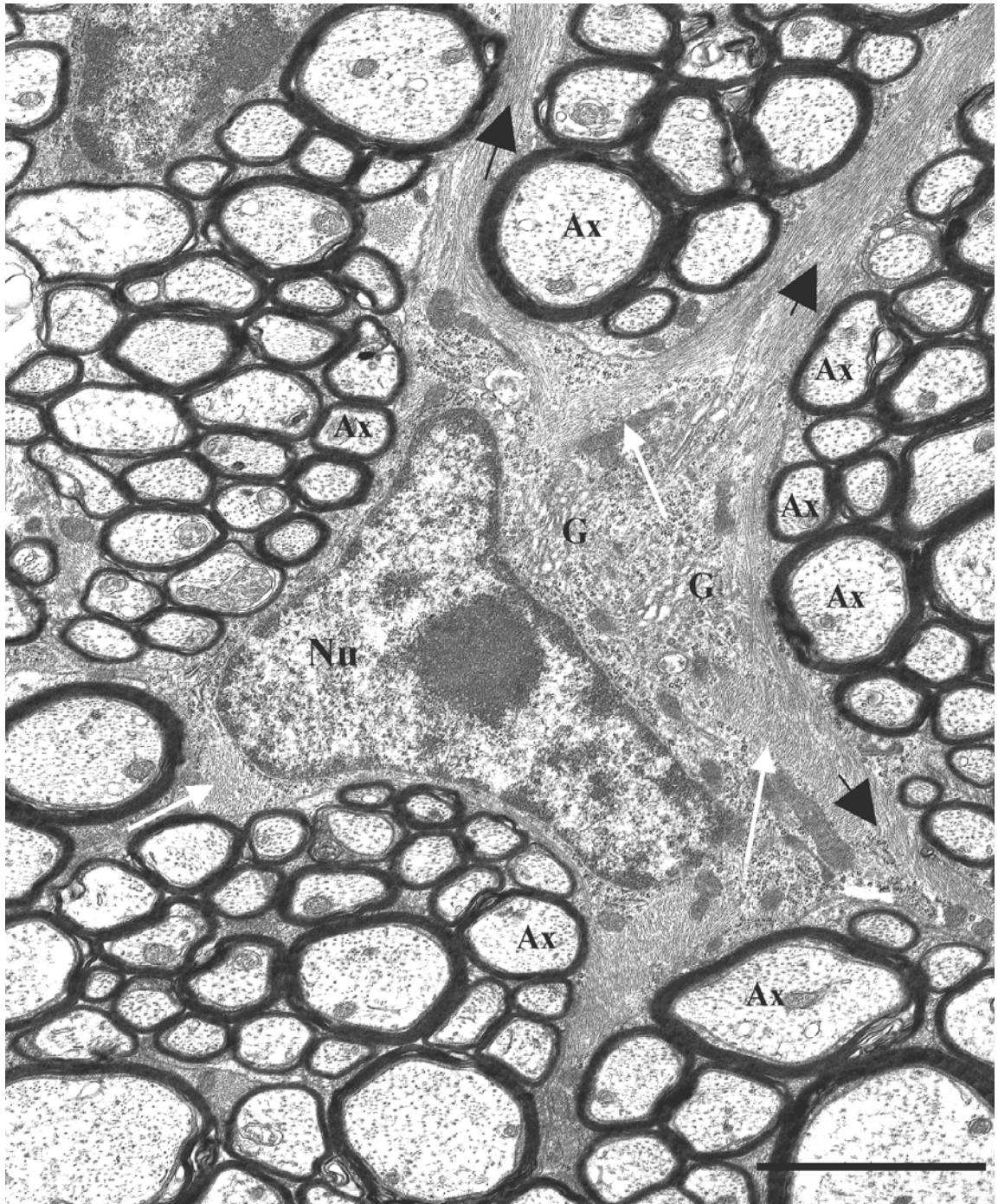


**FIGURE 1.2** Electron micrograph of an astrocyte from the optic nerve of an adult mouse surrounded by myelinated axons (Ax). The astrocyte nucleus (Nu) usually has a more homogenous chromatin than is shown here but the thin rim of chromatin inside the nuclear envelope clearly distinguish astrocyte nuclei from other glia cells. Characteristic for the astrocyte are the bundles of filaments (white arrows) which makes these cells easily recognisable. Note the filament filled processes extending from the cell body, three of which are labelled (black arrows), demonstrating the typical starshape of the astrocyte. Other cellular features are rough ER and Golgi apparatus (G). (Griffiths, unpublished observation). Scale bar = 2  $\mu$ m.

Identification and localisation of astrocytes have become relatively easy and reliable through the advent of immunocytochemistry. Many antigenic markers are now in use but the first and still foremost is glial fibrillary acidic protein (GFAP), discovered by Eng et al (1971) and Bignami et al (1972), the major protein associated with the astrocyte intermediate filaments. Astrocytes have numerous other functions including regulation of the extracellular milieu through their ion channels, neurotransmitter receptors and transporters, modulation of synapses and production of growth factors.

## **1.4 OLIGODENDROCYTES**

Oligodendrocytes are the second type of cells belonging to the subclass of macroglia. Their main function is myelination of axons in the CNS, although the more that is revealed about the oligodendrocytes the more complex these heterogeneous cells appear. Rio Hortega first described oligodendrocytes in 1921 and gave them the name oligodendroglia meaning oligo= few, dendro=tree and glia=glue. He later reviewed his findings and renamed them oligodendrocytes in recognition that they were cells in their own right and also categorised them into interfascicular, perineuronal and perivascular oligodendrocytes. Hortega furthermore subdivided oligodendrocytes into four types, numbered I through IV by characterising their polymorphism using criteria such as size of somata, number of processes, tissue distribution and the manner of interaction with axons. This was later confirmed by Stensaas & Stensaas (1968a, b), who found the same results in toad with no transitional forms between I & II and III & IV. Typically, oligodendrocytes type I and II myelinate multiple internodes on separate small diameter axons, sometimes as many as 40 to 50 axons. Type III and IV oligodendrocytes myelinate fewer axons of larger diameter with the latter type myelinating a single internode just as Schwann cells in the PNS (for a historical perspective of the field from Rio Hortega to current concepts, see Szuchet 1995).

Ultrastructurally oligodendrocytes are moderately dense cells with a round or oval nucleus usually eccentrically located; some clumping of chromatin occurs with a thin rim just below the nuclear envelope. The cytoplasm contains large numbers of ribosomes both free and attached to rough ER and a well-developed Golgi system. Two features that

make oligodendrocytes readily identifiable are the lack of glycogen granules and intermediate filaments which are prominent features in astrocytes (Fig.1.3). Microtubules are also a prominent feature of these cells. In a study of corpus callosum in rats Mori & Leblond (1970) identified three classes of oligodendrocytes, i.e. light, medium and dark. Light oligodendrocytes are the largest and contain most free ribosomes and were found to undergo mitosis; dark oligodendrocytes are smallest with a rough ER and Golgi more prominent and with no evidence of mitosis. The medium class of oligodendrocytes are intermediate with many features of the light but with fewer ribosomes and more limited mitosis. The conclusion would be that these three classes are the representation of the oligodendrocytes lifecycle, light being young and dark being the old oligodendrocyte.

#### **1.4.1 BIOCHEMISTRY OF MYELIN**

Biologically, CNS myelin is an extension of the oligodendrocyte plasma membrane. During myelination processes contact and wrap tightly around axons to form a compact lamellar structure. Although myelin is a continuation of the oligodendrocyte its biochemical composition is complex and distinct (Szuchet et al, 1988)

The major biochemical components of myelin are few and well documented. Depending on species, lipids make up 70 – 85%, protein 15 – 30 % and gangliosides 0.5 % of myelin dry weight. Minor proteins, splice products and post-translationally modified protein isoforms are numerous and the list of such proteins continues to grow as new techniques and molecular markers are discovered.

The molecular architecture of myelin is hypothesised and is based on EM, immunohistochemical staining, X-ray diffraction, surface probe studies, structural abnormalities in mutant mice, correlations between structure and composition in various species and predictions of protein structure from sequencing information (for review see Kirchner and Blaurock, 1991).

It is generally accepted that myelin consist of compaction of normal cell lipid bilayer membrane with proteins, some integral embedded some extrinsic attached to the surface by weaker linkages.

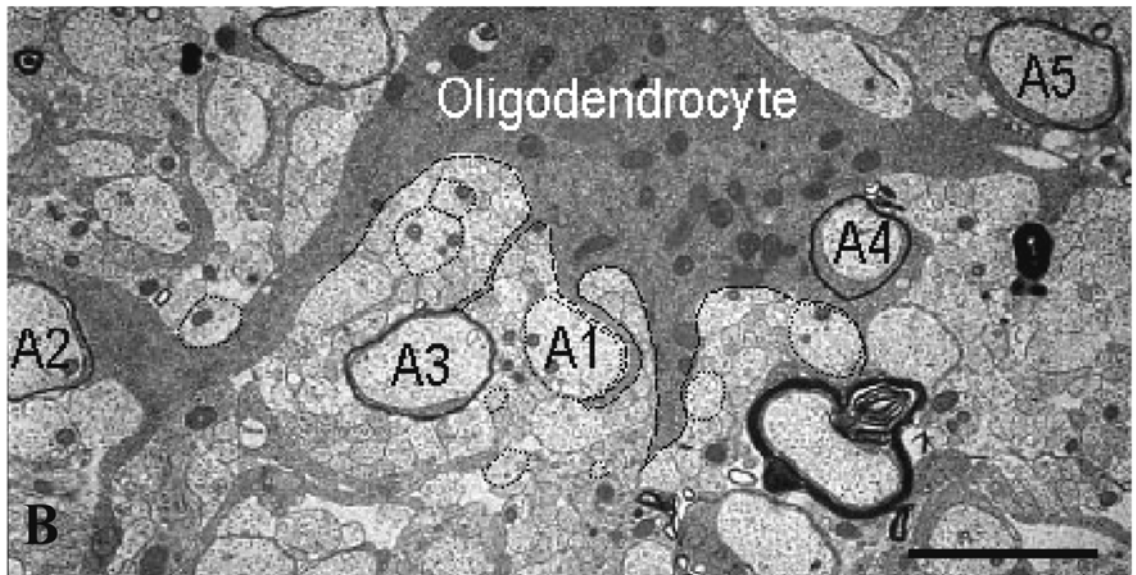
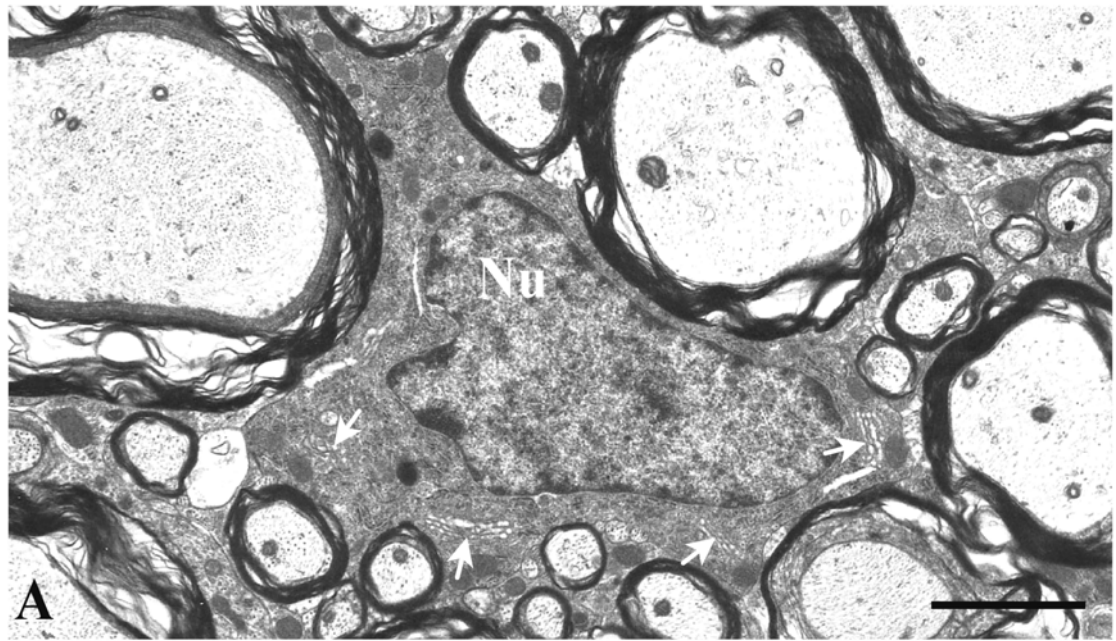


FIGURE 1.3 Oligodendrocyte ultrastructure

**A.** Electron micrograph of an oligodendrocyte from the spinal cord ventral columns of an adult mouse. Note the irregular feature of the nuclear chromatin, the density of the cytoplasm due to considerable amount of free ribosomes and microtubules and prominent Golgi apparatus (white arrows). Also note the lack of intermediate filaments which identifies astrocytes. Nucleus (Nu).

**B.** Oligodendrocytes myelinates axons in the CNS which is clearly seen in this micrograph. The oligodendrocyte processes are ensheathing at least five axons (A1-5).

Scale bar A = 1  $\mu$ m, B = 2  $\mu$ m.

(Griffiths, unpublished observations)

### 1.4.1.1 Lipids

Myelin (dry mass) has a high ratio lipid to protein in contrast to most biological membranes, which have a higher ratio protein to lipids. Biological membranes are formed by lipid molecules, largely phospholipids, consisting of 2 hydrophobic hydrocarbon tails and a hydrophilic head group, where the phosphate is located. Two monolayers of lipid molecules with their hydrophobic tails tightly packed are sandwiched together tail to tail to form a bilayer. The membrane is fluid with individual molecules able to diffuse laterally, rotate or even “flip-flop” across the layers.

Different types of cells have a different mixture of lipids in their membranes depending on function. There are three classes of membrane lipid molecules:

1. Phospholipids, which spontaneously form bilayers
2. Cholesterol, which enhances permeability
3. Glycolipids, which are found exclusively in the non-cytoplasmic half of the bilayer where they are thought to self associate into microaggregates by forming hydrogen bonds with one another. This asymmetrical distribution also suggests some role in interactions of the cell with its surrounding. The most complex glycolipid, ganglioside, carries a net negative charge and might be important for its electrical effect. Glycolipids may also play a role in electrical insulation.

There are no myelin-specific lipids although galactocerebroside, (GalC), is the most typical of myelin constituting 22.7% of myelin lipids (dry mass). In order of abundance, in addition to cerebroside, the major lipids of myelin are cholesterol, ethanolamine, lecithin and sphingomyelin.

Several myelin specific proteins are amphipathic with lipid bilayer spanning domains and as such contribute to the lipid structure of myelin.

### 1.4.1.2 Proteins

The protein composition of CNS myelin is simpler than for other brain membranes with proteolipid protein (PLP/DM20) and myelin basic protein (MBP) making up to 60 – 80% of the total in most species. A variety of minor proteins and glycoproteins are also present. With the exception of MBP none of the myelin proteins is easily extractable or soluble in aqueous solutions, however, they can be solubilised in sodium dodecyl sulphate (SDS) solution. In this state they can be separated easily using electrophoresis in polyacrylamide gels, the so-called SDS-PAGE technique. Current ideas propose PLP to be the major integral protein for stabilizing the intraperiod line and MBP an extrinsic protein localized exclusively at the cytoplasmic surface is believed to be the major protein for stabilizing the major dense line. These hypotheses are supported by ultrastructural abnormalities observed in inherited dysmyelinating conditions or gene targeting studies. For example, the *shiverer* mouse, which lacks MBP due to a major deletion within the *Mbp* gene (Privat et al, 1979; Roach et al, 1985) and the *Plp1* null mouse (Yool et al, 2002; Klugmann et al, 1997), which is deficient in PLP/DM20.

#### (a) Myelin Basic Protein (MBP)

Myelin basic protein constitutes approximately 30 % of the myelin protein in the CNS. The primary structure i.e. the amino acid sequence of MBP was established by Eylar et al (1971) for bovine brain and Carnegie (1971) in humans (for review see Baumann and Pham-Dinh (2001). There are several spliced variants of MBP, up to seven in mice and four in humans ranging from 14 – 21.5 kDa. The gene structure consists of seven exons over a stretch of 32 kb on chromosome 18 in mice and 45 kb in humans on chromosome 18q22-qter (Baumann et al 2001). MBP is a hydrophilic, highly unfolded protein with virtually no tertiary structure in solution. MBP is localised on the cytoplasmic interface of the oligodendrocyte plasma membrane at the major dense line, which is formed by compaction of the oligodendrocyte processes during myelination. The protein is locally incorporated into the myelin sheath by a signal mediated mRNA transport to the periphery (Ainger et al, 1993, 1997). Studies of the *shiverer* mutant mouse, in which MBP is absent, (Roach et al, 1985), provided evidence that MBP is of major importance for formation of the major dense line and myelin compaction.

## (b) Myelin-Associated Glycoprotein (MAG)

Myelin-associated glycoprotein is one of the larger myelin membrane proteins but represents only 1% of the total protein (dry mass) in the CNS. MAG consists of 13 exons distributed over 16 kb stretch on chromosome 7 in mice and 19 in humans. The apparent molecular mass is 100kDa as established with SDS-PAGE. Two isoforms of MAG have been identified: large MAG (L-MAG) and small MAG (S-MAG) 72 and 67 kDa respectively in the absence of glycosylation (Frail et al, 1985; Salzer et al, 1987). MAG is situated periaxonally in the CNS and has one transmembrane, one extracellular and one intracellular domain.

The function of MAG has been elucidated through the use of MAG gene knockout mice (Li et al, 1994; Montag et al, 1994; Yin et al, 1998). These MAG deficient mice show an abnormal formation of the periaxonal cytoplasmic collar and cytoplasmic organelles between lamellae suggesting a blocking or delaying of myelin compaction. A comparatively larger percent of axons in the CNS of knockout mice received myelin sheaths than axons in the CNS of WT mice suggesting a role for MAG in helping oligodendrocytes distinguish between myelinated and unmyelinated axons. MAG also appears important for the long-term survival of myelinated CNS axons (Pan et al, 2005).

## (c) Cyclic Nucleotide Phosphodiesterase (CNP)

2',3' Cyclic nucleotide 3' phosphodiesterase belongs to a group called Wolfgram proteins after fractionation of myelin was performed by Wolfgram (1966) and thereby identified a group of high molecular weight myelin proteins (see Campagnoni, 1988 for review).

CNP is the major component of the Wolfgram fraction proteins that constitutes 4 % of the total myelin with a gene structure of 4 exons over 7kb in man and mouse. Two isoforms are expressed by alternative splicing referred to as CNP1 and CNP2.

The CNP protein has been localised to photoreceptor cells in the retina and oligodendrocyte cytoplasm; specifically the cytoplasm filled inner- and outer tongue processes of non-compact myelin and the paranodal loops at nodes of Ranvier (Trapp et al, 1988), where they are in close contact to the 2 nm gap apposing the axolemma. An

axon/glia function has been proposed for CNP and evidence to this effect has been shown in studies with CNP deficient mice (Lappe-Siefke et al, 2003). In these mice, compact myelin remains normal; however, axons and inner tongues display organelle rich swellings and the axons degenerate with time. In a study of CNP deficient young animals, both inner tongue and axonal organelle filled swellings occur together with axonal degeneration and abnormal, excessive “swirls” of myelin in small diameter axons (Edgar, personal communication). Thus not only is CNP a requirement for normal development of oligodendrocytes that myelinate small axon but absence of CNP possibly also creates a toxic environment for these axons.

#### (d) Proteolipid Protein (PLP) and DM20

The proteolipid protein PLP (with its smaller isoform DM20) is the single most abundant protein in CNS myelin. Proteolipid proteins were discovered by Folch and Lees in 1951 together with other lipid protein complexes extracted by organic solvent mixtures from CNS white matter and retained that name because of its large presence in myelin. PLP constitutes approximately 50% of the myelin proteins in the CNS. The gene encoding PLP has been localised and consists of 7 exons stretching over ~ 17kb. The isoform DM20 is a spliced variant identical to PLP except for exon 3B which is omitted (Nave et al, 1987; Griffiths et al, 1998).

The primary structure of PLP and DM20 has been established by direct sequencing and indirectly from cDNA clones to comprise 276 and 241 amino acids respectively. The amino acid sequence of PLP is strongly conserved among mammalian species with human and murine PLP being 100% identical (Popot et al, 1991; Diehl et al, 1986; Macklin et al, 1987). Human and murine PLP also have a 99% homology with protein from dogs and cattle (Sobel et al, 1994; Lees et al, 1983; Stoffel et al, 1983), a 98% homology with rat PLP, even bird and amphibian PLP show a high degree of homology > 85% which points to an important role for PLP in myelination.

PLP is a highly hydrophobic and polytopic transmembrane protein. Although the exact topology of PLP is unknown it is generally accepted that the model developed by Popot et al (1991) and confirmed experimentally by Weimbs and Stoffel (1992) is the tertiary structure of PLP. The model predicts alpha-helical transmembrane domains spanning the

whole membrane bilayer with two extracytoplasmic and three cytoplasmic domains including an amino and a carboxyl terminal (Fig.1.4). The extracellular loops have been identified through immunostaining with cell surface markers i.e. the O10 antibody (Jung et al, 1996; Thomson et al, 1997). The cytoplasmic loop has been identified with a PLP specific antibody recognising an epitope on residues 116 – 150, which is deleted in DM 20 (Trifilieff et al, 1985; Nave et al, 1987).

Numerous functions have been proposed for PLP and DM20 in CNS. Currently, PLP/DM20, together with claudin-11 (also known as oligodendrocyte-specific protein) is known to be necessary for the formation of the intraperiod line (Chow et al, 2005; Yool et al, 2002; Boison et al, 1995) and appears necessary for the long-term maintenance of small diameter axons (Griffiths et al, 1998). Other functions, such as a secreted C-terminal fragment that can influence proliferation of oligodendrocyte progenitors, have been proposed (Yamada et al, 1999).

Surprisingly, the *Plp1* null mice assemble large amounts of myelin. The myelin is partially compacted but with intermittently condensed or absent IPL which confirms the role for compaction. Demyelination does not occur. However, these mice develop an axonopathy with axonal swellings and degeneration perhaps indicating a role for PLP in glial/axonal interaction (Yool et al, 2002; Griffiths et al, 1998; Edgar et al, 2002). The severe dysmyelinated MBP deficient *shiverer* mice lack similar axonal swellings to PLP null mice but they recur in the MBP/PLP-deficient double mutant which further substantiates the role of glial/axonal communication (Griffiths et al, 1998).

Pelizaeus-Merzbacher (PMD) and its allelic disorder spastic paraplegia type 2 (SPG2) are heterogeneous disorders in man caused by mutations or dosage alterations of the *PLP1* gene (Al-Saktawi et al, 2003; Garbern et al, 1999). Duplication of the *PLP1* locus is the most frequent cause of PMD/SPG2 with a wide variety of missense mutations the major cause of the remaining cases.

Spontaneous point mutations of the *Plp 1* gene occur in a range of animal species where the severity of phenotype varies considerably (for review see Nave and Griffiths, 2004).

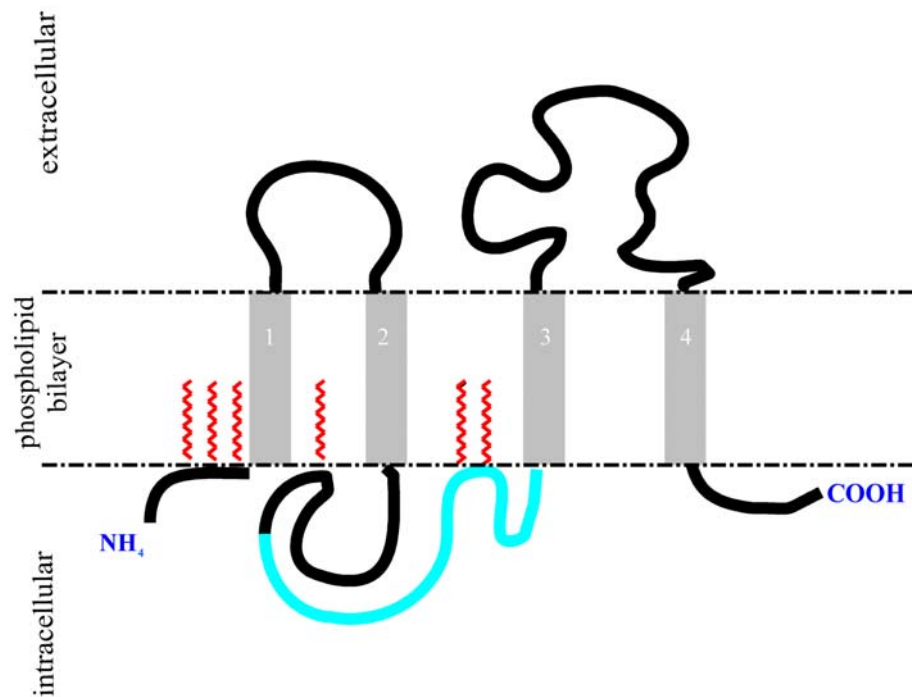


**FIGURE 1.4** Modified schematic model of myelin proteolipid protein (PLP) based on the predicted tertiary structure developed by Popot, (1991). The model predicts 4  $\alpha$ -helical transmembrane domains spanning the whole membrane bilayer with two extracytoplasmic and three cytoplasmic domains including an amino ( $\text{NH}_4$ ) and a carboxyl terminal ( $\text{COOH}$ ). The PLP protein is acylated at six cysteine residues (shown in red) increasing its overall hydrophobicity. The extracellular loops have been identified through immunostaining with cell surface markers i.e. the O10 antibody (Jung et al, 1996; Thomson, 1997). The cytoplasmic loop has been identified with a PLP specific antibody recognising an epitope on residues 116 – 150, which is deleted in DM 20 (shown in turquoise) (Trifilieff et al, 1985; Nave et al, 1987). Anti-PLP226 antiserum (N.P. Groome, Oxford Brookes University, Oxford, UK) which recognises the carboxy terminus (amino acids 271 to 276) of both PLP and DM20 protein isoforms (Fanarraga et al, 1993) was used throughout this thesis.

## 1.4.2 PROTEIN TRAFFICKING

PLP and DM20 have different expression patterns. The murine *Dm20* transcript occurs as early as E 9.5 (embryonic day) (Timsit et al, 1992; Spassky et al, 1998) and the protein at E12 (Dickinson et al, 1996) whereas the *Plp* transcript occurs at P 0 – 2 (postnatal day) coinciding with the onset of myelination. PLP levels peak at P22 when myelination is most active ( Verity and Campagioni, 1988). *Plp* and *Dm20* message isoforms are translated on the rough ER and the proteins progress through the secretory pathway through the Golgi apparatus to the plasma membrane where they incorporate into the myelin (Gow et al, 1994). Two post-translational modifications occur. The amino terminal methionine is lost and the proteins undergo acylation, possibly in both the Golgi apparatus and the myelin membrane. The PLP protein is acylated at six cysteine residues increasing its overall hydrophobicity. The DM20 protein is also acylated but lacks two of the acylation sites that are present in the intracytoplasmic loop. Both isoforms are present in PNS at lower levels. In Schwann cells, PLP gene products are localised to the perinuclear region (Griffiths et al, 1995). DM20 is the major isoform and is localised to the non-compacted regions of the Schwann cell myelin.

Both isoforms, PLP and DM20, appear necessary for normal structure and function in the CNS. *Plp1* null mice, complimented with either PLP or DM20 and mice expressing only DM20 all showed CNS defects (Griffiths et al, 1998; Stecca et al, 2000; Spörkel et al, 2002).

## 1.5 MICROGLIA

Microglia belong to the second group of cells classified as glia cells. Controversially they were classified as microglia of mesodermal origin by del Rio Hortega and although it is generally accepted that microglial progenitors arise from peripheral mesodermal tissue their precise origin is still debated today (Chan et al, 2007). They are considered the immune cells or resident macrophages of the CNS. Microglia are found throughout the entire CNS. They are heterogenously distributed in both grey and white matter and from

one region to another (Lawson et al,1990). In rodent brain, microglia account for 4 to 5.5%, of all cell types in major white matter tracts such as the corpus callosum and optic nerve (Lawson et al, 1990; Mori and Leblond,1969; Vaughn and Peters, 1968). In normal human white matter, the proportion of cells that are microglia is even greater, at 13% (Hayes et al,1987) and in contrast to the rodent, they are more prevalent in white than in gray matter (Mittelbronn et al, 2001).

Microglia have elongated nuclei which are smaller than those of other glial cells, averaging 5.1µm in length and 2.2 µm in diameter (Mori and Leblond ,1969). Ultrastructurally the nuclei are rich in heterochromatin, similar in appearance to dark oligodendrocytes, with a very thin perimeter of cytoplasm around most of the nucleus. However, the two cell types can be differentiated by the convoluted outline of the nuclear membrane and the clear space which separates the nucleus from the cytoplasm in microglia. Cisterns of endoplasmic reticulum, Golgi stacks and mitochondria are present, and dense bodies, including lysosomes and phagosomes, are frequent (Karasek et al, 2004; Mori and Leblond ,1969). Microglia also contain filamentous actin and a few microtubules, but glial filaments and glycogen granules, which are prominent in astrocytes, are absent (Mori and Leblond, 1969).

The morphology of microglia changes in response to CNS injury and neurodegenerative disease as the cells acquire an 'activated' phenotype. These 'activated' microglia have larger cell bodies and thicker and shorter processes than the ramified microglia of the healthy brain and are usually found in increased numbers (Perry et al, 2007; Ip et al. 2006; Lawson et al, 1994; . Perry et al, 1994; Zhang et al, 2001). Microglia are influenced by systemic infection or inflammation (Perry et al, 2007) and can be seen filled with phagocytosed material and engulfing dying CNS cells (Streit et al, 2002).

## **1.6 EPENDYMAL CELLS**

Ependymal cells are the third class of glia cell, identified by Purkinje in 1836 who described a ciliated epithelium lining the cerebral ventricles (see Pannese 1994).

Ependymal cells are, flattened, cuboidal or columnar spongioblasts, of ectodermal origin.

During embryonic development they proliferate, overlying the neural tube assisting the formation of an external limiting membrane. After neural folding, the ependymal cells are restricted to lining the ventricular system including the spinal central canal or form part of choroid plexus. Mature ependymal cells are proposed to be involved with secretion, absorption, transport, receptor as well as a barrier function between cerebrospinal fluid/blood and brain (Berry et al 2003). Morphologically the cells differ depending on region but all have an indented nucleus with cytoplasm rich in mitochondria, lysosomes, microtubules and microfilaments (Brightman and Palay 1963; Berry et al, 2003) and are of varying length, 0.2  $\mu\text{m}$  – 15  $\mu\text{m}$  in mammals (Westergaard, 1970).

Ependyma does not regenerate and hence injury to the ventricular lining has serious consequences resulting in discontinuity of the neuropil and reactive gliosis by subventricular astrocytes (Pekny and Nilsson, 2005). Recently, the subventricular zone beneath the ependymal lining is the subject of growing interest due to the fact that it is a neurogenic region containing neural stem cells (Nait-Oumesmar et al, 2008). These stem cells are thought to be of astrocytic origin and generate migratory neurons. Subventricular zone astrocytes have also been detected in active repair of the ependyma in geriatric animals, with electron micrographical evidence of astrocytes gaining ependymal cell like cilia (Romanko et al, 2004).

## **1.7 ULTRASTRUCTURE**

The first electron microscope was built in the 1930s by a German company Knoll and Ruska (Ham, 1974) and commercially available EMs appeared later in that decade. However, it was not until the mid 1960s after numerous problems such as sectioning, fixation, embedding medium were sufficiently resolved by renowned scientists (Fernandez-Moran, Sjostrand, Sabatini, Glauert, Afzelius are but a few of the pivotal individuals) that biological ultrastructural research began in earnest.

The ultrastructure of biological tissue are components of cells only visible beyond the light microscopy level i.e. electron microscopy, where magnifications of 500 to 1,000,000 times are possible. The resolving power, i.e. the distance at which 2 points can be

distinguished, of the electron microscope is 0.2 nm or even sub-Ångstrom levels in high resolution EM as opposed to LM which is 0.2 µm. Although some subcellular features can be seen at light microscopy level through staining, eg. Nissl substance in neurones, what is seen is the stain not the feature itself. In the EM it is clear that Nissl substance consists of aggregates of rough ER with numerous ribosomes each distinguishable, both attached and scattered in between the flattened cisternae.

EM studies used to be restricted to purely morphological investigations. Although biochemical investigation using EM techniques were at its height in the 1970s and 1980s, speciality skills and equipment needed made this a very narrow research field. Preparation of tissue and subsequent staining protocols, time, cost and methods available, served to make EM studies increasingly unpopular. However interest was resumed during the late 1990s when molecular biology and immunohistochemical investigations needed sub-cellular levels of resolution. Methods for EM developed progressively and are still evolving.

## **1.7.1 ULTRASTRUCTURAL ANATOMY OF MYELINATED FIBRES**

### **1.7.1.1 Axon**

The ultrastructure of axons is well defined (see Peters et.al, 1976). Although the axon and its hillock is an extension of the nerve cell, it lacks the Nissl substance that characterises the perikarya and dendrites, which are easily identified even at LM level through basophilic staining. At EM level, the axolemma, the plasma membrane of the axon is a trilaminar feature 7-8 nm in thickness and distinct. The cytoplasm of the axon contains neurofilaments, microtubules, mitochondria, agranular ER (axoplasmic reticulum), vesicles and multivesicular bodies but lacks Golgi apparatus, rough ER and most other components which are involved in protein synthesis.

Neurofilaments (nf) are a prominent feature of axons which are also present in perikarya and dendrites. On entering both axons and dendrites, neurofilaments converge and align themselves parallel to the length of the processes. Fernandez-Moran and Dahl (1952) were first to describe and classify these structures. They were later found to be tubes rather than rods measuring 90-100Å in diameter (Peters et al, 1976 for review).

Microtubules also known as neurotubules are also tubular, slightly larger than neurofilaments, measuring 200-250Å. While neurofilaments predominate in large axons, the proportions of neurofilament and mitochondria are progressively reversed with the decrease of axon diameter so that mitochondria predominate within small axons (~0.1µm or less in diameter).

### **1.7.1.2 Myelin**

Ultrastructurally, myelin is a spiral encasement of the axon where the oligodendrocyte cytoplasm is squeezed out during compaction of the membranes. Thus, the characteristic periodic structure of alternating concentric electron-dense and electron-light layers is formed. The major dense line consists of a fusion between the two apposing intracellular membranes and the minor, light, intraperiod line consists of a close apposition of the apposing extracellular membranes of the spiralling oligodendrocyte process. An inner and outer tongue, each running longitudinally along the entire myelin sheet can be seen in cross sections as loops containing cytoplasm (Fig.1.5). In longitudinal section at the node of Ranvier paranodal terminal loops similarly containing cytoplasm are present (Fig.1.6). Transverse bands, which are septate-like junctions and connect the myelin sheath to the axolemma can be seen in the 2nm gap at the paranodal loops (Rosenbluth, 1999; Scherer et al, 2004; Hirano and Dembitzer, 1982).

## **1.7.2 ULTRASTRUCTURAL IMMUNOHISTOCHEMICAL TECHNIQUES**

There are now several techniques available for immunohistochemical procedures at EM level. The most published are immunolabelling techniques such as immunogold, peroxidase-anti-peroxidase (PAP), ultracryostat techniques and to a lesser extent the photo-oxidation technique. There are disadvantages with all of them and the investigator has to evaluate the criteria that are of most importance to them.

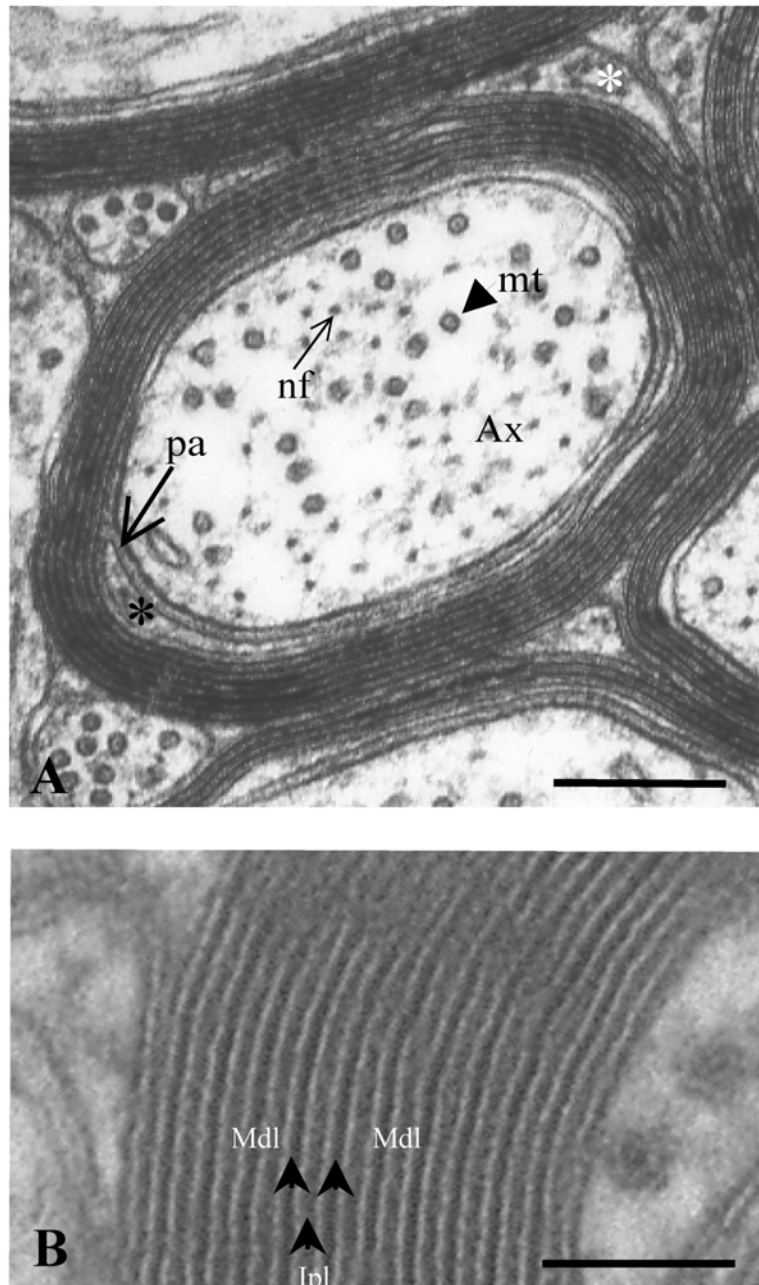


**FIGURE 1.5** Transverse sections of myelinated axons from the spinal cord ventral columns of an adult mouse. Note the characteristic periodic structure of alternating concentric electron-dense and electron-light layers of the myelin sheath.

**A.** The inner tongue (black asterisk) and the outer tongue (white asterisk) of the myelin sheath can be seen as loops containing oligodendrocyte cytoplasm. A periaxonal space (pa) is maintained between the oligodendrocyte and the axon (Ax) throughout their apposed positions with specialisations occurring at the paranodal loops only. The cytoskeletal features within the axon consists of microtubules (mt) and neurofilaments (nf).

**B.** High magnification of the compact myelin sheath showing the major dense lines (Mdl) formed by fusion between the two apposing intracellular membranes and the minor light intraperiod line (Ipl) formed by close apposition of the extracellular membranes during the ensheathment of the axon.

Scale bars A = 250 nm, B = 50 nm. (Griffiths, unpublished observations)

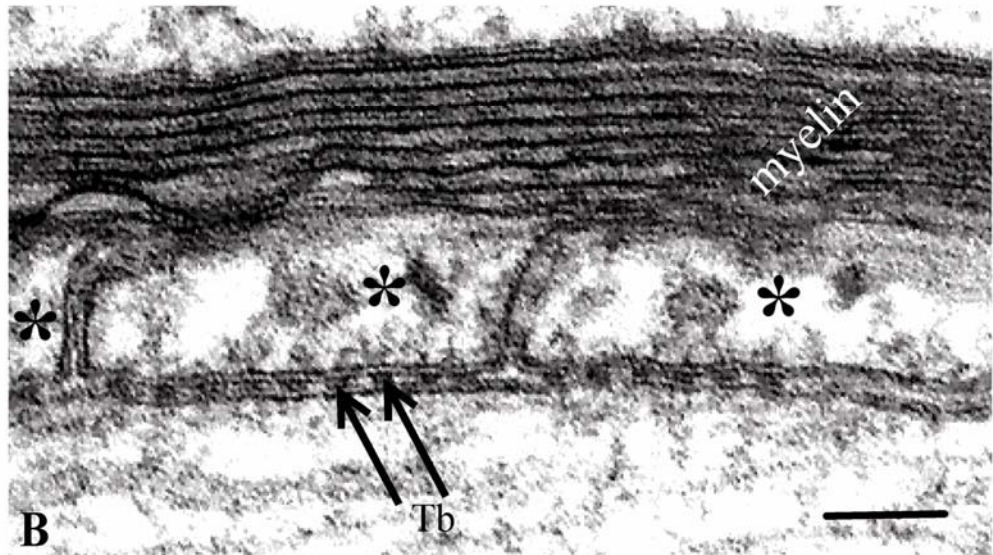
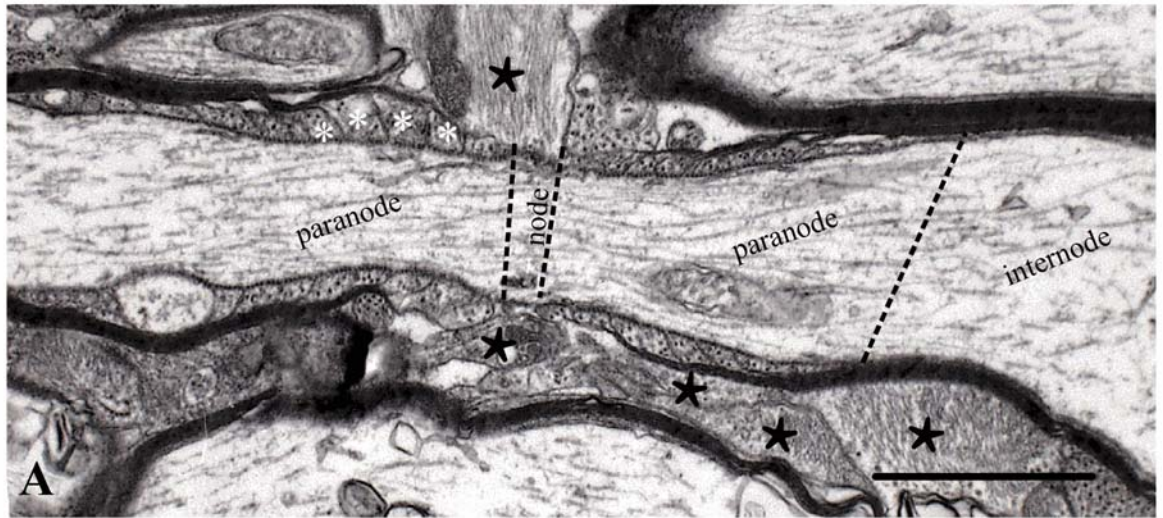


**FIGURE 1.6** Electron micrograph of a longitudinally sectioned myelinated axon from the optic nerve of an adult mouse.

**A.** A node of Ranvier (node) occupies the nerve in the centre of the picture where astrocyte processes ( black star) can be seen adjoining the unmyelinated part of the axon. On either side of the node, paranodes (paranode) with their terminal loops (white asterisk) containing oligodentrocyte cytoplasm are present. Internodes runs in between paranodes and can be seen in this picture on the right hand side labelled (internode).

**B.** Part of a paranode showing cytoplasmic loops (black asterisk). Transverse bands (Tb) which are septate-like junctions can be seen in the gap between the myelin sheath and the axolemma.

Scale bars A = 2 $\mu$ m, B = 50nm. (Griffiths, unpublished observations)

### **1.7.2.1 Immunogold**

Immunocytochemistry and EM have been combined since the 1950s. In their review, Afzelius and Maunsbach (2004) highlight Singer, in 1959, who introduced ferritin as an electron-dense antibody tracer and later Faulk and Taylor (1971) who developed gold particles for immunolocalisation purposes at the EM level. These techniques are still used today. The indirect labelling technique, that is most commonly used today, consists of introducing a tagged secondary antibody against an untagged primary antibody. This two-layer technique was pioneered by Baxandall et al (1962). Although elegant results are generated, it is notoriously difficult to get consistent and reliable results with this method because of the many steps involved. Fixation is certainly an issue and a compromise between preservation of the tissue and preservation of antigenicity will often have to be reached. There is also an issue whether a quantification of labelling is possible. Last but not least the processing and embedding of specimens are of considerable concern. Standard resins like Durcupan™ and even Araldite™ have been used with some success on brain tissue (Maxwell et al, 1995; Maxwell and Riddell, 1999). However specialist resins for immuno-EM are now available i.e LowiCryl™, LRWhite™ and LRGold™ (Scherer et al, 1995; Tait et al, 2000). The negative aspect in the use of these resins is the requirement for special equipment to either cure or cut the embedded tissue.

Investigations of myelin proteins using the immunogold have been explored but with limited success. Most publications on this subject use immunogold in combination with the ultracryo technique (Trapp et al, 1989; McLaurin et al, 1993; Sobel 1994; Yin et al, 1998, 2006).

### **1.7.2.2 PAP and ABC**

Peroxidase-antiperoxidase (PAP) and avidin-biotinylated enzyme complex (ABC) are similar peroxidase activity labelled immunological techniques. The latter, an intensified labelling version of PAP was introduced by Hsu et al (1981a, b). These indirect labeling techniques employ a secondary antibody linked to a peroxidase complex which forms a reaction product that is revealed with a chromogen. Usual chromogens are diaminobenzidine derivatives. The reaction product can be enhanced with heavy metals

i.e nickel, cobalt and more commonly osmium. The techniques are used successfully for light microscopy but have a limited use for electron microscopy mainly because the reaction product tend to be shallow and diffuse, situated away from the reaction site. Publications using these techniques on the CNS were most prolific in the 1980 and 1990s (see Deerinck et al, 1997; Sekirnjak et al, 1997; McMahon et al, 2000 as elegant illustrative examples).

### **1.7.2.3 Ultracryosectioning**

Ultracryosectioning is a technique introduced by Tokuyasu in 1973 and involves infusing fresh or fixed tissue with polyvinylpyrrolidone (PVP), directly fitted onto stubs followed by rapid freezing in low temperatures approx -187 C. The tissue is then sectioned in an ultracryomicrotome, picked up onto copper mesh grids, embedded in resin and stained for viewing in an EM. It is perhaps more widely used now but is still a very difficult technique. Not only is it difficult to orientate the tissue during freezing and identify areas of interest after freezing, but the need to embed the tissue when it is situated on the grid in contrast to conventional EM techniques where sectioning takes place after embedding, makes this a technique suitable only for people with considerable experience. To couple this technique with immunogold labelling and its disadvantages makes this method capricious and time-consuming.

### **1.7.2.4 Photo-Oxidation**

Fluorescence photo-oxidation with eosin is a high resolution immuno-localisation method (Deerinck et.al, 1994). Eosin, a fluorescent marker, conjugated onto a secondary antibody is excited in a fluorescence microscope (FM) by UV light in the presence of diaminobenzidine tetrahydrochloride (DAB). DAB is oxidized and an osmiophilic reaction product is formed. The advantage with this method is that the reaction product is highly insoluble making it easily visible by LM. Since it is osmiophilic, enhancement with osmium tetroxide (OsO<sub>4</sub>) makes it visible by EM. A further advantage is that the same tissue can be viewed by all three options e.g. a specific fluorescing site can be identified by FM, photo-oxidized and verified by LM, processed for EM while orientation of the oxidized site is visibly aligned.

Eosin or eosin-5- isothiocyanate (EITC) is a brominated derivative of fluorescein. It is essentially identical but has 4 bromine atoms added, which significantly increases the non-fluorescent dissipation of energy from the excited dye molecule, which in turn increases the generation of singlet oxygen molecules ( $^1\text{O}_2$ ).

Fluorescein and rhodamine are commonly used for immunolabelling because of their high fluorescence quantum yields, but they yield low quantities of singlet oxygen, which makes them less suitable for photo-oxidation. Even with intense immunolabelling Deerinck's group found it difficult to detect staining using FITC and rhodamine in the EM. EITC has a singlet oxygen quantum yield approximately 19 times greater than FITC and it still has a moderate fluorescence property, although it is only ~ 20 % as bright as fluorescein.

Because EITC is a small molecule penetration of labelling reagents is high, hence specificity is optimised and very different from e.g. avidin-biotin complexes and colloidal gold conjugates (Hsu et al, 1981; Sternberger, 1986). This method therefore appears to be suitable for the detection of the membrane bound myelin proteins PLP and DM20.

## **1.8 AIM OF STUDY**

The aim of this study was to critically evaluate sub-cellular localisation techniques for the purpose of studying the biology of proteolipid proteins in myelin.

Ultrastructural techniques will provide the best resolution to establish the sub-cellular localisation of the two myelin protein isoforms encoded by the *Plp1* gene in mice and from these data postulate functions for the two isoforms. The *Plp1* gene encodes the two proteins DM20 and PLP. The gene is expressed primarily by oligodendroglia of the central nervous system (CNS), with some expression (primarily of DM20) in the Schwann cells of the peripheral nervous system. In the CNS, the DM20 isoform is expressed both prior to and during myelin initiation and maintenance. It is of unknown function. The expression of the PLP isoform appears to be related to myelination and has a structural role in compact myelin. An objective was to establish an immunolocalisation technique which would allow the hypothesis to be tested that DM20 is expressed in non-compacted

regions of the oligodendrocyte (premyelinating, ensheathing and myelinating) as well as compact myelin, whilst PLP expression is confined to the compact myelin sheath.

The EM techniques most suitable for immunolocalisation of the PLP isoforms are immunogold and fluorescence photo-oxidation with eosin. Immunogold labelling of myelin proteins (Arvanitis et al, 1992, Trapp et al, 2006) has traditionally been used but the immunogold technique is renowned for being difficult and morphological resolution may be impaired due to the inaccessibility of the targeted PLP epitopes. Fluorescence photo-oxidation with eosin in the presence of diaminobenzidine tetrahydrochloride provides a high-resolution depiction of sub-cellular antigen distribution (Deerinck et al, 1994) and may be more suitable. Antibodies for this study are already well established and used in our laboratory. The PLP226 antibody recognises the C-terminal of both PLP and DM20. PLP A antibody recognises the exon specific to PLP only. Differential immunolabelling may allow us to determine the sub-cellular location of the two protein isoforms on separate sections. Both antibodies are recognised by a goat-anti-rabbit IgG secondary antibody to which the eosin fluorophore for the photo-oxidation method or colloidal gold for immunogold method will be conjugated.

Myelin is a notoriously difficult membranous structure to study morphologically due to its high lipid content interspersed with protein. Lipids are difficult to preserve without undesirable extraction during processing resulting in distortion and membranes are difficult to penetrate without physical damage. It was recognised at the outset that this study would be difficult due to the criteria deemed necessary, i.e. firstly the structure of tissue should be preserved and secondly there should be a differential labelling of myelin to non-myelin tissue suitable for statistical analysis.

## **CHAPTER 2 MATERIALS AND METHODS**

### **2.1 GENERAL TISSUE PREPARATION**

#### **2.1.1 TISSUE SOURCE**

The wild type mice were an inbred hybrid C3H/101 strain, which were bred in house for over 15 years. The *Plp1* null mice were derived by gene targeting using Sv129 embryonic stem cells in C57BL/6 mice with subsequent generations being bred on the C57BL/6 background (Klugmann et al, 1997).

#### **2.1.2 FIXATION**

Transcardiac perfusion fixation was performed in a fume cupboard according to COSHH regulations. General solutions are detailed in Appendix 5.1.

Wild type and *Plp1* null mice were humanely euthanased using an overdose of carbon dioxide or halothane in a closed chamber. Perfusion took place through a thoracotomy. The right atrium was nicked to ensure flow of the perfusate. Depending on the size of the animal, a 21-23 gauge hypodermic needle was introduced into the left ventricle. Perfusion was initiated with a flushing of ~10 ml PBS (see appendix 5.1.1) using a perfusion circuit consisting of two 20 ml syringes (one for PBS and one for fixative) attached to a three way tap connected to a line leading to the hypodermic needle. The initial flushing with PBS to clear blood from the circulatory system was followed by perfusion with 20-40 ml fixative. Composition of the fixative varied depending on specific procedures.

#### **2.1.3 DISSECTION**

Following perfusion, animals were wholly immersed in fixative 1-24 hours prior to dissection. Dissection was carried out under a low power dissection microscope and fixative fumes extracted via a fume extractor.

The top of the cranium was removed to expose the brain. The meninges were severed and the whole brain carefully extricated using microsurgical instruments. When needed, the optical nerves were removed still attached to the optic chiasm. The orbits were also left attached to allow orientation after disconnection to the brain. The cervical part of the spinal cord was similarly extricated and stripped of meninges after severing the nerve roots.

#### **2.1.4 CELL CULTURE**

Oligodendroglial cultures were established and grown by Anne Hunter Appl. Neurobiology Group (see Thomson et al, 1999).

Cells were grown for 5-7 days in vitro before being stained for both PLP/DM20 (using the 226 antibody) or PLP only (using PLPA antibody). The stained cells were visualised by fluorescence microscopy.

##### **2.1.4.1 Staining protocol**

The staining protocol was performed on a staining platform consisting of Eppendorf™ caps glued onto an inverted lid of a tissue culture dish, thus, able to hold individual coverslips. To prevent coverslips drying out overnight, the bottom of the inverted lid was moistened with water and the base tray of the culture dish used as cover. All steps except for the primary antibody application were carried out at room temperature.

Oligodendrocyte cultures were fixed in 4% paraformaldehyde, 0.1% glutaraldehyde/PBS for 10-15 min. After 3x10 minutes washes in PBS the cell membranes were permeabilised in 0.5% or 0.1% Triton X-100 for 30-60 minutes. To block non specific antibody staining, the coverslips were immersed in DV blocking buffer (see appendix 5.1.3) for for 30-60 minute. Coverslips were drained and incubated with a primary antibody, PLP 226 IgG fraction diluted in DV buffer 1:50, overnight at 4° C. A wash in PBS, 3x10 minutes, was followed by incubation in the secondary antibody, either EITC diluted as necessary or FITC diluted at 1:80. A further wash in PBS, 3x10 min, was followed by nuclear staining with 4, 6-diamidino-2-phenyl-indole (DAPI, Sigma)/PBS diluted to 1:1000 for 1 min. A short wash in distilled water was performed prior to

mounting the coverslips onto glass slides in either Citifluor mounting media or PBS. The edges of the coverslips were sealed with nail varnish. Stained cells were kept on slide trays, covered with aluminium foil at 4°C.

### **2.1.5 CRYOSTAT SECTIONS**

Frozen tissue sections were used to establish the titre for the conjugate EITC. Controls were always included; the positive where the EITC conjugate was substituted for a FITC conjugate and the negative where no primary antibody was applied. Animals were perfused as described in 2.1.2. The whole brain was dissected out as described in 2.1.3, thereafter immersed in a 20% sucrose solution. Freezing took place by dropping the brain into isopentane (-56°C) chilled with liquid N<sub>2</sub>. Frozen tissue was stored in a freezer at -20°C.

Sections were cut on a Bright cryostat at a thickness of 10 – 15 µm.

### **2.1.6 ANTIBODIES**

For all methods, well-established primary antibodies routinely used in our laboratory were applied. Anti-PLP226 antiserum (N.P. Groome, Oxford Brookes University, Oxford, UK) raised in rabbit, which recognises the carboxy terminus (amino acids 271 to 276) of both PLP and DM20 protein isoforms (Fanarraga et al, 1993). A rabbit polyclonal antibody specifically created to recognise an epitope in exon 3B (amino acids 117-129), solely expressed by the PLP isoform (PLPA) (E.Trifilieff, University of Strasbourg, Strasbourg, France).was used. A rat monoclonal antibody, AA3, (S Pfeiffer, University of Connecticut, USA) was also used to recognise the C-terminal of PLP and DM20. As a positive control, a polyclonal astrocyte specific marker recognising glial fibrillary acidic protein (GFAP) from DAKO and an anti-myelin basic protein (MBP) polyclonal antibody (Chemicon) were also used. Negative controls were created by omitting primary antibodies.

Secondary antibodies used were specific for each method and are described in the appropriate section of this thesis.

## 2.1.7 EM PREPARATION

Cerebellum and cervical cords were used, mainly. The cerebellum was halved with a razor blade following on from the mid line of the longitudinal fissure of the cerebrum. 1 mm sagittal slices were removed from the cerebellum and divided into 4 pieces. 1- 2 mm and 2-4 mm transverse slices of cervical cord were taken and either left whole or halved along the median fissure through the central canal dorsal to ventral and then quartered laterally through the central canal, if required. The slices were embedded and orientated for either transverse or longitudinal sectioning.

Processing for electron microscopic study was carried out in a routine fashion in an automatic, programmable Lynx Processor™ (Leica). Tissues were loaded into plastic mesh baskets, lids fitted and threaded on to a metal arm assembly used to suspend the tissues in vial for automatic processing. Vials contain up to 20ml of liquid. Agitation and temperature adjustment was applied. A temperature of 4°C was applied for initial rinse and secondary fixation. Room temperature was used for dehydration and initial resin infiltration and 30°C applied to final full resin. The routine processing programme is as follows:

1	isotonic cacodylate buffer	50 min
2	1% OsO <sub>4</sub> in cacodylate buffer	2hr
3	isotonic cacodylate buffer	30 min
4	50% ethanol	5 min
5	50% ethanol	10 min
6	70% ethanol	5 min
7	70% ethanol	10 min
8	80% ethanol	5 min
9	80% ethanol	10 min
10	90% ethanol	5 min
11	90% ethanol	10 min
12	ethanol	20 min
13	ethanol	20 min
14	propylene oxide	15 min
15	propylene oxide	15 min
16a	1:2 resin: propylene oxide	13 hr
16b	1:1 resin: propylene oxide	6 hr
17	2:1 resin: propylene oxide	18 hr
18	resin	4 hr

After infiltration, tissues were embedded in resin (see appendix 5.1.5). For blocking out the tissues were orientated in resin-filled silicon moulds and placed in an oven at 60°C for a minimum of 24 hours to polymerise.

Microscopy sections were first cut on glass knives as semi-thin sections, collected with a glass rod and floated out on a water droplet placed on microscope glass slides. They were then dried and stained with 1% azure II and 1% methylene blue in 1% borax (see appendix 5.1.6) on an 80°C hotplate for light microscopy. Thin sections were then cut with a Diatome™ diamond knife on a Reichert Ultracut E™ at a thickness of 70 – 80nm, floated out on water and collected on 200 and 300 mesh copper grids and air dried. They were stained by placing them on droplets in a closed Petri dish lined with Nescofilm™ first with a saturated solution of uranyl acetate in 50% ethanol for 10 min, washed by ~10 dips in 100ml 50% ethanol and 2 x 100ml washes with 10 dips each in dH<sub>2</sub>O. Secondly, they were contrast stained with lead citrate (see appendix 5.1.7) for 10 minutes similarly placed on droplets on Nescofilm but with an added filter paper moistened with 1% sodium hydroxide (NaOH) on the bottom of the Petri dish to absorb oxygen which reacts with the lead citrate to form a precipitate that can be picked up on the sections. This was followed by 3 washes consisting of 10 dips each in 100ml NaOH (0.01%) and 2x100ml dH<sub>2</sub>O, blotted on filter paper and left to air dry.

## **2.1.8 GENERAL IMAGING**

### **2.1.8.1 Fluorescence Microscopy**

Microscopy sections, cultured cells and photo-oxidation preparations were examined using an inverted Olympus IX70 research microscope with 100x 1.25NA oil, 60x 1.4NA, 40x 0.40NA objective lenses. Images were captured using Image Pro® Plus 6 software (MediaCybernetics).

FITC absorbs light at a wavelength of 495nm and emits it at 525nm, which can be visualised as green light using a blue filter. DAPI provides a fluorescent light with excitation of 345 nm and emission of 455nm. Excitation wavelength for EITC is 526nm and emission is 545nm. A triple cube allowing visualisation of all 3 fluorophores, as well as individual filters, was used.

### **2.1.8.2 Electron Microscopy**

Sections were examined in a JEM CX-100 II transmission electron microscope. Photographs were taken on Kodak 4469 cut plate films. Films were developed 10 min in Universal™ developer diluted 1:10. Developing was stopped in a waterbath with a few drops of acetic acid added and fixed for 10 minutes in Ilford Hypam™ fixer diluted 1:10. Films were then washed in running water for 20 minutes and left to air-dry.

### **2.1.8.3 Image capture**

Negatives were scanned (Epson Perfection) into a PC using Photoshop CS2 (Adobe) software.

## **2.2 PHOTO-OXIDATION**

### **2.2.1 ANIMAL SOURCE AND TISSUE PREPARATION**

In total, 11 wild type mice (see section 2.1.1) were used. Ages ranged from P17 to P180. In total, 30 photo-oxidation experiments were performed (see section 2.2.3.2). For every experiment 4- 8 vibratome sections were used. Vibratome sections were trimmed and cut into 4 segments suitable for EM. Approximately 5-10 grids were cut from each segment (see section 2.2.4).

#### **2.2.1.1 Fixation**

##### **ESTABLISHING FIXATIVE**

The fixative for the photo-oxidation protocol was established to ensure the maximum level of morphological preservation without compromising antigenicity. Glutaraldehyde cross-links different regions of proteins and may hide or destroy epitopes. Therefore, a compromise to preserve antigenicity as well as keeping a reasonable morphological preservation had to be reached.

## **ANIMAL SOURCE**

Three, P180, wild type female mice were used (see section 2.1.1). Perfusion was carried out as described in section 2.1.2.

## **PERFUSION FIXATIVE**

To optimise the photo-oxidation protocol the animals were perfused with different fixatives, i.e.:

1. 4% paraformaldehyde/0.1 % glutaraldehyde/0.1 M sodium cacodylate buffer pH 7.2
2. 4% paraformaldehyde/0.5% glutaraldehyde/0.1 M sodium cacodylate buffer pH 7.2
3. 4% paraformaldehyde/1% glutaraldehyde/0.1 M sodium cacodylate buffer pH7.2

Transverse cervical spinal cord sections were dissected from each animal and processed and cut using routine EM protocol see section 2.1.7 and section 2.1.8.

A control mouse of same strain and age was added from the Applied Neurobiology Group existing archive of routine strong fixed (5% glutaraldehyde) embedded tissue. Tissues are routinely perfused with a modified version of Karnovsky's fixative (see appendix 5.1.2) and left in fixative at 4°C for at least 2 hrs, but most often overnight.

### **2.2.1.2 Vibratome sectioning**

Vibratome sections were cut on a 1000 Plus® (Vibratome). Whole cerebellum and spinal cord were dissected out and mounted directly onto the Vibratome metal trough using a small spot of superglue. The tissue was aligned so that sagittal sections of cerebellum and transverse sections of cervical cord would be produced. The trough was flooded with PBS so that the mounted tissue was completely submerged. Sections were cut at a thickness of 50-100µm, cutting speed was 3-5mm/sec. Sections were picked up with a fine tipped paintbrush and transferred to a 5ml Petri dish filled with PBS.

## **2.2.2 IMMUNOHISTOCHEMISTRY**

### **2.2.2.1 Primary antibody concentration**

Four primary antibodies were used for photo-oxidation experiments. PLP226, dilution 1:600; GFAP, dilution 1:1000; MBP, dilution 1:500 and AA3, dilution 1:300. Negative controls were always included (see section 2.1.6).

### **2.2.2.2 Secondary antibodies concentration**

#### **CONJUGATION OF EOSIN**

For the photo-oxidation method a conjugated secondary antibody was created with the help of Douglas Kirkham (Applied Neurobiology Group) as follows:

Conjugation of the fluorophore eosin via its 5-isothiocyanate moiety to goat-anti-rabbit IgG was carried out using FluoReporter Eosin Protein Labelling Kit ® F-1023 and protocol (Molecular Probes Europe BV). Two conjugations using goat-anti-rabbit IgG, (Sigma-Aldrich), was carried out. One conjugation using goat-anti-rat IgG, (Sigma-Aldrich), was carried out.

The conjugation protocol was initiated by adding eosin 5-isothiocyanate (EITC) to a reaction tube with goat-anti-rabbit IgG or goat-anti-rat IgG in a 1M bicarbonate solution, pH 9.0. The reaction was stirred at room temperature for 1 hour whilst being protected from light and then stopped by the addition of hydroxylamine. The solution was stirred for a further 30 minutes at room temperature. The conjugate was separated from unreacted dye by loading the sample into spin columns, containing 30,000 MW size exclusion resin. After allowing the solution to be absorbed into the gel it was then spun on a Heraeus Instruments Labofuge 400 R centrifuge at 1100 x g. The requirement for further purification was assayed by dialysis using a Pierce Slide-A Lyzer Dialysis Cassette® with a molecular weight cut off (MWCO) of 10 kDa and dialysed against 0.1 M PBS at 4°C. A single fluorescence staining on oligodendrocyte cultures was performed to establish if purification was necessary.

Degree of labelling was determined by measuring the absorbance at a wavelength of 524nm ( $A_{542}$ ) in an Ultrospec III/ Pharmacia spectrometer and using calculation formulas as provided in the labelling kit.

### **SDS-PAGE**

A sodium dodecyl sulfate polyacrylamide gel electrophoresis was carried out to establish that the conjugations of EITC to the IgG were successful. It was also a useful tool to compare EITC against FITC. The assays were carried out by Dr Mark McLaughlan. A 12.5 % acrylamide gel was prepared (see appendix 5.2.2) on a PAGE gel rig (ATTO Corporation).

Samples were prepared in SDS/DTT (see appendix 5.2.2) and denatured by boiling 90° C for 4 minutes. Samples were loaded onto the gel as follows:

First a neat sample of EITC then 3 dilutions each of EITC and FITC i.e. 1:10, 1:20 and 1:100. A final lane was loaded with a molecular weight marker (Biorad). The gel was run in 1X SDS-PAGE running buffer (see appendix 5.2.2) at a constant 100 V. On completion the gel was transferred to a UV transilluminator (Herolab) to visualise and record the fluorescent bands with a photographic printer (Sony).

### **ESTABLISHING TITRES**

Titres for goat-anti-rabbit EITC were established using both primary cultured cells and cryosections. Initially, 5 dissociated oligodendrocyte cultures between 5 and 7 days in vitro were used followed by 1 explant oligodendrocyte culture, 21 days in vitro. Finally, tissue was tested from a P20 wild type mouse. Evaluation of titres on sections was performed on 10 µm thick cryostat sections of sagittal mouse cerebellum (perfused tissue). Initially, oligodendrocyte cultures stained with EITC at dilutions of 1:10, 1:50, 1:75, 1:100 and 1:250. To establish a titre for tissue, cryostat sections were incubated with EITC at dilutions of 1:50, 1:75, 1:85 and 1:100. Staining protocol was carried out as described in section 2.1.4.

## **2.2.3 PHOTO-OXIDATION PROTOCOL**

### **2.2.3.1 Materials**

Photooxidation was performed on a fluorescence microscope (see section 2.1.8). An extraction fan was used in the microscope room to eliminate DAB vapour. Gloves, mask, goggles and protective clothing were used according to COSHH regulation. The microscope and surrounding area was dressed in polythene sheets to avoid any splashes of DAB. The stage was chilled with ice packs to reduce the oxidising rate of DAB. The sections were irradiated using a 100W mercury burner light source and a triple cube with an excitation spectrum 490-510. EITC IgG conjugate exhibits an absorption maxima at 526nm and an emission maxima at 545 nm. A solution of chilled (~4°C) 2.8 M DAB in 0.1M sodium cacodylate buffer (see appendix 5.1.4) was constantly suffused with pure oxygen to keep the DAB from oxidising. The solution was kept in a fume cupboard and transferred to the microscope in small amounts, packed in ice and administered drop wise over the section. Specialised glass “bottomed” plastic tissue culture Petri dishes (MatTek Inc) were used. These tissue culture dishes provide a high resolution microscopic image.

### **2.2.3.2 Photo-oxidation**

Vibratome sections were processed in glass Petri dishes and manipulated with a fine tipped paintbrush. Buffer used throughout the protocol was 0.1M sodium cacodylate, pH 7.4, unless otherwise stated.

Initially sections were washed in buffer for 30 minutes in three baths. They were then permeabilised in buffered 0.1% Triton X-100 for 30 minutes before blocking of non-specific IgG binding to reduce background staining. Blocking buffer consisted of photo-oxidation buffer (see section 5.2.1) and incubation was 45 minutes. The sections were then incubated in primary antibody, either PLP226, dilution 1:600 or GFAP, dilution 1:1000, overnight but minimum of 12 hours in a 4°C fridge. A further three washes in buffer took place before the sections were incubated for an additional hour in goat anti-rabbit IgG-eosin conjugate at room temperature. Two more washes of 10 minutes each, followed by 15 minutes fixation in 2% glutaraldehyde (EM grade) diluted in buffer at 4°C the 4°C. After five washes of three minutes each the sections were treated with 100mM

glycine and 50mM aminotriazole in buffer to reduce non-specific staining. The sections were then transferred to the glass “bottomed” plastic Petri dishes, that had been pre-treated with 0.1% polyethyleneamine (see appendix 5.2.3). The pre-treatment is important to keep the vibratome sections flat and adhered to the base during photo-oxidation. The dish was filled with buffer; the sections transferred and gently pushed down to adhere to the base with a paintbrush. The buffer was sucked out taking care to keep the sections in place and refilled very gently. Next, photo-oxidation took place in a microscope prepared as described above. The Petri dishes containing sections were placed on the chilled microscope stage and held in place with tape. A line with a 10 ml syringe attached was also taped to sit inside the Petri dish and provide the means of extracting excess fluid. An irradiation site was identified through the x40 objective lens using transmitted light and commenced by changing to a x60 objective lens, introducing the triple cube before adding the DAB solution drop by drop. Photo-oxidation took place during continuous observations to establish a visual image of a brown spot where the higher lens created a field limit easily observed in the larger field of the lower magnification lens with darker brown reaction product appearing (see Fig 3.4 and 3.5a, b).

### **2.2.3.3 Propidium iodide**

To check that the protocol was working, propidium iodide, a nuclear marker, was substituted for the primary antibody. The secondary antibody/conjugate was omitted. Otherwise the protocol was followed as described above.

## **2.2.4 EM PREPARATION**

All washes, post-fixation and dehydration were carried out in Petri dishes sitting on crushed ice to keep the vibratome sections flat. After photo-oxidation the vibratome sections were washed for 5 x 3 minutes in 0.1M sodium cacodylate buffer and then post-fixed with 1% osmium tetroxide made up in the same buffer, for 30 minutes. The sections were transferred to individual glass Petri dishes washed a further 2 x 3 minutes in buffer and dehydrated in increasing concentrations of ethanol, starting at 50% continuing to 70%, 80%, 90% finishing at absolute. Each step lasted 15 minutes and absolute

ethanol consisted of 2 changes of 15 minutes each. Finally, the sections were infiltrated with Durcupan resin B which does not contain a hardening accelerator (see appendix 5.2.4), diluted 1:1 with ethanol for 30 minutes and left overnight in Durcupan B diluted 3:1 with ethanol. The following day, the sections were left in Durcupan resin A, which contains hardening accelerator(see appendix 5.2.4) for 1hr in a 50°C oven, then embedded in Durcupan A by placing each section on a glass slide coated with a compound release agent (Formen-Trennmittel, Hobbytime). A small amount of resin was carefully pipetted on to the section and a second coated glass slide placed on top. The two slides were clamped together with stationary bullfrog clips. The slides were left in a 50°C oven for the resin to polymerise a minimum of 24 hours.

A razorblade was used to detach the resin sheet from the glass slides, the sections trimmed and then glued on to blank resin blocks with a drop of resin.

Sections were cut for EM and grids stained as described in 2.1.8

## **2.3 PAP and ABC**

Vibratome sections (see section 2.2.1.2) were used for both PAP and ABC staining. All staining was carried out at room temperature unless otherwise stated.

For the PAP method, a secondary antibody (rabbit PAP complex) diluted 1:40 and a goat anti rabbit link antiserum, diluted 1:10, was used

For the ABC method, a biotinylated secondary antibody was used together with a Vectastain ABC avidin biotin complex kit™ to enhance the signal.

### **2.3.1 PAP STAINING**

Endogenous peroxidase activity was blocked with freshly made 0.3% hydrogen peroxide/dH<sub>2</sub>O for 30 minutes.

After washing with running water, sections were treated with 10% normal goat serum (NGS) in PBS for about 2 hours at room temperature. Excess NGS was removed and the primary antibody, diluted in 1% NGS/PBS, was immediately applied and sections were incubated overnight at 4°C. The following day, sections were allowed to warm to room temperature and washed in PBS, 6 changes, for 30 minutes. The appropriate link antibody diluted in 1% NGS was applied for 1 hour at room temperature and washed in PBS, 6 changes for 30 minutes. Sections were incubated with PAP complex, 30 minutes at room temperature and washed in PBS, 6 changes, for 30 minutes. The chromogen reaction was developed in filtered PBS containing 0.5 mg/ml DAB and 0.003% hydrogen peroxide/dH<sub>2</sub>O until the required colour change was seen (30 seconds to 5 minutes). DAB was removed by washing in PBS for 2 minutes and running water for 5 minutes. Sections were immersed in 1% osmium tetroxide/cacodylate buffer for 2 minutes before washing.

Sections were dehydrated through alcohols, cleared and mounted in DPX. For EM, sections were processed after osmication as for routine EM i.e dehydrated through graded ethanol, propylene oxide and embedded in Araldite similarly to the photo-oxidation method.

### **2.3.2 ABC STAINING FOR EM**

100µm thick vibratome sections were transferred from a Petri dish to a 24 well tissue culture dish (NUNC), separated to single slices per compartment. The slices were submerged in solutions except for primary and secondary antibody solutions where the slices were merely kept covered in as little solution as possible, without drying out. Adding and withdrawing solutions were performed with a Gilson Pipette™. Primary antibodies consisted of PLP226, AA3 and GFAP as a positive control. Negative controls consisted of primaries being omitted and instead kept in blocking buffer, the rest of the schedule was performed as follows:

The slices were washed in three changes of 20 minutes each with PBS, thereafter endogenous peroxidase activity was blocked with a solution of 0.3% hydrogen peroxide in dH<sub>2</sub>O for 30 minutes. A blocking buffer consisting of 10% NGS, 0.2 % Triton X-100 in PBS to reduce non specific background staining and permeabilise cell membranes was

applied for 1 hour. Slices were then incubated for 1 to 5 days with primary antibody solution made up in the same buffer as used for blocking except for NGS concentration being reduced to 1%. Incubation was carried out in a 4°C fridge and solutions topped up as necessary. The slices were thoroughly washed three x 20 minutes in 0.2 % Triton X-100/PBS. Next, incubation in a biotinylated secondary antibody solution, made up in the same buffer as for the primary, for 2 hours to overnight followed. Further three x 20 minutes washes in the same buffer was applied before an Avidin Biotin Complex.

## **2.4 IMMUNOGOLD**

### **2.4.1 TISSUE PREPARATION**

#### **2.4.1.1 Animal source**

Altogether 26 mice, 20 wild type and 6 *Plp1* null, were used (see section 2.1.1 for detail). Ages ranged from P8 to P69. In addition, tissue from 5 animals previously used for the photo-oxidation study, suitably fixed, was initially used. Fixation varied and is described for the particular studies, see table 1.

#### **2.4.1.2 Fixation**

Several methods for fixation were explored to establish best possible preservation of antigenicity and morphology. Animals were perfused and left for 8-12 hrs in 4°C,

1. 1% glutaraldehyde and 1% paraformaldehyde in 0.1M phosphate buffer (PB) pH 7.4 (Maxwell and Riddell, 1999).
2. 15% picric acid, 1% glutaraldehyde and 1% paraformaldehyde in 0.1M PB pH 7.4 (Li et al, 2001).
3. 4% paraformaldehyde and 0.1% glutaraldehyde in 0.1M PB pH 7.4 (Tait et al, 2000).

## 2.4.2 EM PREPARATION

Tissues were dissected as in section 2.1.3 extracting transverse sections of corpus callosum, transverse ventral columns and longitudinal dorsal columns sections of cervical spinal cord and whole optic nerves.

Processing fixed tissue, for fixation methods 1 and 2 (see section 2.4.1.2), were as follows:

The tissues were rinsed 6 times in 0.1M PB for 30 minutes followed by secondary fixation in 1% OsO<sub>4</sub> in 0.1M PB for 30 minutes to 1 hour. Dehydration was carried out in rising concentrations of ethanol starting with 50% and finishing with 2 x 100%, 15 minutes each. Infiltration of resin (Durcupan) was carried out with 100% ethanol/Durcupan B (without hardener), dilution 1:1 for 1.5 hours, then 100% ethanol/Durcupan B, dilution 1:3 overnight, finishing with Durcupan A (with hardener) only for 2 hours prior to embedding and curing in a 60°C oven for 24 hours.

Processing fixed tissue for fixation method 3 (see section 2.4.1.2), was as follows:

Tissue blocks were kept in perfusion fixative for a further 2 hours (after perfusion) and then washed several times in 0.1M PB pH 7.4 (see appendix 5.3.1) containing 3.5% sucrose for 20 minutes. Next, tissues were stained with 0.25% tannic acid made up in the wash buffer at 4°C for 1 hour. To quench aldehydes 50mM ammonium chloride (NH<sub>4</sub>Cl) in 0.1M PB pH 7.4 was used for 30 mins. Several washes in 0.1M maleate buffer pH 6.2 (see appendix 5.3.2) containing 4% sucrose for 20 minutes was followed by *en bloc* staining with 1% uranyl acetate in the same maleate/sucrose buffer for 1 hour also carried out at 4°C. Dehydration and embedding followed as for methods 1 and 2.

Semi-thin sections (0.5µm) were cut and stained with routine azureII/methylene blue protocol (see 2.1.8) for light microscopy to identify areas to be cut for grids. Thin sections (70nm) were then cut with a diamond knife (see section 2.1.8), floated out on water and picked up either directly on formvar coated slot (see appendix 5.3.3) or uncoated 200 mesh nickel grids or picked up together with a droplet of water on a nickel

loop and placed on coated slot grids. Excess water was blotted off with a piece of filter paper and care taken to orientate sections on the grid.

## **2.4.3 IMMUNOCYTOCHEMISTRY**

### **2.4.3.1 Primary antibodies**

Titres for PLP226 were established using ~70nm thin sections cut for EM, embedded both in Araldite and Durcupan. Dilutions were approximated from routine use at 1:600 and increased in concentration to 1:450 and 1:300. Similarly, titres for PLPA were tested at routine concentration of 1:1000 and further tested at 1:500 and 1:2000. Anti-GABA (donated by Prof. Maxwell) and anti-GFAP were used at 1:1000.

### **2.4.3.2 Secondary antibodies**

For the IG method initially a 10µm gold particle conjugate donated by Prof D. Maxwell was used, followed by a 10µm and a 2µm gold particle conjugated to an anti-rabbit IgG from Biotech. The 10µm conjugate was put into Eppendorf vials in aliquots of 20µl, frozen and stored at -20°C. Dilutions were initially kept to the same titre as used by Prof D. Maxwell (Maxwell et al, 1997)

## **2.4.4 IMMUNOGOLD LABELLING**

### **2.4.4.1 Pre-embedding immunogold**

For pre-embedding IG staining vibratome sections were created as before (see sections 2.2.1.2), to include sagittal cerebellar and transverse cervical spinal cord sections at 50µm thickness. Staining protocol was used as by Prof Maxwell's spinal cord research group (Olave et al, 2002)

Immediately after cutting, the 50µm thick sections were transferred to a Petri dish with 50% ethanol for 30 minutes to permeabilise. After several washes in PBS the sections were left for 3 days in primary antibody solution, PLP226/PBS, concentration 1:600.

#### **2.4.4.2 Post-embedding immunogold**

Staining protocol for tissue processed as per methods 1 and 2 (see section 2.4.1.2) were as follows:

Grids were floated on droplets, of various protocol solutions, placed on Nescofilm™ in a Petri dish lined with water soaked tissue paper to prevent the grids drying out. All steps were carried out at room temperature except that primary antibodies were applied overnight at 4°C.

Controls included sections where primary antibody was omitted (-ve) or a different primary antibody (+ve) was applied.

Initially, the sections were treated with a blocking solution (PBST, pH, see appendix 5.3.4) containing 10% NGS, to reduce non-specific binding and 0.1% Triton X-100 to increase membrane permeability in PBS for 1 hour. The sections were then incubated with primary antibodies diluted in PBST with a reduced concentration of NGS to 1%. After overnight incubation, grids were subsequently washed thoroughly; first, in PBST then in TBST (Tris buffered saline containing 0.1% Triton X-100, pH 8.2, see appendix 5.3.5) altogether for 1 hour. The grids were then incubated for 2 hours with goat anti-rabbit secondary antibodies conjugated to 2 or 10nm particles of colloidal gold (BBI) diluted in TBST. Thorough washing followed; first, with TBST 2 x 10 minutes then distilled water 2 x 10 minutes. If 2nm gold particles were used, grids were place on droplets of freshly mixed silver enhancing solution (Vectastain) for 5 to 10 minutes. Grids were then either left unstained or stained briefly with uranyl acetate and/or Reynold's lead citrate.

Staining protocol for tissue processed as per method 3 (Tait et al, 2000) (see section 2.4.1.2) were as follows:

Sections were blocked for 40 minutes with 1% BSA, 0.5% fish skin gelatine, 0.05% Triton X-100 and 0.05% Tween 20 made up in 10nM Tris buffer, pH 7.4, containing 500nM NaCl and then incubated with primary antibodies diluted in the same buffer overnight. The sections then went through 4 washes in blocking buffer before a 1 hour incubation

with secondary antibody IG conjugate took place. After several washes in distilled water the sections were fixed in 2.5% glutaraldehyde/dH<sub>2</sub>O, further washed in a stream of dH<sub>2</sub>O before a secondary fixative consisting of 2% OsO<sub>4</sub>/ dH<sub>2</sub>O was applied. The sections were finally stained with uranyl acetate and Reynold's lead citrate.

## **2.5 FREEZE SUBSTITUTION**

### **2.5.1 ANIMAL SOURCE**

Four wild type and 2 *Plp* null mice, aged P20-21 were used.

### **2.5.2 PROTOCOL**

Animals were humanely euthanased as described before (see 2.1.2). Brain and spinal cord were immediately dissected out. The tissue was kept submerged in PBS during dissection and transferred to be frozen as quickly as possible. Areas of interest were chosen as before, see 2.4.2, to consist of transverse slices of corpus callosum, longitudinal and transverse slices of spinal cord. Tissues were "rapid frozen" in liquid propane at -187C° using a Reichert KF 80 cryo chamber; propane was liquefied and kept at a constant temperature with liquid nitrogen; tissues were mounted on aluminium pins, attached to a plunger and propelled semi-automatically into the cryogen. After freezing, the pins were transferred to NUNC tubes kept in liquid nitrogen. The tubes were filled with pre-chilled 100% acetone, to dehydrate the tissue, and kept in a -90°C freezer for 7 days. The tubes were refilled daily with fresh pre-chilled acetone. The tissues were slowly brought to room temperature by transferring the tubes first to a -20°C freezer for 2 hours and then to a 4°C fridge for 2 hours. Osmication followed with freshly made 1% OsO<sub>4</sub> in 100% acetone for 1 hour, dehydration for 2 x 15 minutes in acetone. Infiltration and embedding with Durcupan resin followed as described in section 2.2.4 with acetone replacing ethanol.

## **CHAPTER 3 RESULTS**

### **3.1 CRITERIA FOR SUCCESSFUL LABELLING**

The aim of this thesis was to evaluate techniques for subcellular immuno-histochemical labelling which could be applied to the study of PLP biology. PLP is localised predominantly in the compact myelin sheath. Therefore myelinated tract from the spinal cord and from the cerebellum of mice were used to critically evaluate a number of methodological aspects. Outcome was assessed by visual observation to determine if the sections satisfied following criteria

(I) The structure of tissue should be preserved.

(II) There should be a differential labelling of myelin to non-myelin tissue.

As part of an independent audit, approximately 50% of the sections were assessed by Dr C. Thompson and there was 100% concordance between her assessment and my assessment whether the sections satisfied these criteria.

### **3.2 PHOTO-OXIDATION**

Photo-oxidation of eosin was used because the technique is verifiable at each stage and all equipment necessary was available. The labelling can be confirmed at light microscopic level before proceeding to the electron microscopic level which eliminates unnecessary and time consuming processing of unlabelled tissues.

### **3.2.1 FIXATION**

Three fixatives, of varying glutaraldehyde concentrations were examined to establish a protocol for the photo-oxidation investigation which produced an adequate level of morphological preservation. These results were contrasted with the excellent morphological preservation of myelin achieved by high concentrations of glutaraldehyde.

Fixation with glutaraldehyde (0.1%) failed to produce acceptable myelin morphology. The intraperiod lines of the myelin were completely disrupted, myelin distorted as was the axons, see Fig. 3.1. Furthermore the low concentration of glutaraldehyde left the tissue very soft resulting in wavy tissue thus making the nodes of Ranvier difficult to identify.

Fixation with glutaraldehyde (0.5%) was also suboptimal for the myelin morphology displaying similar artefacts, although to a lesser degree.

Fixation with glutaraldehyde (1%) produced acceptable morphological preservation for the myelin. Intraperiod lines were still disrupted but key morphological features (myelin periodicity and axons) could be discerned and thus glutaraldehyde (1%) satisfied criteria I.

### **3.2.2 CONJUGATION OF EOSIN**

Three conjugations were performed where the fluorophore eosin was attached to a goat antibody; firstly to a goat-anti-rabbit IgG which recognise PLP226 (two conjugations); secondly to a goat-anti-rat IgG which recognise AA3 (one conjugation). Both antibodies target myelin proteins PLP and DM20.

Using spectrometry measurements the two goat-anti-rabbit conjugates consisted of 2 molecules of eosin per IgG and 5.9 molecules of eosin per IgG, respectively. The goat-anti-rat conjugate consisted of 9.5 molecules of eosin per IgG.

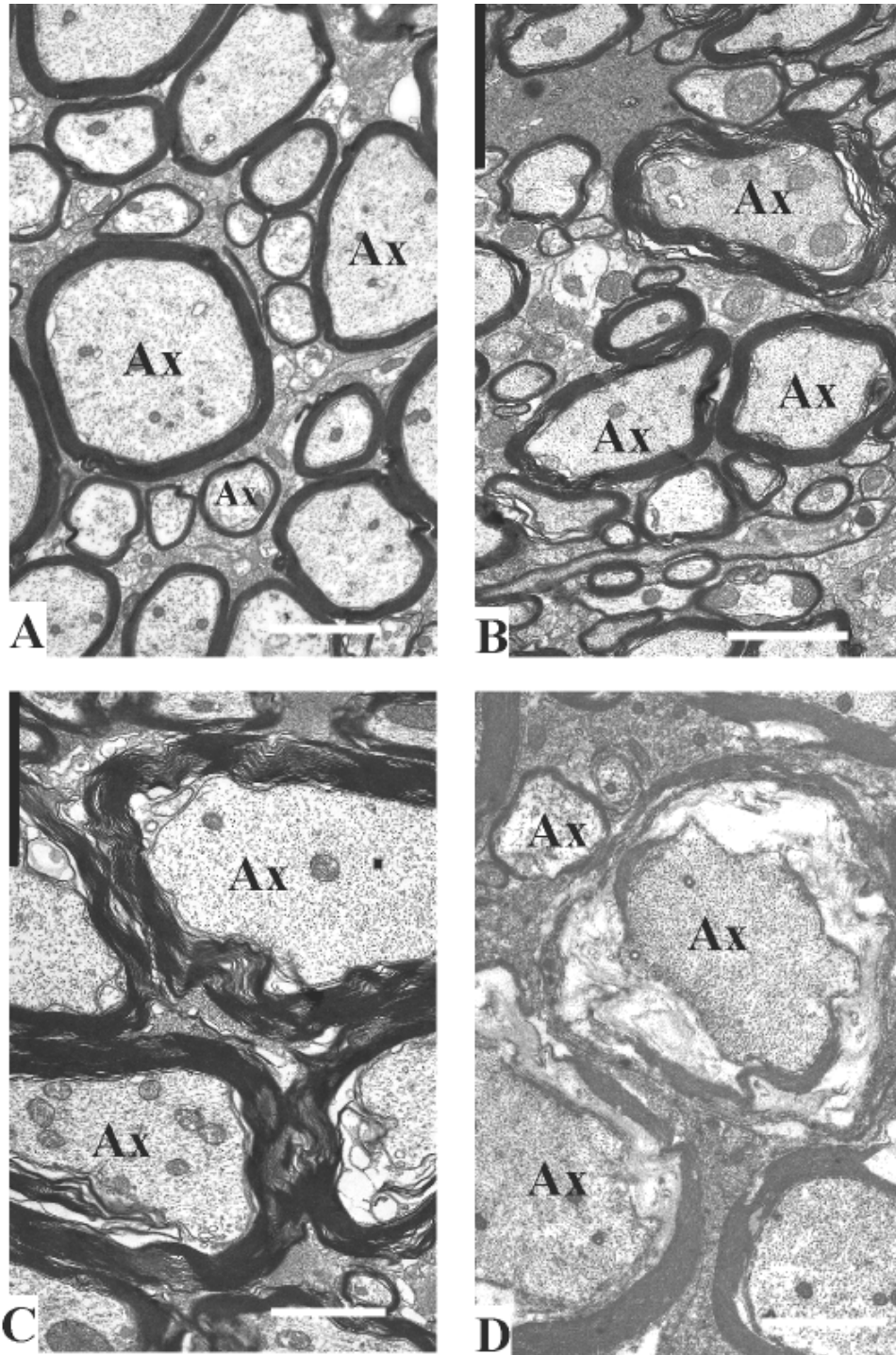


**FIGURE 3.1.** Electron micrographs of myelinated axons in the spinal cord ventral columns from adult mice showing the influence of glutaraldehyde concentration.

**A.** Tissue fixed with 5% glutaraldehyde.

**B.** Tissue fixed with 1% glutaraldehyde.

**C.** Tissue fixed with 0.5% glutaraldehyde.

**D.** Tissue fixed with 0.1% glutaraldehyde.

Note the correlation in deterioration of myelin compactness and axon (Ax) shape to decreasing glutaraldehyde concentration.

Scale bar = 2 $\mu$ m

No significant difference was apparent on visual inspection in oligodendrocyte cultures stained with dialysed and undialysed solutions of eosin conjugated goat antibodies.

SDS-PAGE gel electrophoresis confirmed that the conjugations were successful but EITC fluorescent output was at a much lower level than FITC. The EITC was of the order of 20% of the FITC in accord with published data (Deerinck et al, 1994) (Fig. 3.2).

### **3.2.3 TITRE**

Titres for the EITC to be used in the photo-oxidation method were established for each conjugate on dissociated oligodendrocyte cultures which were chosen because they were readily available, easily stained and avoided the need for sacrificing additional animals. Dilutions of 1:10, 1:50, 1:100 and 1:250 were examined because the FITC is used at a dilution of 1:80.

EITC at a dilution of 1:10 had poor signal to noise because of the high background. EITC at a dilution of 1:250 had a faint signal, although fine oligodendrocyte processes could still be seen. EITC at dilutions of 1:50 and 1:100 both showed clearly labelled oligodendrocyte processes.

Further tests between 1:50 and 1:100 were made. The first eosin conjugate, goat anti-rabbit was optimal at a dilution of 1:75, the second at a dilution of 1:85. The third, an eosin goat anti-rat conjugate was optimal at a dilution of 1:50 (Fig. 3.3).

These antibody titres were tested on cryostat sections to determine if the concentrations were appropriate for photo-oxidation and that PLP could be distinguished in sections. PLP was readily visible in the white matter of cerebellar folia (Fig. 3.4) using all three conjugates.

### **3.2.4 PHOTO-OXIDATION**

Propidium iodide, a nuclear marker, was used instead of a primary antibody to test the photo-oxidation protocol. Photo-oxidation of propidium iodide produced excellent results at LM level but equivocal results at the EM level.

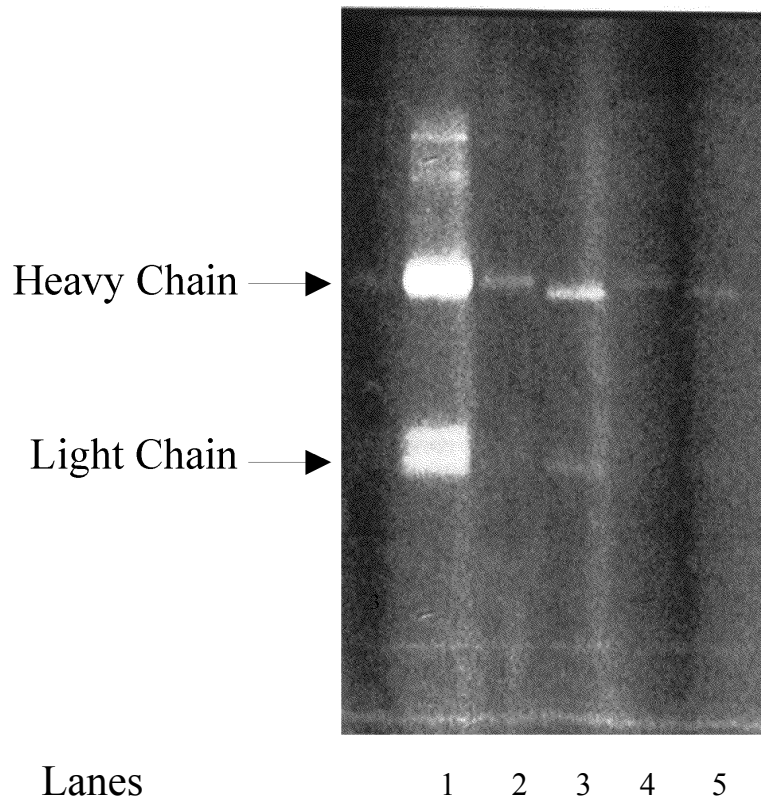


**FIGURE 3.2** SDS-PAGE acrylamide gel to confirm successful conjugation of EITC to rabbit IgG and comparison to FITC, visualised using a UV light

**Lane 1.** Denatured EITC conjugate separated into fragments. Light chain (25 kDa ) and heavy chain (50 kDa). Bands are prominent in the undiluted sample.

**Lane 2.** Diluted EITC conjugate 1:10. The heavy chain band can be discerned together with a faint band for the light chain. Both bands are approximately 20% of the equivalent band in lane 3.

**Lane 3.** Diluted FITC conjugate 1:10. A clear band for the heavy chain and a lighter band for the light chain are clearly visible.

**Lane 4.** Diluted EITC conjugate 1:50 Faint bands for the heavy chain can be discerned.

**Lane 5.** Diluted FITC conjugate 1:50 Faint bands for the heavy chain can be discerned

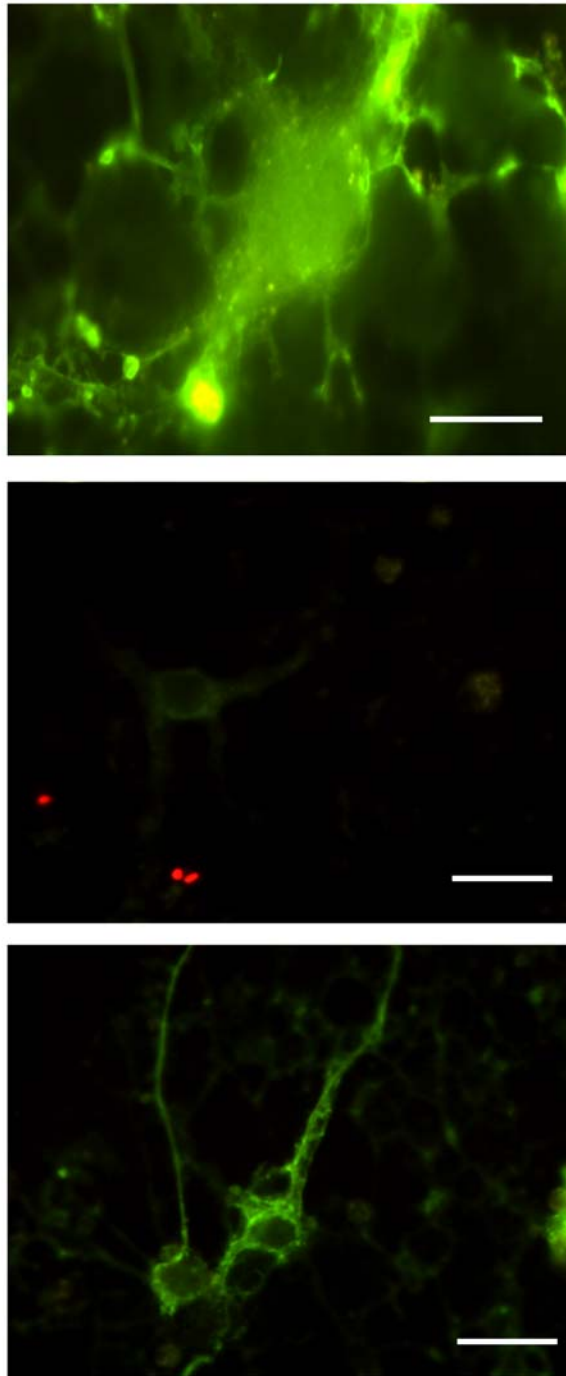


**FIGURE 3.3** Cultured oligodendrocytes immunostained with a PLP/DM20 primary antibody to determine secondary antibody concentration for optimal fluorescence.  
**Upper.** Goat anti-Rabbit conjugated EITC 1:75  
**Middle.** Negative control without primary antibody, goat anti-Rabbit EITC 1:75  
**Lower.** Goat anti-Rabbit FITC 1:80.  
Scale bar A = 10 $\mu$ m, B, C = 20 $\mu$ m

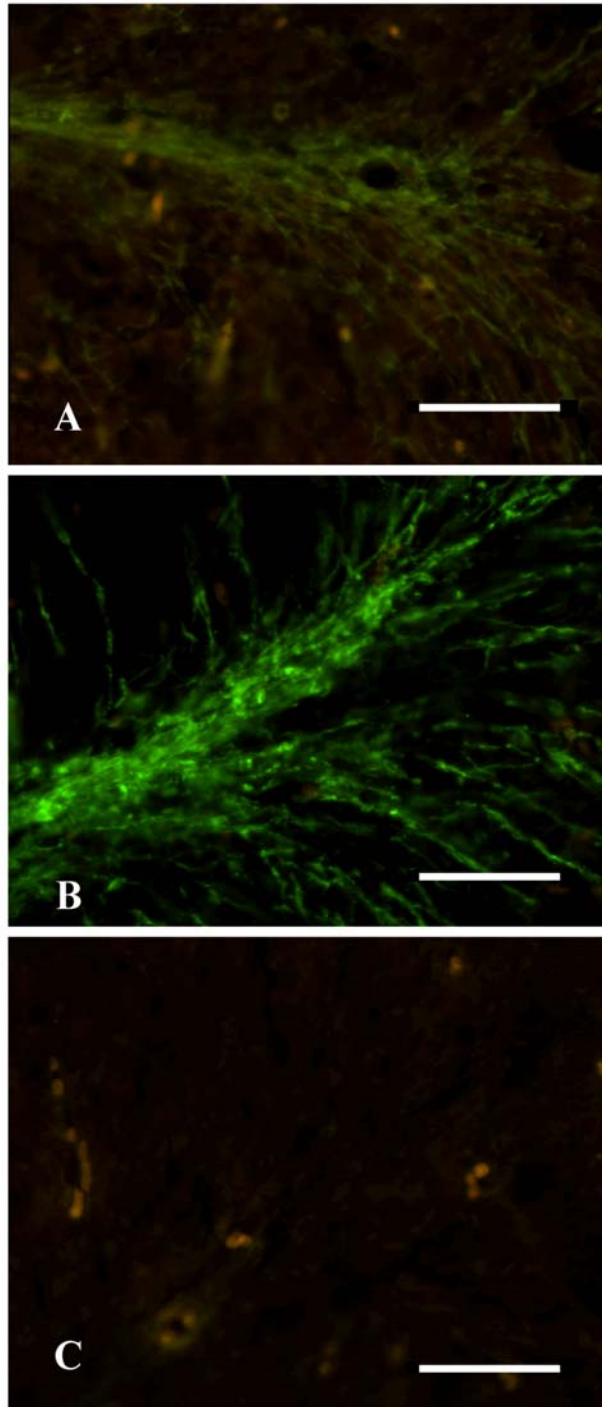


**FIGURE 3.4** Fluorescent images of myelinated axons in cerebellar folia to confirm appropriateness of titres.

Indirect immunolabelling performed on 12  $\mu\text{m}$  cryostat sections with a PLP/DM20 antibody.

**A.** Myelin immunolabelled with a goat anti-rabbit IgG conjugated EITC secondary antibody.

**B.** Myelin similarly immunolabelled but with a FITC conjugated secondary antibody. Compare the intense staining of the axons with the less intense staining with EITC shown in image A above.

**C.** Negative control in the form of omission of the primary antibody PLP/DM20 .

Scale bars = 20 $\mu\text{m}$

During photo-oxidation, the EITC conjugate is irradiated in the presence of DAB, which is subsequently converted to a brownish reaction product by the excitation of the EITC molecule. Propidium iodide reacts directly with DAB, forming a similar reaction product. Cerebellar sections, focused on the folium with both grey and white matter was used. The photo-oxidation process were stopped by halting the irradiation which could easily be defined with continuous observation. A medium brown spot, matching the restricted area formed by objective aperture size, with darker brown nuclei both in the grey and white matter, was clearly seen under the light microscope (Fig. 3.5a & b). However, at EM level no discernable staining could be detected. This observation must be treated with caution. If a light homogenous “sprinkling” of very fine grains it could easily be missed due to contrast staining of the tissue.

The photo-oxidation protocol was applied to both cerebellar and cervical spinal cord vibratome sections. An antibody (PLP226) against PLP and DM20, targeting the C-terminal of the proteins, was used. This antibody was very reliable on LM and FM preparations.

After photo-oxidation the tissue appeared well labelled at LM level. Dark brown “strands” corresponding to myelinated processes could be seen in the white matter of sagittal cerebellar sections (Fig.3.6) and similarly in longitudinally sectioned spinal cord sections. In transverse section, the myelin around axons was easily observed as brown rings surrounding pale axonal centres. Because photo-oxidation took place in a fluorescence microscope, I was able to check that the tissue was labelled by switching between a FITC cube for fluorescence viewing and a triple cube for photo-oxidation viewing (Fig.3.6). The optical density of the reaction product was established through timed exposure ranging from 5 min. to 30 min. At 5 minutes exposure, no specific labelling was observed although the brown background labelled circle had appeared and at 30 minutes overexposure had obscured the specific labelling against the darker background. Although the LM result appeared positive and labelled as expected, there was no evidence of labelling at EM level in contrast stained sections. On 30 occasions (each with 4 sections) successful labelling was observed at LM level with no reaction product seen at EM level in contrast stained sections (see Table 1).

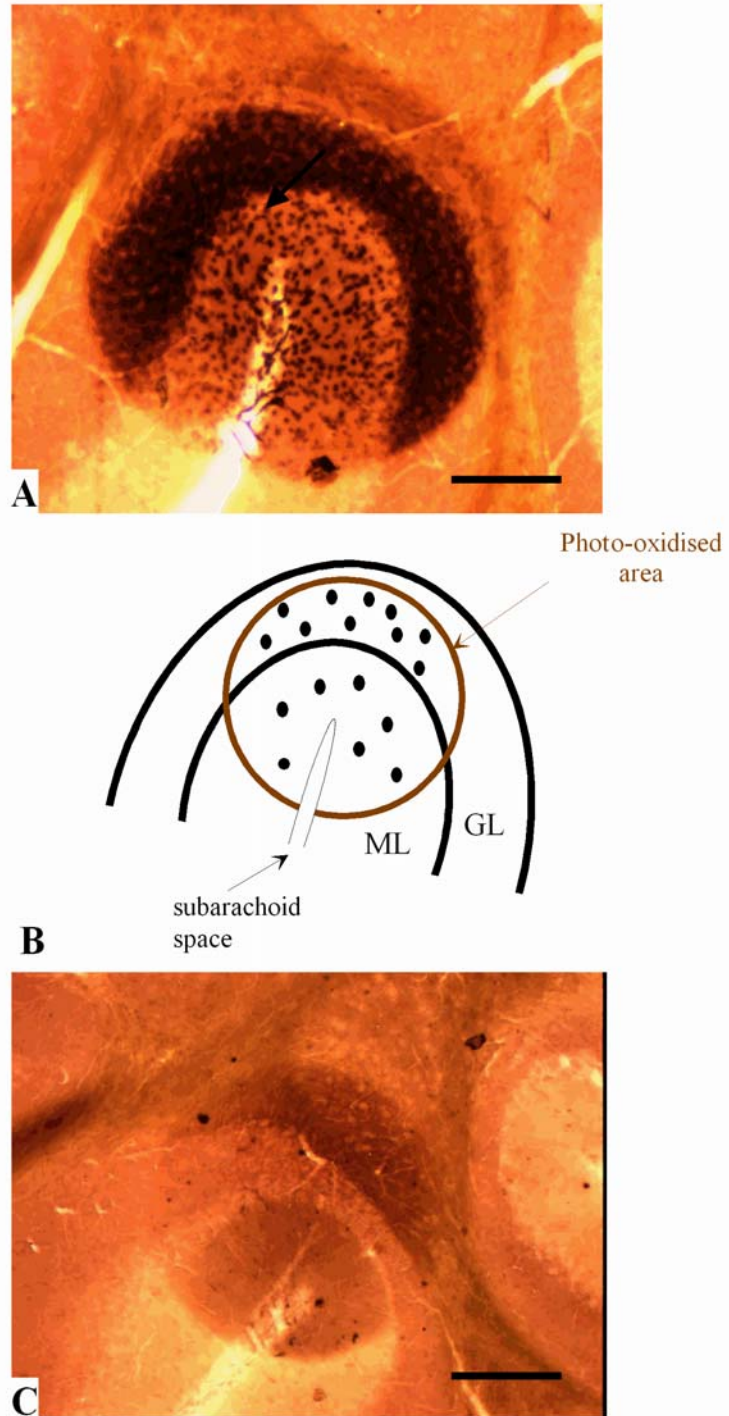


**FIGURE 3.5a** Light microscopy images of cerebellar folium, showing photo-oxidised area restricted by objective aperture size.

**A.** Nuclei, in molecular and granular layer, labeled with propidium iodide after photoconversion

**B.** Schematic representation of photo-oxidised sections in A and B. Two layers in the cerebellar folia are visible, the molecular layer (ML), granular layer (GL). Black dots represent stained nuclei seen in section A only;

**C.** Control showing photo-oxidised area of section with no propidium iodide incubation. Note lack of stained nuclei.

Scale bars A, C

= 100 $\mu$ m.

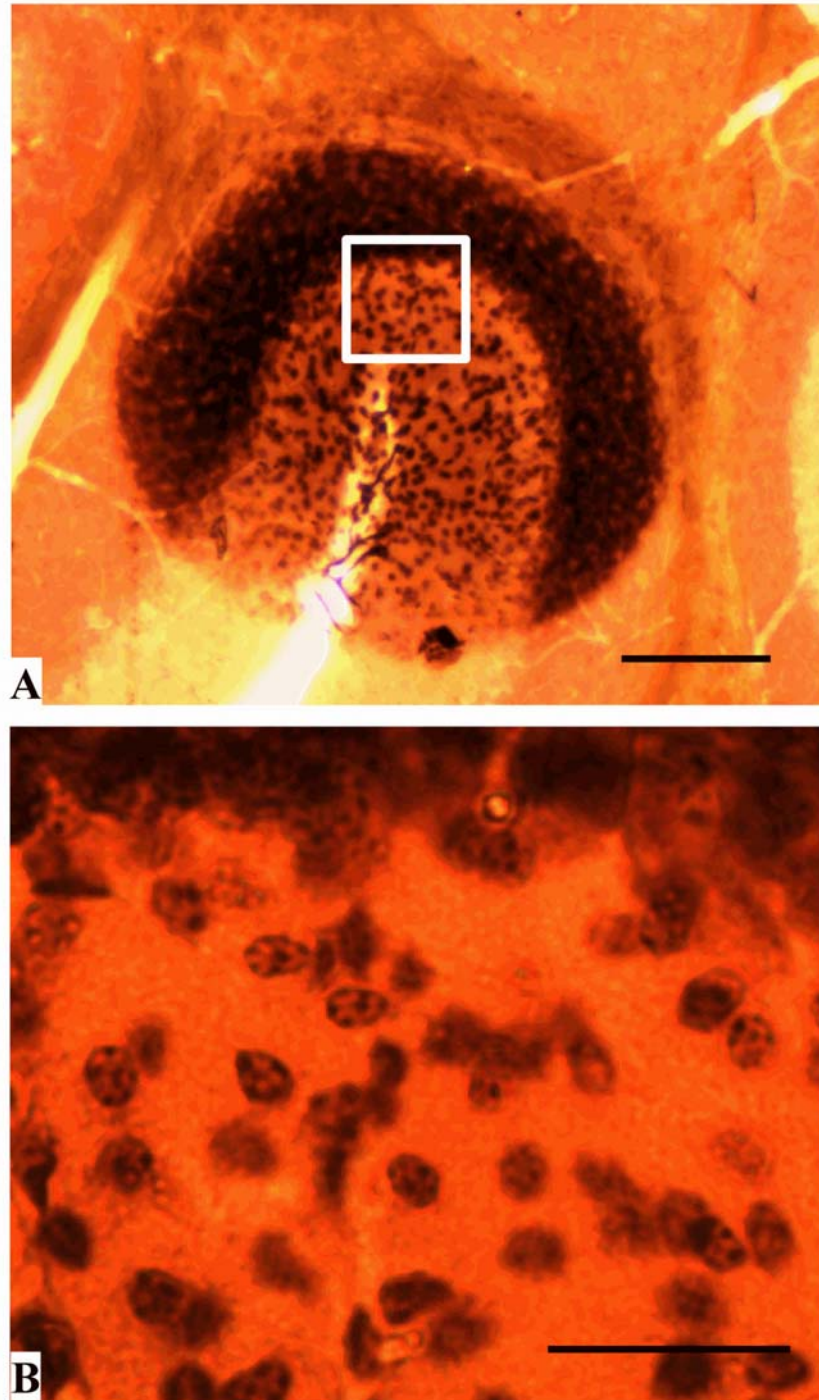


**FIGURE 3.5b** Light microscopy images as in figure 3.5a (at higher magnification) highlighting labelled cell nuclei.

**A.** Cerebellar folia showing photo-oxidised area restricted by objective aperture size. Inset area representing figure B;

**B.** High magnification of photo-oxidised cerebellar molecular layer showing labelled cell nuclei.

Scale bars A = 100 $\mu$ m. B = 20  $\mu$ m

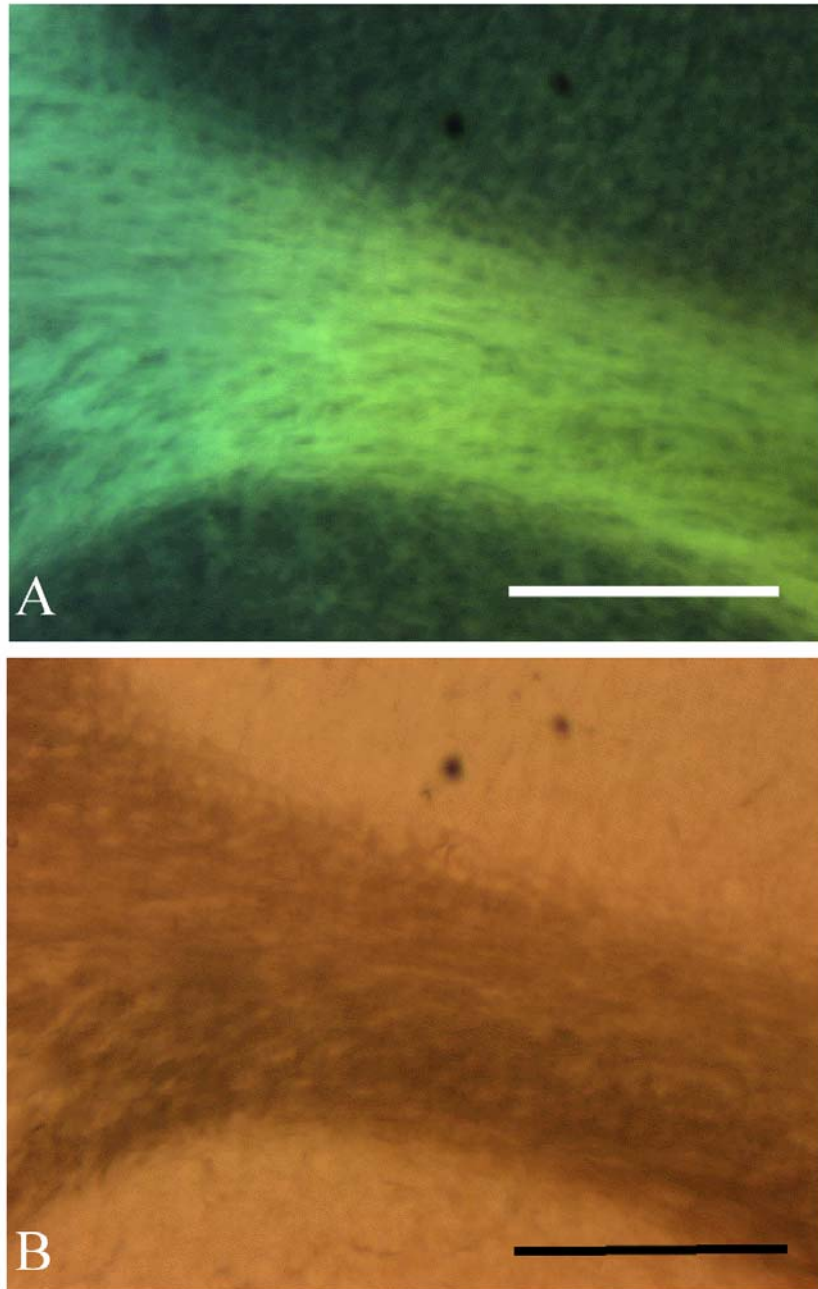


**FIGURE 3.6** Successful photo-oxidation of myelin at LM resolution.  
**A.** Fluorescence image of myelin (prior to photo-oxidation) in white matter between cerebellar folia labelled with rabbit anti-PLP antibody followed by a goat anti-rabbit eosin conjugate  
**B.** The same section after photoconversion.  
Scale bars A, B = 100 $\mu$ m.

**TABLE 1: Optimisation of Photo-oxidation : Factors varied**

Exp no	Animal	Genotype	Tissue	Age	Fixation	Type experiment	Ab1	Ab2
PO 1	mouse	WT	sag cereb 50µm		4% para add 0.1% glut	po	PI	
PO 7	mouse	WT	sag cereb,cerv 50µm	P6weeks	4% para 0.1% glut	po	PLP226	EITC#1
PO7A	"	"	"	"	"	po	PLP226	EITC#1
PO7B	"	"	"	"	"	po	PLP226	EITC#1
PO7C	"	"	"	"	"	po	PLP226	EITC#1
PO7D	"	"	"	"	"	po	PLP226	EITC#1
PO 8	mouse	WT	sag cereb,cerv 50µm	P6mo	4% para 0.5% glut	po	PLP226	EITC#1
PO 9	mouse	WT	sag cereb,cerv 50µm	P6mo	4% para 1% glut	po	PLP226	EITC#1
PO 9C	"	"	sag cereb 70µm	"	"	po	PLP226	FITC
PO 9D	"	"	sag cereb,cerv 50µm	"	"	po w NaBH4	PLP226	EITC#1
PO 16	mouse	WT	sag cereb,cerv 50µm	P22	4% para 1% glut	po	PLP226/GFAP	EITC#2
PO 16A	"	"	sag cereb vibs 50µm	"	"	po	PLP226/GFAP	EITC#2
PO 16B	"	"	sag cereb vibs 50µm	"	"	po	PLP226/GFAP	EITC#2
PO 16C	"	"	"	"	"	po	PLP226/GFAP	EITC#2
PO 17	mouse	WT	sag cereb,cerv 70µm	P22	4% para 1% glut	po	PLP226/GFAP	EITC#2
PO 18	mouse	WT	"	P19	4% para 1% glut	NA		
PO 19	mouse	WT	"	P19	4% para 1% glut	po	PLP226/GFAP	EITC#2
PO 19A	"	"	sag cereb vibs 50µm	"	4% para 1% glut	po	PLP226/GFAP	EITC#2
PO 19B	"	"	sag cereb vibs 50µm	"	4% para 1% glut	po	GFAP	EITC#2
PO 19E	"	"	sag cereb vibs 70µm	"	4% para 1% glut	po	PI	
PO 20	mouse	WT	sag cereb vibs 50µm	P16	4% para 1% glut	po	GFAP	EITC#2
PO 20B	"	"	cereb vibs 50µm	"	4% para 1% glut	po	GFAP	EITC#2
PO 20E	"	"	cereb vibs 50µm 70µm	"	4% para 1% glut	po	GFAP	EITC#2
PO 21	mouse	WT	"	P17	SF	po	PLP226/GFAP	EITC#2
PO 22	mouse	WT	"	P17	SF	po	PLP226/GFAP	EITC#2
PO 22A	"	"	"	"	"	po	PLP226/GFAP	EITC#2
PO 26	"	"	"	"	4% para 1% glut	po	AA3	EITC#3
PO 26B	"	"	"	"	4% para 1% glut	po	AA3	EITC#3
PO 27	mouse	WT	Astro TC	7 div	4% para 0.1% glut	po	GFAP	EITC#2
PO 29	mouse	WT	Astro TC	7div	4% para 0.1% glut	po	GFAP	EITC#2
PO 31	PO 22	WT	sag cereb vibs 50µm	P17	SF	po	PI	

No compelling demonstrations of photo-oxidation product associated with myelin were obtained in these experiments (see text for details)

Age: Postnatal ages for mice days, weeks, months For astrocytic cultures days in vitro (div)

Tissue: Vibratome sections of sagittal cerebellum (sag cereb), cervical spinal cord ventral columns (cerv), astrocyte tissue cultures (Astro TC).  
Section thickness is indicated.

Ab1: Type of primary antibody used  
P1: propidium iodide for nuclear labelling  
PLP226 for PLP/DM20, GFAP for astrocytes

Ab2: Type of secondary antibody used :  
EITC #1 and #2 represent two different conjugations of eosin 5-isothiocyanate, FITC represents fluorescein 5-isothiocyanate

Type experiment: photo-oxidation (PO), photo-oxidation with tissue quenched for autofluorescence (PO w. NaBH4)

To determine if the lack of staining at EM level was due to weak immuno-labelling of PLP and DM20, an antibody against GFAP was used as this provides a strong labelling of intermediate filaments in astrocytes. Sagittal cerebellar sections were used because astrocytes in the shape of Bergmann glia run densely through the molecular layer of the folium. The photo-oxidation protocol was applied as before and Bergmann glia was observed at LM level but not at EM level in contrast stained sections.

### **3.2.5 IMMUNOHISTOCHEMISTRY**

Failure to detect photo-oxidation labelling of EITC at EM level may be a consequence of inadequate signal, either because the 70nm EM sections cannot hold enough of the reaction product or that the low fluorescing ability of eosin is not enough to be detected at EM level. Therefore I employed the ABC method. Using ABC, anti-GFAP gave excellent labelling at dilution of 1:1000 at LM level. Bergmann glia in the cerebellar molecular layer was strongly labelled (Fig.3.7). PLP226 had to be tested at various dilutions, 1:300, 1:600 and 1:1200. The ABC labelling of PLP226 at the dilution of 1:1200 clearly showed visible strands, identifiable as longitudinally orientated myelinated axons. Higher concentrations of PLP226 gave a high background. A different antibody (AA3) against PLP and DM20 was tested to preserve our group's finite pool of PLP226. This antibody gave an identical labelling to PLP226 although slightly finer and weaker (Fig. 3.7). The EM picture for both antibodies was found to be unsatisfactory for our main purpose of differential localisation for PLP and DM20. To critically assess if the photo-oxidation technique would give an adequate EM picture of the oxidised DAB product, I used GFAP since it gives a stronger signal than PLP226 and AA3 at LM level. The filaments are found throughout the cytoplasm of astrocytes and its processes, which should be easily identifiable. At EM level, the fine reaction product at lower concentration levels was difficult to recognise and at higher concentration tended to destroy the morphology of the tissue. The DAB product was diffuse and covered large areas around the filaments. Whole processes of Bergmann glia were heavily stained (Fig. 3.8) resulting in excessive hardening of the tissue during processing, therefore rendering the tissue fragile and easily prone to ripping. Additionally the reaction product was not readily found in every section.

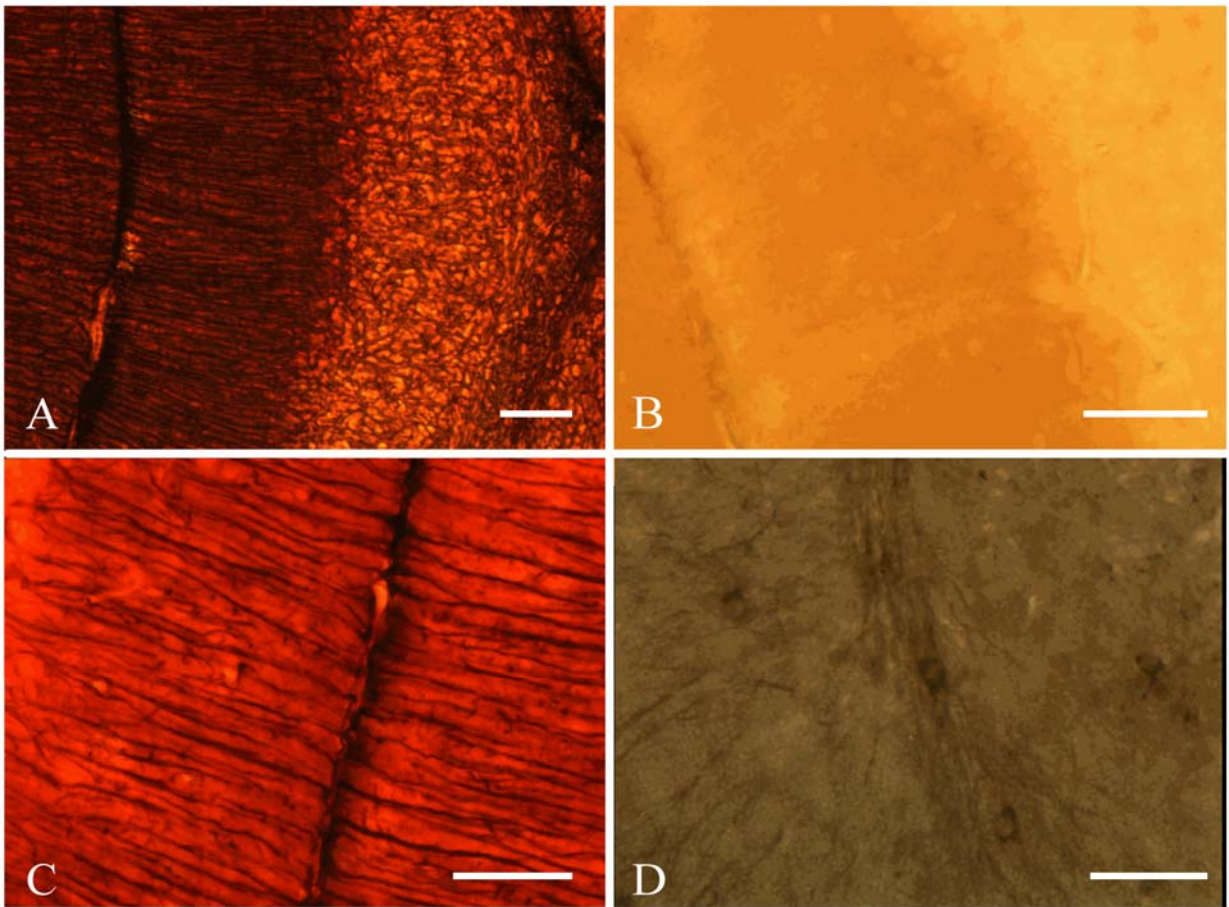


**FIGURE 3.7** Astrocytes and myelinated axons in cerebellar folium, labelled with anti-GFAP or anti-PLP antibodies and stained with an avidin-biotin complex (ABC) at LM resolution.

- A.** Bergmann glia in the molecular layer and protoplasmic astrocytes in the granular layer;
- B.** Negative control section showing unlabelled molecular and granular layer;
- C.** High magnification of Bergmann glia;
- D.** Myelinated axons in cerebellar folium white matter.

Scale bars = 20  $\mu$ m

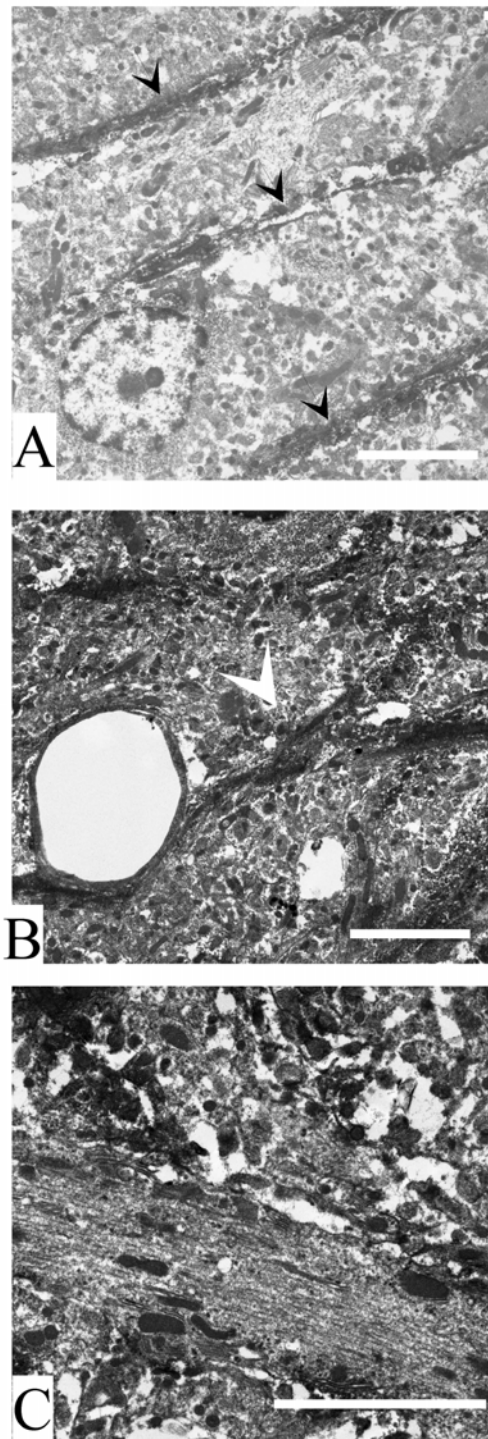


**FIGURE 3.8** Astrocytes in cerebellar folium, labelled with anti-GFAP and stained with an avidin-biotin complex (ABC) at EM resolution.

Three illustrative examples of labelled astrocytes (Bergmann glia) processes (arrows) in the cerebellar molecular layer at different levels of magnification showing morphological disruption of the tissue. The reaction product was difficult to recognise at low concentrations whereas in these examples of higher concentrations tended to destroy the morphology of the tissue. The EM results contrasted with excellent labelling at LM resolution (see figure 3.7).

Scale bars 5 $\mu$ m.

Failure to detect photo-oxidation labelling of EITC at EM level may be due to obscuring the reaction product by contrast staining with uranyl acetate and lead citrate which is needed to view sections in the electron microscope (see section 2.1.7). To determine if this was the case I examined unstained sections after photo-oxidation and EM processing. Sections without contrast staining appear white and translucent in the EM and such sections are difficult to focus on or to see fine details. The JEM CX-100 II transmission electron microscope has 4 different objective lens apertures numbered 1-4 in decreasing order of size, creating higher contrast with decreasing size. Routine viewing takes place with a number 2 objective lens and with this size no labelling was immediately apparent. With the smallest size objective aperture i.e. number 4, I was able to detect very fine lines of dotted reaction product using anti-PLP antibody 226 (Fig.3.9). Only after negatives were scanned into a computer and the pictures further contrast enhanced with Adobe Photoshop software was a confirmation of labelling was possible. Controls were examined in the form of anti-GFAP and anti-PLP antibody AA3 and labelling using the photo-oxidation method confirmed (Fig. 3.10).

The photo-oxidation technique was found to be unsuitable for subcellular differential localisation of PLP/DM20 because of the difficulty in producing a viable EM image of the DAB reaction product. Although the product might be seen and recorded after some manipulations, the possibility of finding specific regions i.e. nodes of Ranvier in unstained sections would be a formidable task. The challenge of labelling myelin trans-membrane proteins requires a technique that produces a reaction product that is larger and has a more specific reaction product than the diffuse DAB reaction product. Together these findings led me to discontinue further research with the photo-oxidation method.

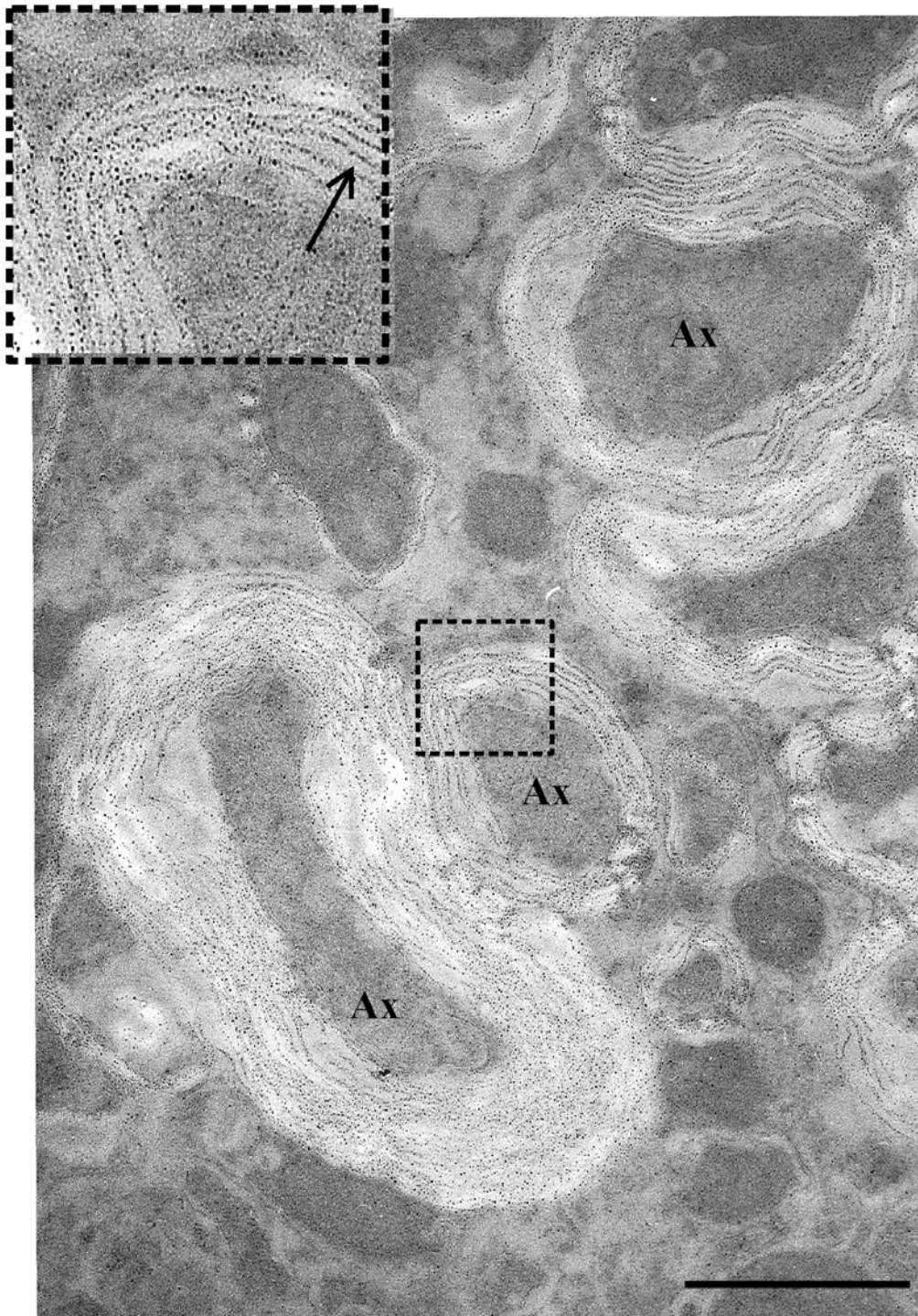


**FIGURE 3.9** Electron micrograph of myelinated axons (Ax) in cerebellar white matter from an adult mouse after photo-oxidation of EITC in the presence of DAB. The EITC was conjugated to a secondary antibody recognising a primary antibody against PLP/DM20. The sections appeared immunolabelled, although the labelling was only detectable when sections without contrast staining for EM and high contrast objective aperture were used. Note the alignment of the reaction product seemingly following myelin membranes. Whether the reaction product was situated on the intraperiod line was not possible to ascertain due to lack of resolution at high magnification. There appear to be an unlabelled membrane (see arrow in inset) possibly the major dense line. Scale bar = 1  $\mu\text{m}$ .

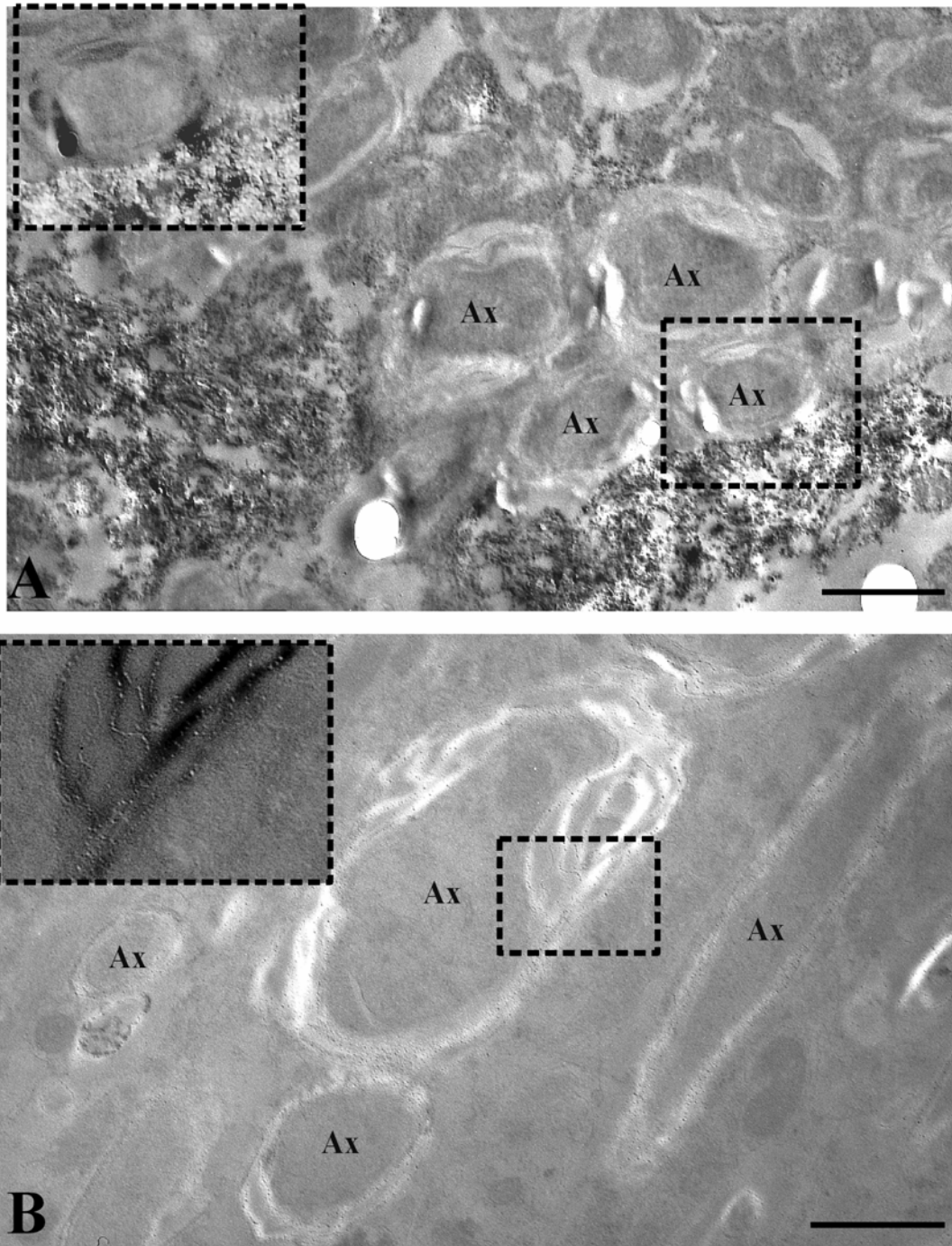


**FIGURE 3.10** Electron micrograph of myelinated axons (Ax) in cerebellar white matter from an adult mouse after photo-oxidation of EITC in the presence of DAB.

**A.** The section was labelled with an anti-GFAP antibody. Note the heavy deposit of reaction product that although covering underlying structure is in concordance with the anatomical localisation of astrocyte processes. Also note the apparent lack of labelling of the myelin around the axons (Ax) (see inset) in contrast to the reaction product in Figure 3.9.

**B.** The section was labelled with a different anti-PLP/DM20 antibody from the antibody used in Figure 3.9. The myelin appear similarly labelled although with a much finer reaction product in concordance with findings at light microscopic level. The inset shows an inverted higher magnification, note the fine lines of product different from the labelling in A.

Scale bars A, B = 1  $\mu$ m

### **3.3 EVALUATION OF IMMUNO GOLD TECHNIQUES**

The immunogold technique was used to evaluate if PLP/DM20 can be labelled at EM level because unlike the photo-oxidation technique the immunogold method produces a specific and distinct reaction product (Fig. 3.11).

#### **3.3.1 PRE- AND POST-EMBEDDING TECHNIQUES**

One pre-embedded and one post-embedded immunogold schedule were performed. For pre-embedded, silver-intensified staining, two wild type mice were perfused with glutaraldehyde (1%) / paraformaldehyde (1%) in phosphate buffer (0.1M). The spinal cord was dissected and left in fixative over night. Vibratome sections were stained as described in detail in section 2.4.4. Formvar coated nickel (Ni) slot grids were obtained and stained.

For the post-embedded method glutaraldehyde (1%) fixed tissue, previously embedded for the photo-oxidation method was used. Formvar coated Ni slot grids were obtained and stained.

In white matter of the spinal cord (with the intrinsic problems connected with the high lipid content) the pre-embedded method yielded no result i.e. few gold particles could be found in the tissue. Due to either long incubation time or the permeabilising technique the morphology of the tissue was unacceptable for my purpose. Therefore, the pre-embedding method was excluded at this stage.

The post-embedded method appeared to have the potential to produce successful labelling of white matter of the spinal cord. However, the specificity of the observed labelling was difficult to evaluate. Most grids had wrinkled tissue or support film (formvar), which promotes staining contamination, and so obscured results. The spread of gold particles were patchy with high background labelling. Nonetheless, the presence of some labelling provided a basis for optimisation of the immunogold method for spinal cord investigation.

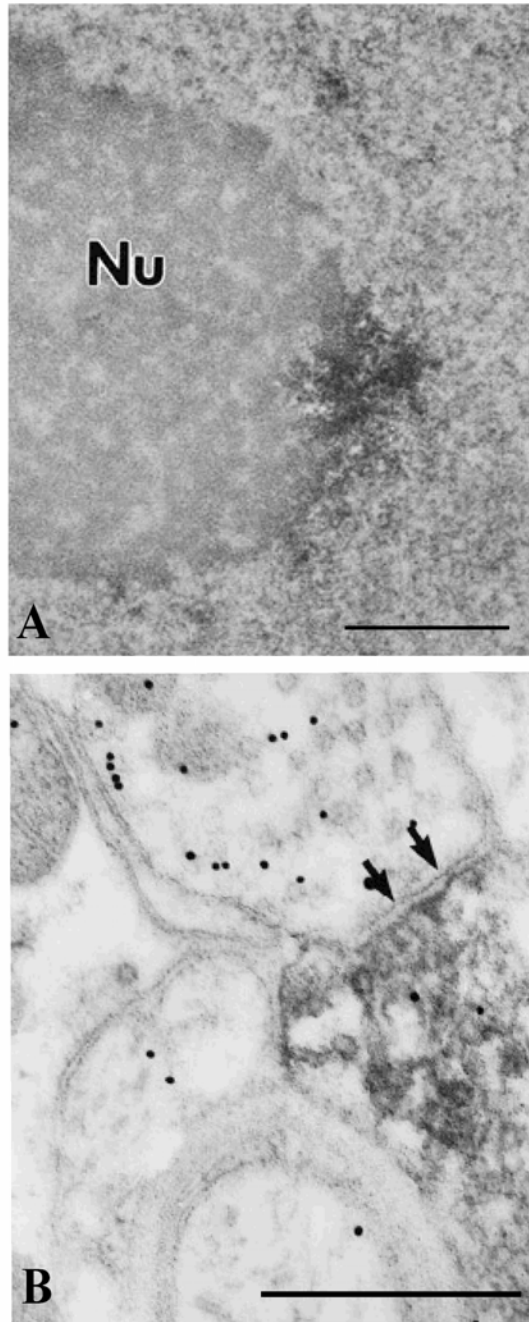


**FIGURE 3.11** Comparison of two different immunocytochemical reaction products.

**A.** Modified electronmicrograph (from Huang et al, 1997) of the reaction product from photo-oxidation of an antibody labelling the perinucleolar compartment in HeLa cells. The photo-oxidation took place in the presence of DAB which was converted to an electron-dense reaction product. Note the diffuse nature of the labelling arranged both inside the nucleolus (Nu) and the nucleoplasm.

**B.** Modified electronmicrograph (from Maxwell et al, 1997) of immunogold reaction product (10-15nm gold particles) used to label glutamate in the bouton of a dorsal horn interneuron. Note the large, smooth electron-dense gold particles of this product compared to the product of DAB in A. Scale bars A = 1  $\mu$ m, B = 50.5  $\mu$ m.

### **3.3.2 IMPROVING QUALITY AND SPECIFICITY OF IMMUNOGOLD LABELLING**

A systematic analysis of constituent elements of the immunogold labelling techniques was undertaken to evaluate the post-embedding method as applied to tissue with high lipid content such as spinal cord white matter. Types of grids were changed to assess if support film was necessary thus avoiding wrinkles. All solutions were filtered to eliminate contamination that can be mistaken for label. Controls were introduced to corroborate specificity of labelling. Three different fixatives were used to evaluate if the strength of signal could be improved. Freeze substitution was employed, which circumvents the initial use of a chemical fixative thus rendering hydrophobic epitopes immobile during processing and more accessible to immunostaining. Lastly the age of animals were varied to determine whether immature and less compact myelin allows greater access to the PLP/DM20 antigen than mature, fully compacted myelin.

#### **MESH GRIDS**

Many EM techniques advocate the use of a support film (formvar, see appendix 5.3.3) for the tissue sections in order to use grids with a larger mesh (see section 2.1.7). This has the advantage of allowing observation of the tissue section either in its entirety or in large segments without grid bars obscuring the view. The disadvantages are that thickness is increased which reduces microscope resolution and wrinkles can be formed both in the film and the tissue. To avoid wrinkles on formvar coated slot grids (see appendix), eliminate contamination and improve labelling, uncoated Ni mesh grids were used (Fig.3.12). The immunolabelling was stronger, possibly due to antibodies reaching the tissue on both sides of the section. However the sections were very unstable in the electron beam due to the low level of fixation and long staining protocol (compared to routine contrast staining for EM sections). Also, longitudinal sections of nervous tissue become physically weak due to the anatomical features of nerves with shearing between the neuropil and the compact, fatty myelin. Too many sections were lost to make this a viable option other than confirm labelling on transverse sections.

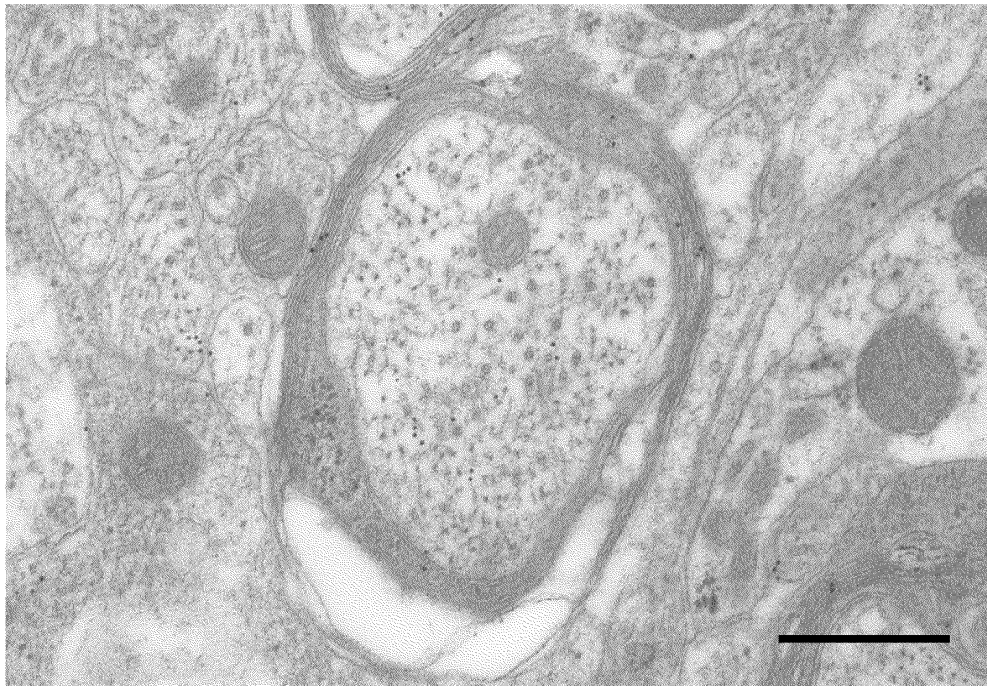
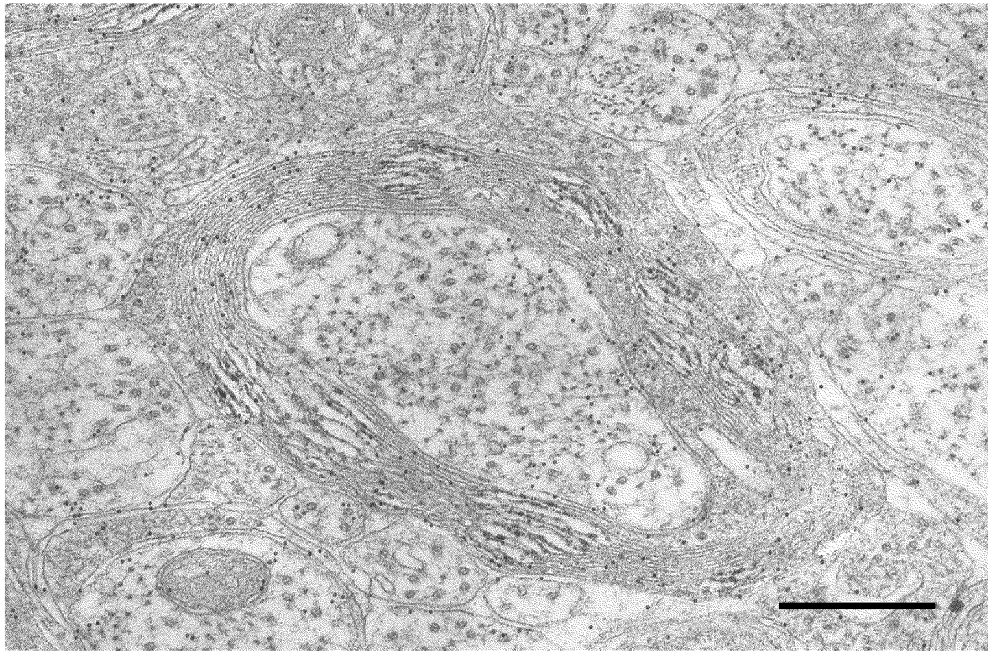


**FIGURE 3.12** Influence of grid type on immunogold labelling.

Electron micrographs of myelinated axons in spinal cord ventral columns. The sections were labeled with a PLP antibody and immunogold stained with a secondary rabbit IgG conjugated to 10nm gold particles.

**A.** Section is carried on an uncoated 300 mesh Ni grid. Note increased label and high background;

**B.** Section is carried on a formvar coated Ni slot grid. Note the lower level of immunogold labeling but with low background compared to that in uncoated grid.

Scale bars. A, B = 0.5 $\mu$ m

## **FILTERING**

Due to the long staining schedule, sections were very prone to pick up foreign material (e.g. dust, impurities in reagents, unconjugated components of IgG sera) in solutions that were amplified by contrast staining with uranyl acetate and lead citrate. Elimination of a large proportion of contamination was achieved by micro filtering all solutions. The rest of the contamination could usually be eliminated as artefacts during observation in the EM because gold particles were perfectly round, dense and smooth whereas the contamination had an irregular or less dense appearance.

## **POSITIVE AND NEGATIVE CONTROLS**

A series of positive and negative controls were employed to assess the immunogold method or specificity of PLP labelling. An antibody against GABA, a neurotransmitter, kindly donated by Prof Maxwell, compatible with the rabbit IgG-coupled gold as a positive control displayed a widespread and intense labelling pattern in the ventral columns of the spinal cord. The utility of GABA immunogold labelling was rejected as a suitable positive control because of its anatomical location (grey rather than white matter) and intensity. A second positive control, the same anti-GFAP as for the photo-oxidation method, was used. The GFAP antibody was confirmed as positively labelling astrocyte cytoplasm (Fig.3.13). The GFAP antibody also provided a negative control since the lack of label in myelin was confirmed. Additional negative controls were added in the form of omission of primary antibody with no other modification of the experimental protocol. These negative controls were almost always devoid of gold particles, as expected, thus confirming that loose particles would not adhere by themselves. Further and more important negative controls were added using tissue from the *Plp1* null mice (Fig.3.13).

## **FIXATION**

Fixation with glutaraldehyde (1%) yielded tentative immunogold labelling of spinal cord myelin and I had already demonstrated this fixation was preferred option for photo-oxidation. Two additional fixatives which had been employed with success in immunogold labelling of CNS tissue, one fixative in grey matter (Li et al, 2001) and one fixative in paranodal loops of white matter myelin (Tait et al, 2000) were investigated.

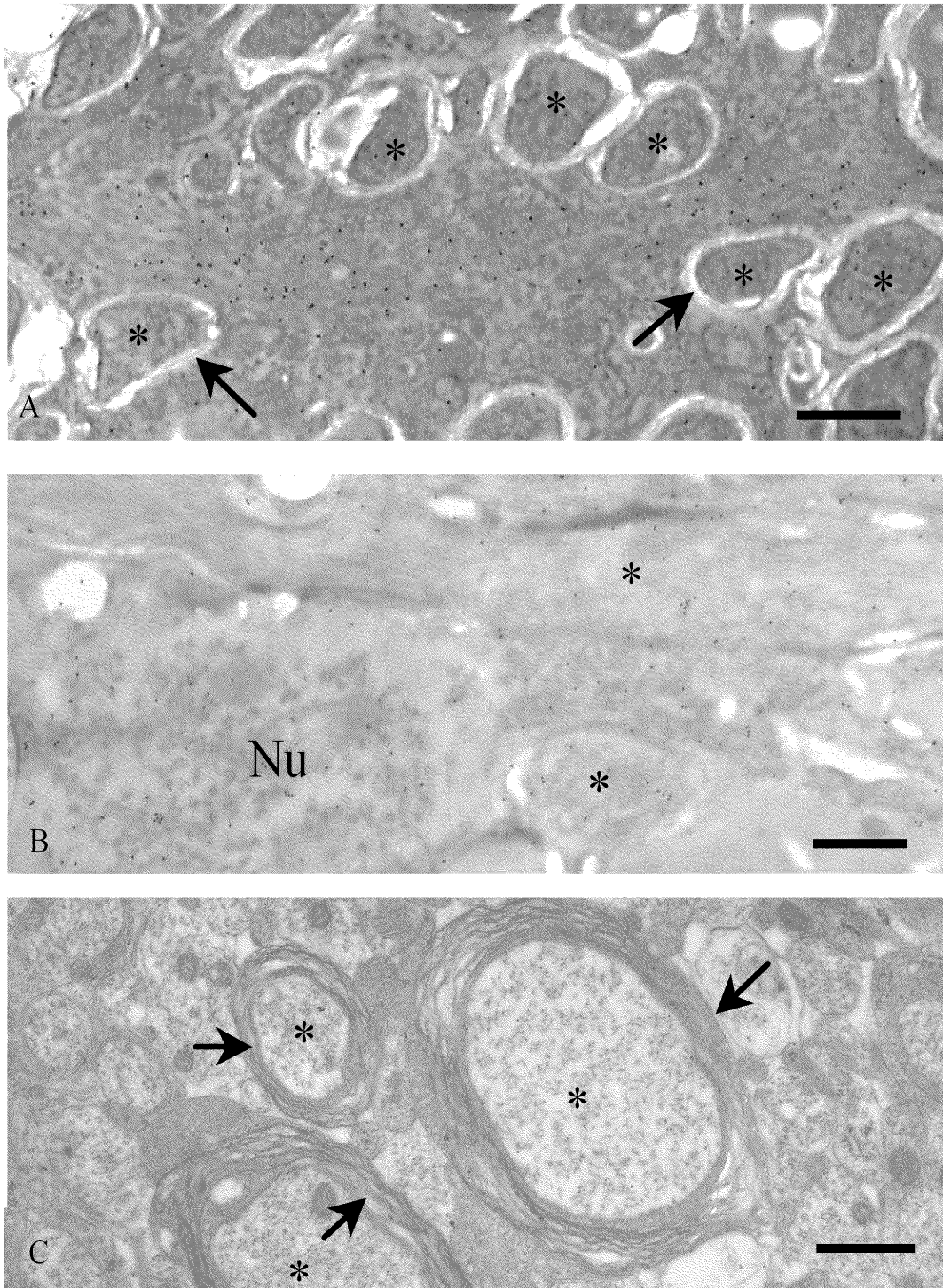


**FIGURE 3.13** Electron micrographs of spinal cord sections, stained with immunogold, and used as positive and negative controls for the antibody PLP 226.

Axons are indicated by asterisks, neuronal nucleus is indicated by Nu.

**A.** Positive control. Shows an antibody (GFAP) labelling intermediate filaments found in astrocytes. Note gold particles following an astrocyte process and lack of labelling in myelin (see arrows);

**B.** Positive control. Shows and antibody (GABA) labelling neurotransmitter substance found in neurons. Note general spread of gold particles and lack of high specificity;

**C.** Negative control. Shows a section of transgenic PLP null tissue stained with the antibody PLP 226. Note the lack of gold particles in myelin (see arrows). Scale bars=1 $\mu$

Three different fixatives were compared; fixative a) glutaraldehyde (1%) and paraformaldehyde (1%) in phosphate buffer (0.1M). This provided a baseline for optimisation. Fixative (b) comprising picric acid (15%), glutaraldehyde (1%) and paraformaldehyde (1%) in phosphate buffer (0.1M), to investigate addition of picric acid and fixative (c) comprising paraformaldehyde (4%) and glutaraldehyde (0.1%) in phosphate buffer (0.1M) to compare a lower concentration of glutaraldehyde.

The results showed that there were no systematic differences in labelling between fixative (b) and fixative (c). There was no systematic improvement in overall utility with either fixative (b) or fixative (c) compared to the reference fixative (a). With fixative (b) and (c), the tissue had a much cleaner background and better labelling than with fixative (a) however the morphological preservation of tissue was inferior than with fixative (a) see Fig 3.14.

### **FREEZE SUBSTITUTION**

Freeze-substitution was used to avoid primary chemical fixation leaving the hydrophobic PLP/DM20 proteins static (frozen) whilst the tissue was dehydrated, secondarily fixed with osmium tetroxide and embedded.

Previous immunogold staining, using chemical fixations (see section 3.3.2), frequently showed gold particles more concentrated in disrupted myelin (Fig.3.15). This pattern could be caused either by a physical artefact or because access to membrane-bound epitopes are increased due to the separation of the myelin lamellae.

The results using freeze-substitution as primary fixation method greatly increased specific labelling. However, axons and surrounding neuropil tended to be ice damaged to various degrees (Fig.3.16).

### **EVALUATION OF GOLD PARTICLES SIZE**

Two different gold particle sizes were used to evaluate if access to the PLP/DM20 protein using the primary antibody PLP226, which targets the intracellular C-terminal, could be improved.

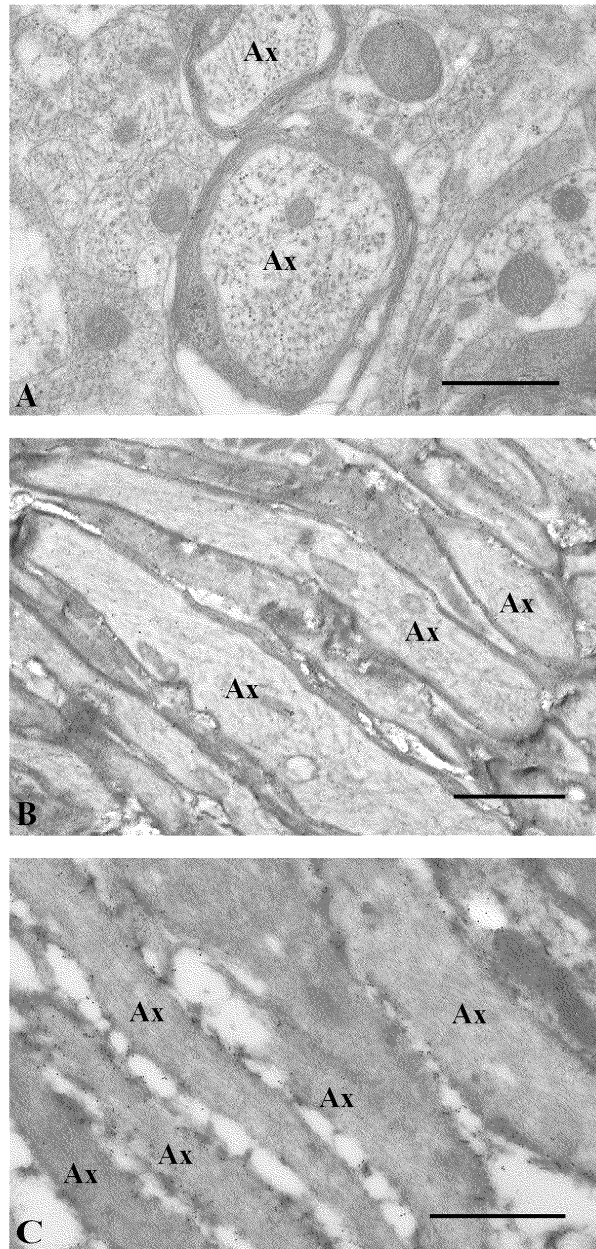


**FIGURE 3.14** Electron micrographs of myelinated axons (Ax) in spinal cord ventral columns displaying the impact of various fixatives.

Sections were labelled with a PLP/DM20 antibody and immunostained with a secondary rabbit IgG conjugated to 10nm gold particles. The immunostaining were used to compare three different fixations, facilitating a comparison for choosing suitable fixation to labelling of myelin. All fixatives were made up in 0.1M phosphate buffer pH 7.4.

**A.** Tissue fixed with glutaraldehyde (1%) and paraformaldehyde (1%)

**B.** Tissue fixed with picric acid (15%) and paraformaldehyde (1%)

**C.** Tissue fixed with glutaraldehyde (0.1%) and paraformaldehyde (4%)

Note the poor preservation of myelin in B and C, clearly inferior to A.

Scalebar A = 0.5 $\mu$ m, B, C = 1 $\mu$ m.

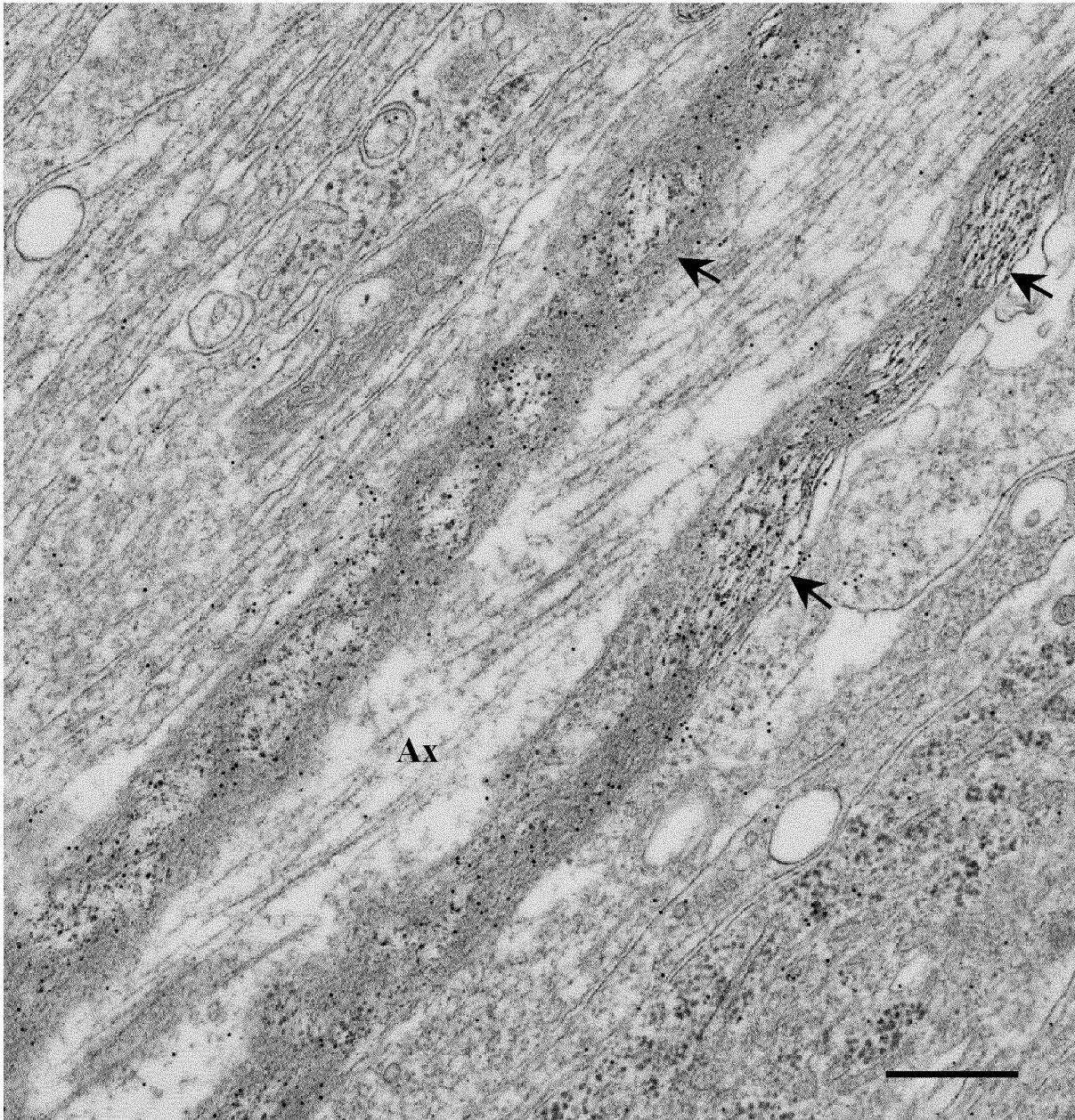


**FIGURE 3.15** Immunogold labelling associated with myelin disruption. Electron micrograph of myelinated axons (Ax) in the spinal cord ventral columns fixed in a glutaraldehyde (1%), paraformaldehyde (4%) solution. The section was labelled with a PLP antibody and immunogold stained with a secondary rabbit IgG conjugated to 10nm gold particles. Note the prevalence for labelling in disrupted myelin (arrows). Scale bar = 0.5 $\mu$ m.

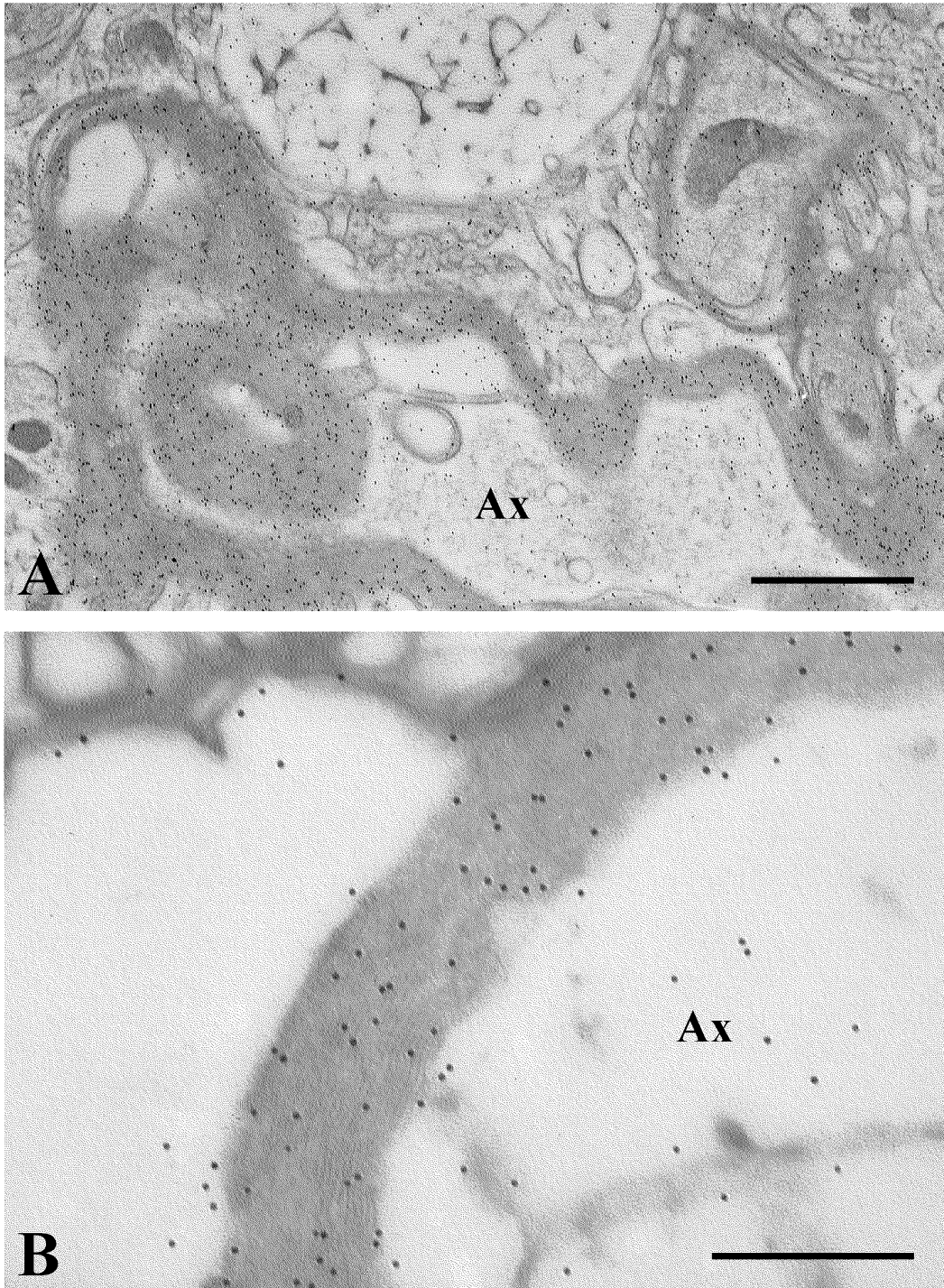


**FIGURE 3.16** Freeze substitution increased specific immunogold labelling. EM micrographs of myelinated axons (Ax) in spinal cord ventral columns using freeze substitution fixation. The sections were labelled with a PLP antibody and immunogold stained with a secondary IgG conjugated to 10nm gold particles. The two illustrative examples shows well labeled myelin with ice damage in the neuropil. Note the lack of ice damage to the myelin and excellent resolution of myelin lamellae. Scale bar A = 1 $\mu$ m, B = 0.3 $\mu$ m.

Medium and small sized gold particles, 10 $\mu$ m and 2 $\mu$ m respectively were used (Fig.3.17).

The 2 $\mu$ m particle was used to increase the penetration of membranes but gave no discernible label. A silver intensification of the applied 2 $\mu$ m particle was used to increase the size resulted in a reaction product that became too large, obscuring true label. The silver intensification method was however important in confirming that the myelin of *Plp1* null mice was not being labelled and could therefore be used as negative control (Fig.3.18). The medium sized gold particle was clearly seen in the EM and was used for the majority of immunostaining.

### **3.3.3 IMMUNOLABELLING OF PLP**

With improved immunogold technique the pre-specified criteria i.e. that the structure of tissue should be preserved and that there should be a differential labelling of myelin to non-myelin tissue, were met to an adequate level for localisation of PLP/DM20, however, not to a standard necessary for a quantitative morphometric study. Assessment was made on 400 grids, 30 immunostainings with 10-15 grids each time. Negative controls in the form of omission of primary antibody, were always included and always negative. Further negative controls were created by the use of PLP null animals. Positive controls were included as anti-GFAP and anti-GABA. Anti-GFAP were included in 11 immunostainings and were positive in 8. Anti-GABA were included in 6 immunostainings but rejected as previously described. Tissue from PLP null animals was included in 16 immunostainings and varied in labelling although the silver enhanced small gold particle preparation showed a convincing lack of PLP label thus confirming that wild type myelin was labelled (Fig.3.18). Assessments were confirmed independently by Dr C Thomson who was in 100 % concordance with my findings. Assessments were made using anti-PLP226 both in mature animals (P17-P20) with PLP at its peak of production, the myelin compacted and well established and young animals (P8-P10) with PLP in its beginning of production and less compacted. Ventral columns in cervical spinal cord which has a dense population of medium to large myelinated axons were used. The labelling was surprisingly low in young animals with a rough estimate of 5-30 gold particles per medium size axon in the transverse plane (Fig.3.19). The axon itself contained approximately between 1-10 gold particles. In mature animals labelling was much higher although background was increased as well, therefore, specific labelling was probably much less than it appeared to be (Fig.3.19).

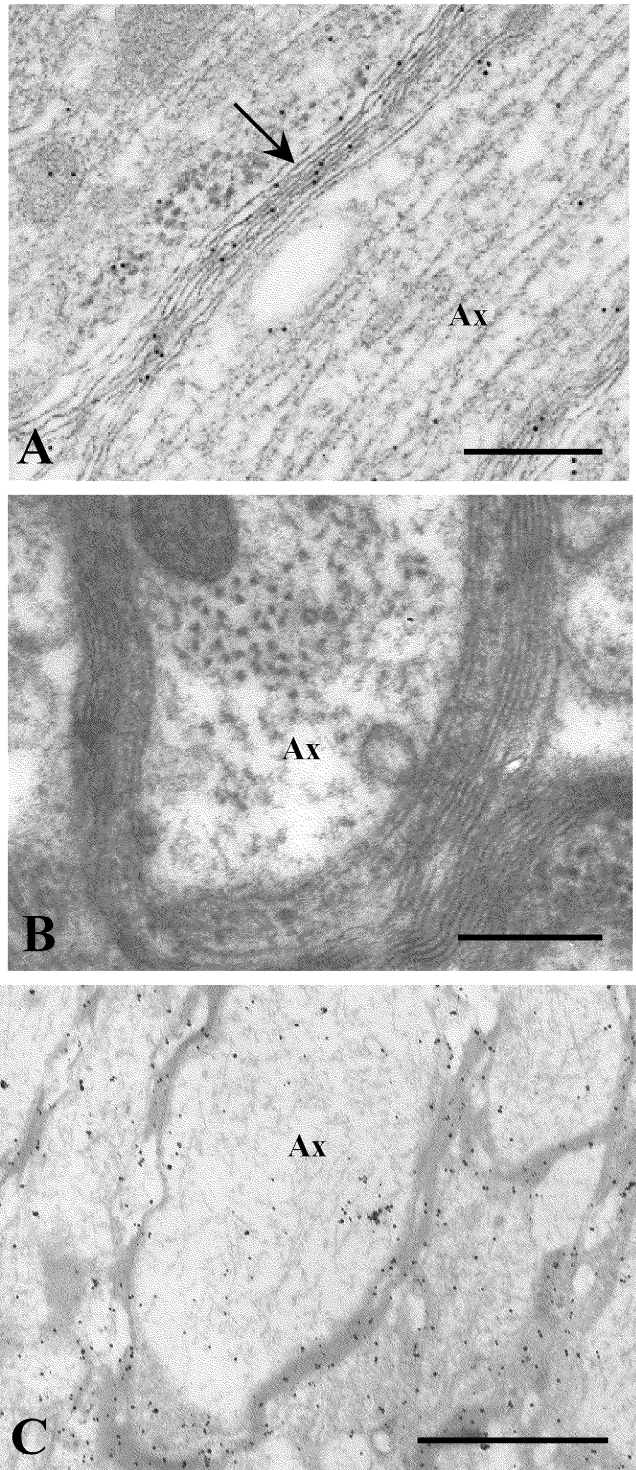


**FIGURE 3.17** Influence of gold particle size on immunolabelling. EM micrographs of myelinated axon (Ax) in spinal cord ventral columns. The sections were labelled with an anti-PLP antibody and immunogold stained with a secondary rabbit IgG conjugated to different sizes of gold particles.

**A.** 10nm goldparticles. Note the well defined labelling with these larger gold particles in the myelin sheath;

**B.** 2nm goldparticles. Note the absence of recognisable labelling;

**C.** 2nm gold particles with silver enhancement Note the high level of specific labelling.

Scalebar A = 0.3 $\mu$ m, B = 0.2 $\mu$ m, C = 1 $\mu$ m

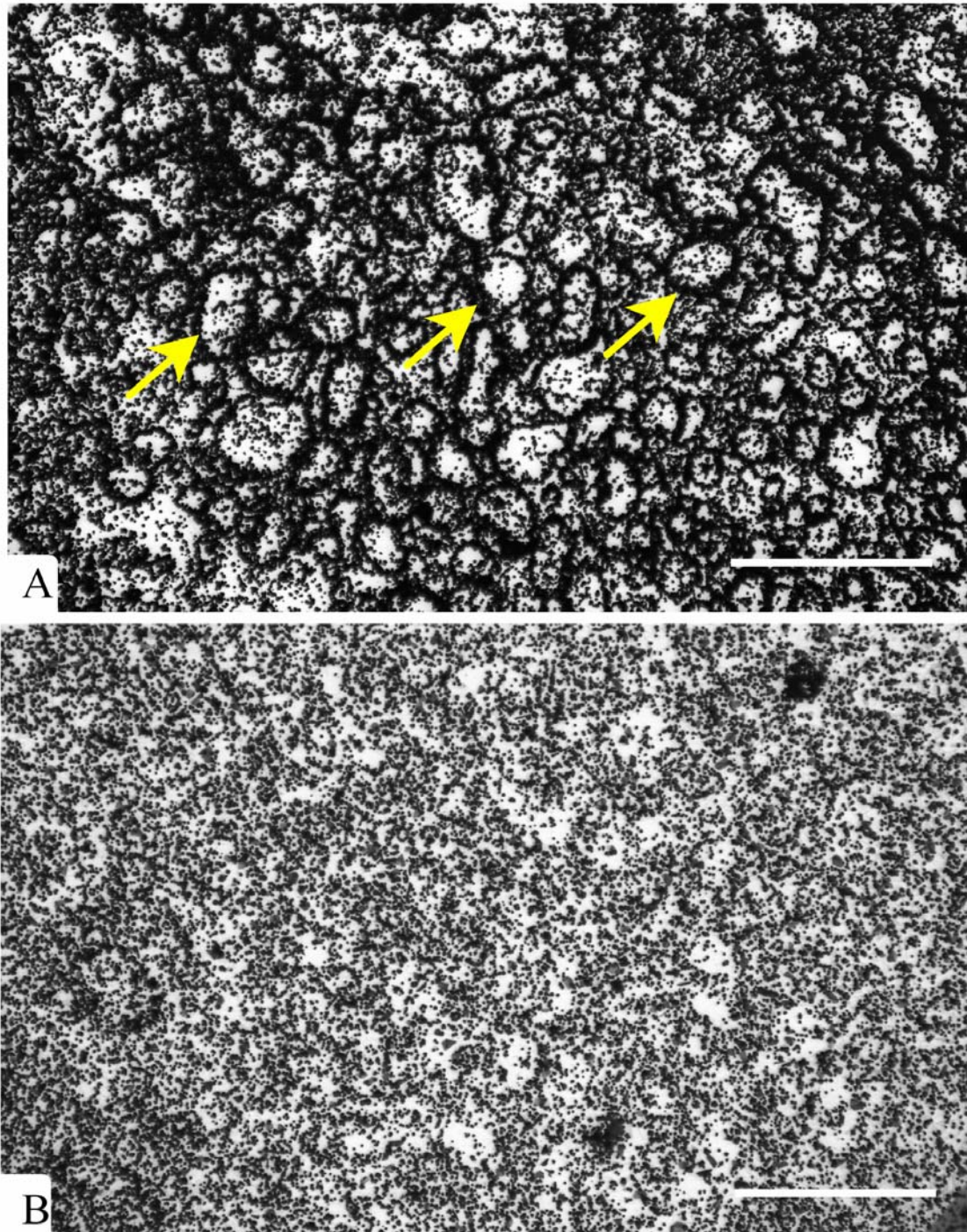


**FIGURE 3.18** Confirmation of immunogold labelling using knockout mice. Electron micrographs of, silver intensified immunogold labelled, central columns in cervical spinal cord sections. Comparison of distribution of immunoreactivity of PLP/DM20 between (A) wild type and (B) *plp*/null mouse. Although high background staining, clearly defined axons can be seen in the wild type tissue (A) see arrows. Scale bars A, B = 10 $\mu$ m.

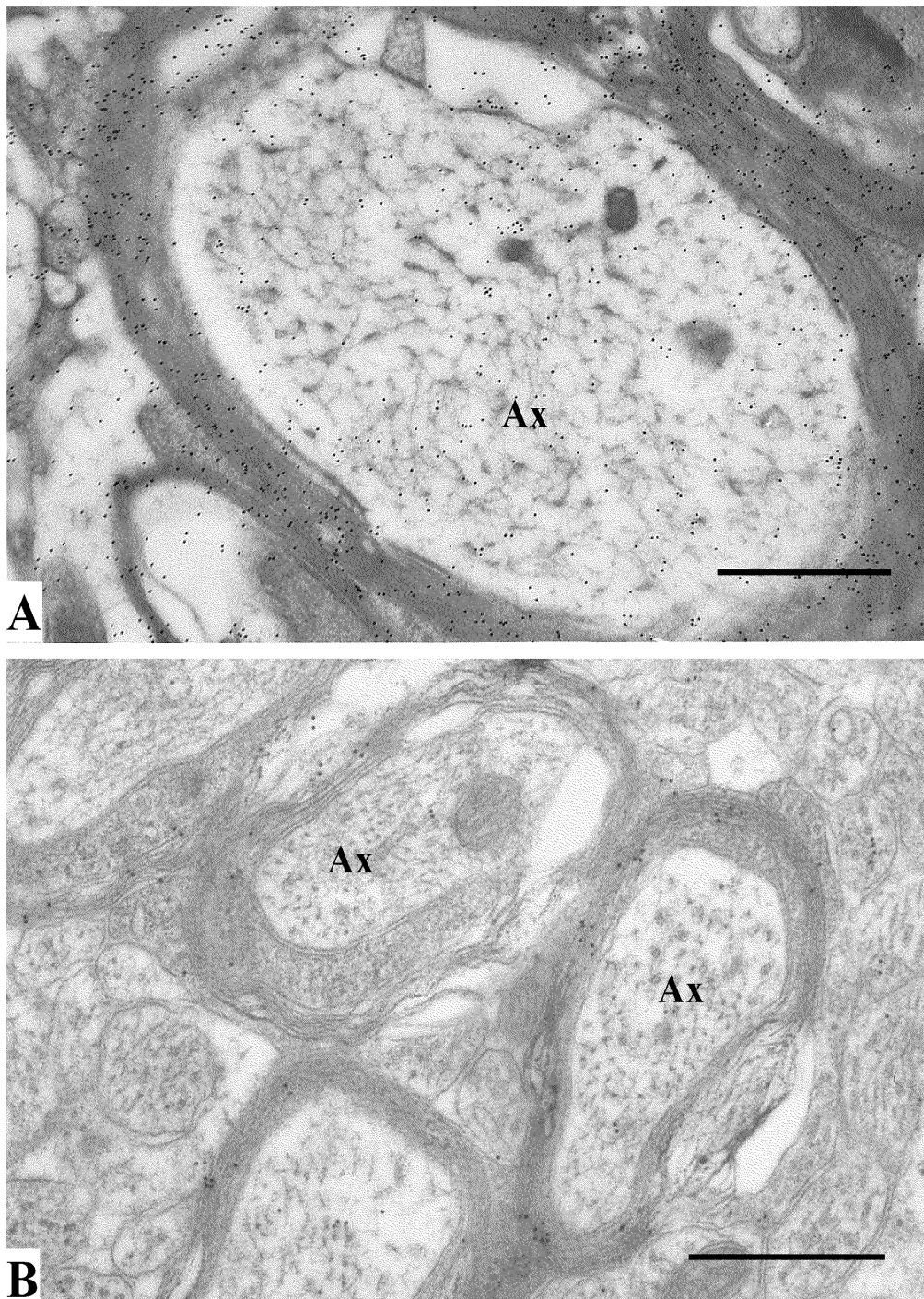


**FIGURE 3.19** Comparison of immunogold labelling of myelin in young and mature animals. Electron micrographs of immunogold stained, anti-PLP labelled myelinated axons (Ax) in spinal cord ventral columns.  
**A.** 20 day old mouse with mature myelin using freeze substituted tissue  
**B.** 8 day old mouse with immature myelin using tissue fixed with glutaraldehyde(1%)/ paraformaldehyde (1%). Note the higher level of staining in mature animals compared to younger animals. Scale bar A, B = 0.5 $\mu$ m.

The labelling was often more concentrated in disrupted myelin, an artefact due to the compromise in choice of fixative. In longitudinal sections the labelling was clearer, particularly if an axon was cut slightly obliquely with myelin lamellae sheared off at one end (Fig.3.20). The gold particles were then denser at the disrupted layers of myelin perhaps through increased access to the antigen. Gold particle distribution was often intermittent and sometimes closely grouped. The low and intermittent phenomenon could perhaps be explained as a difficulty in labelling an amphipathic transmembrane protein with its limiting access to the epitope of interest or the limited amount of epitopes available in a 70nm section. The clumping was almost certainly an artefact, either of the gold conjugate itself (it is not an uncommon problem with gold) or background labelling. Very few paranodal loops were observed since the internodes are comparatively long in the ventral columns; hence, few nodes of Ranvier are present in a 70nm section. The few loops that were observed were always either completely devoid of gold particles or had very few particles sprinkled in the cytoplasm (Fig.3.21).

On 6 occasions, assessment was also made of anti-PLP A, targeting exon 3B which is missing in the DM20 molecule thus specifically reacting with PLP only. Ventral columns in spinal cord sections were used, in mature animals only, together with the freeze substitution method. The need for strong labelling eliminated the use of young animals and the chemical fixation protocols. The results were similar to anti-PLP226 but with a weaker signal therefore making a comparison difficult. For an overview see tables 2& 3.

The decision not to pursue the study further with a morphometric method, suitable for robust quantitative analysis, was taken because the labelling was too weak and the background too high. The staining was also very patchy and varied from staining to staining, although not in itself a problem, making this study too labour intensive, expensive and time-consuming.

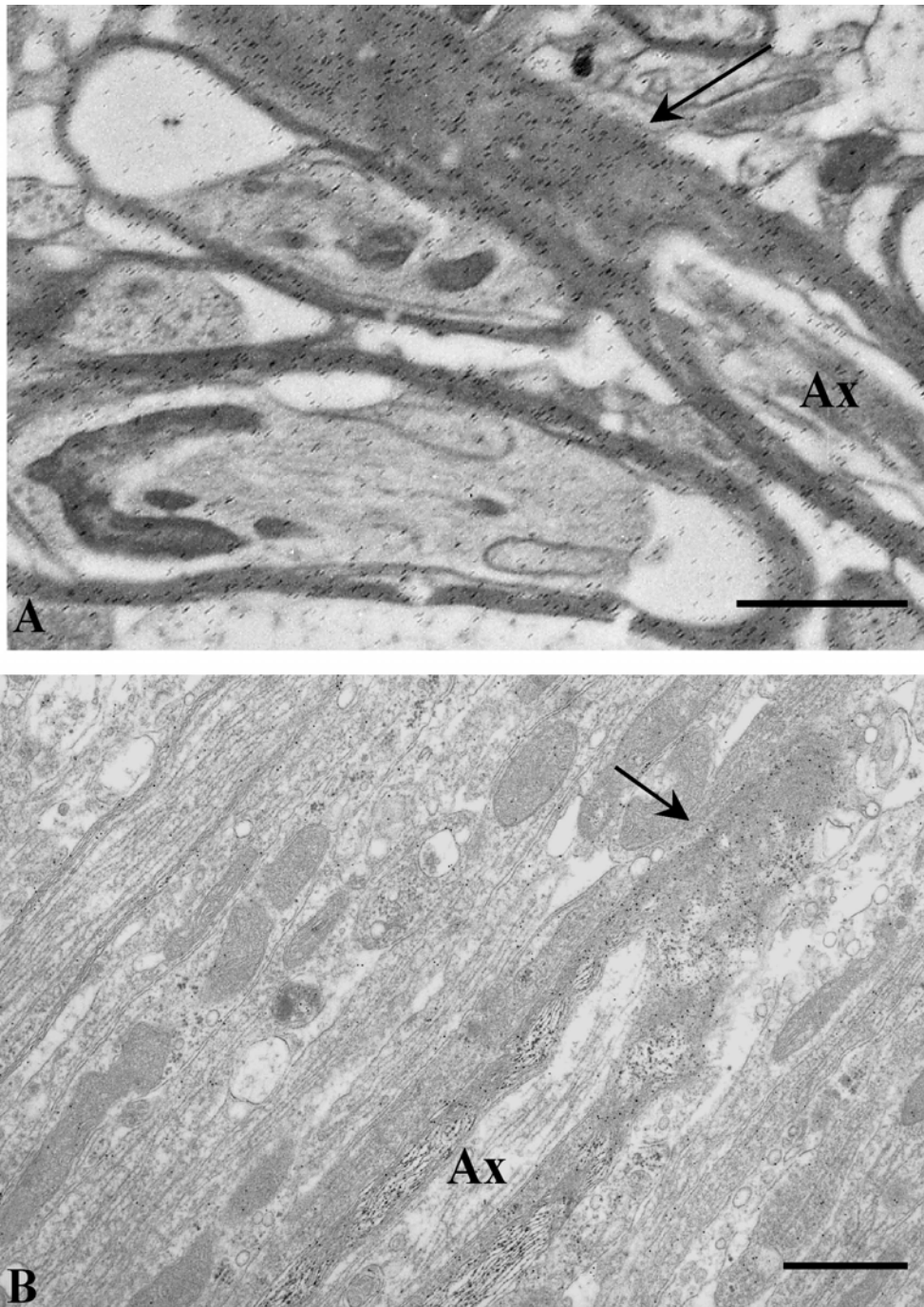


**FIGURE 3.20** Electron micrographs of myelinated axons in spinal cord ventral columns, oblique orientation, displaying level of immunogold labeling. Sections were labelled with an anti-PLP antibody and immunogold stained with a secondary rabbit IgG conjugated to 10 nm gold particles. Note (arrows) increased gold particles in the myelin at oblique end of axons (ax) which confirms the inaccessibility of PLP. Scale bar A, B = 1 $\mu$ m

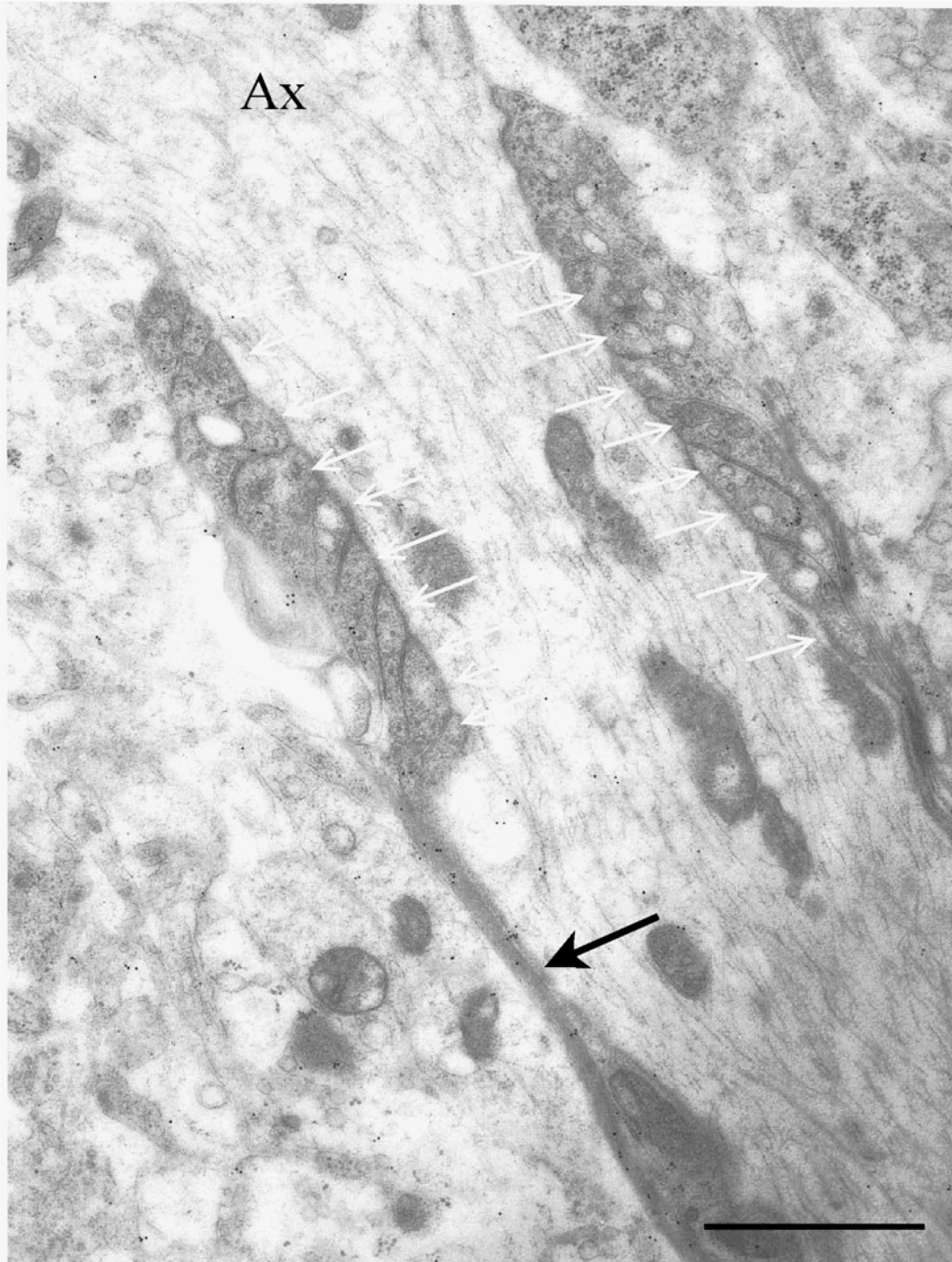


**FIGURE 3.21.** Electron micrograph of paranodal loops at the node of Ranvier displaying level of immunogold labeling in young animals.

The tissue was taken from spinal cord white matter, containing myelinated axons (Ax), of an 8 day old mouse. The section was immunogold stained and labelled with an antibody recognising PLP/DM20. Note the low level of label in both the compact myelin (black arrow) and paranodal loops (white arrows).

Scale bar = 1  $\mu$ m

**TABLE 2 Evaluation of immunogold labelling : Fixation**

Animal Code	Fixative	Age	Type	Label	Background
				PLP226	PLP226
Au 1	picric 15%/1% PF/1% glut/0.1MPB pH7.4	p28	WT	xxx	x
Au2	picric 15%/1%PF/1% glut/0.1MPB pH7.4	p28	WT	xxx	x
Au3	1%PF/1%glut/0,1M PB pH7.4	p28	WT	xxx	xx
Au4	4%PF/5%glut/NaCac pH 7.2	p28	WT	xx	xx
Au5	picric 15%/1% PF/1% glut/0.1M PB pH7.4	p69	KO	x	o
Au6	picric 15%/1% PF/1% glut/0.1M PB pH7.4	p69	WT	xxx	xx
Au7	1%PF/1%glut/0.1M PB pH7.4	p69	KO		
Au8	1%PF/1%glut/0.1M PB pH7.4	p69	WT	xxx	xxx
Au9	4%PF/0.1%glut	p8	WT	xx	o
Au10	1% PF/1%glut/0.1M PB pH7.4	p8	WT	xx	x
Au11	1% PF/1%glut/0.1M PB pH7.4	p11	KO	o	x
Au12	4%PF/0.1%glut	p11	KO		
Au13	1% PF/1%glut/0.1M PB pH7.4	p8	WT	x	x
Au14	4%PF/2.5%glut	p8	WT		
Au15	1%PF/1%glut/0.1M PB pH7.4	p8	WT	xx	o
Au16	1% PF/1%glut/0.1M PB pH7.4	p8	WT	xx	x
Au17	1% PF/1%glut/0.1M PB pH7.4	p8	WT	xx	x
Au18	1% PF/1%glut/0.1M PB pH7.4	p8	WT	xx	xx
Au19	1% PF/1%glut/0.1M PB pH7.4	p8	WT	x	o
Au20	1% PF/1%glut/0.1M PB pH7.4	p8	WT	o	o
Au21	1% PF/1%glut/0.1M PB pH7.4	p8	WT	xx	x

Fixatives : Detailed information on the fixative is to be found in methods sections  
paraformaldehyde (PF), gluteraldehyde (glut), Phosphate buffered saline (PB), sodium Cacodylate (NaCac)

Age: Post natal age (days)

Type: WT : wild type mouse, KO : plp null mouse

Label: The extent of gold particles associated with myelin with anti-PLP antibody (PLP 226)

Background: The extend of gold particles in the neuropil or in axons not associated with myelin

\*\*\* Abundant

\*\* Moderate

\* Few

o none

- not available for retrospective analysis

**TABLE 3**  
**Evaluation of immunogold labelling : Freeze Substitution**

<b>Animals</b>	<b>Processing</b>	<b>Age</b>	<b>Geno- type</b>	<b>Label</b>	<b>Background</b>	<b>Label</b>	<b>Background</b>
				PLP 226	PLP 226	PLP A	PLP A
IG-FS1	Freeze substitution	p20	WT	xxx	x	xx	x
IG-FS2	Freeze substitution	p20	WT	xxx	x	x	x
IG-FS3	Freeze substitution	p21	WT	o	o	o	o
IG-FS4	Freeze substitution	p21	WT	o	o	o	o
A2414	Freeze substitution	p20	WT	xxx	o	xx	x
A2418	Freeze substitution	p20	KO	xx	x	x	x

Processing : Detailed information on the processing is to be found in methods section

Age: Post natal age (days)

Type: WT : wild type mouse

KO : plp null mouse

Label: The extent of gold particles associated with myelin with 2 different antibodies (i.e. PLP226 & PLPA)

Background: The extent of gold particles in the neuropil or in axons not associated with myelin

\*\*\* Abundant

\*\* Moderate

\* Few

o none / poor quality precluding analysis

- not available for retrospective analysis

## CHAPTER 4 DISCUSSION

The aim of this thesis was to evaluate subcellular immunohistochemical techniques for the purpose of studying myelin biology, specifically possible differential localisation of the transmembrane proteins PLP and DM20. Two different types of immunological techniques (photo-oxidation and immunogold) to label PLP and DM20 at the subcellular level were investigated and it is clear that these both techniques have merits but are of limited utility for the study of myelin biology. The two techniques produce quite different patterns of labelling. The first technique (photooxidation) generates a very fine grainy and diffuse product that is too faint when applied to PLP antigen to be visualised at EM level other than in sections not contrast stained. The second technique (immunogold) produces a well-defined electron dense particle that, depending on size, does not reach enough epitopes to produce a measurable result when conventional fixations are used.

There are many problems to overcome when studying myelin. The major challenge is the large amounts of lipid the compact myelin contains which make morphological preservation difficult. Lipids are extracted from the tissue during EM processing therefore requiring a strong fixation. CNS myelin is commonly perfusion fixed with a glutaraldehyde concentration and acts by cross linking protein molecules leaving some free aldehyde groups tissue bound but still reactive. This reactivity creates difficulty when histochemical solutions are introduced by forming non-specific fluorescent products i.e autofluorescence (Baschong et al, 2001). Fluorescence photo-oxidation with eosin as performed by Deerinck et al, 1994 used low levels of glutaraldehyde. Together with the fact that our laboratories had all equipment necessary, ease of use and that the experiment could be verified at LM level, this method was therefore chosen for my project.

The challenge of ensuring adequate ultrastructural preservation of myelin constrained both the investigations of photo-oxidation and immunogold labelling. With high concentrations (e.g. 5%) glutaraldehyde and paraformaldehyde excellent ultrastructure of myelinated fibres is achieved (see Griffiths et al, 1986, Fannaraga et al 1992, Yool et al, 2002, Edgar et al 2008 for published examples of this in my hands). However, high concentrations of fixatives destroy or alter the antigen and successful immunohistochemical labelling has been achieved only with low/very low concentrations of fixative.

Fixatives containing glutaraldehyde at markedly different concentrations were evaluated in this thesis and at concentrations of 1%, the integrity of the myelin was barely adequate (i.e. interperiod lines

were discernible). Concentrations below this level leave CNS tissue very soft and prone to mechanical damage during handling. At microscopic level the tissue is wavy with broken up myelin making it very difficult to find and recognise structures. Being forced to use glutaraldehyde for morphological integrity, autofluorescence then had to be taken into account. To reduce autofluorescence, sodium borohydride was tested and found to make a substantial difference in fluorescence emission (not reported). The background emission was less and specific emission looked much sharper however the reaction when vibratome sections were incubated in sodium borohydride was very violent and broke up or curled the sections. I decided not to pursue this option until the photo-oxidation method was established. Having high background fluorescence was irrelevant at this point, the need to establish labelling was of greater importance.

In the photo-oxidation studies, the minimal success of photo-oxidation analysis of myelin at the ultrastructural level contrasted with the excellent labelling achieved at the level of the light microscope. The limited success of photo-oxidation at the ultrastructural level may be a consequence of either the sub-optimal conjugation of eosin with the secondary antibody or alternatively that the EM sections are too thin to hold enough antigens to be strongly labelled. Conjugating the fluorophore EITC onto the secondary antibody IgG was necessary since these were not commercially available. Three conjugations were performed and confirmed by SDS-PAGE electrophoresis, two with a goat-anti-rabbit IgG and one with a goat-anti-rat IgG. The anti-rabbit IgG conjugations were very successful. Titres for the use of the two anti-rabbit IgG conjugations were independently tested first on oligodendrocyte cultures. Cultures were used because they are readily available in our laboratories, and reduce the unnecessary use of animals. The labelling of PLP in cell culture is excellent (Mitchell et al, 1992; Thomson et al, 2006). The titres were then confirmed on CNS tissue sections. The fluorescent labelling with EITC was estimated by visual inspection as emitting light at approximately 20% of that of FITC which was in concordance with published data (Deerinck et al, 1994). The anti-rat IgG conjugation was performed to be used in conjunction with an alternative primary antibody for labelling PLP/DM20, since the anti-rabbit antibody PLP226 previously used was of limited availability to me. The primary antibody (AA3) used with the anti-rat IgG conjugation displayed a similar labelling to PLP226; staining was fine (i.e. more specific) but signal was weaker.

Photo-oxidation was easily carried out and easily recognised both during and after the procedure (Fig.3.5a & b, Fig.3.6), however the labelling was only apparent in LM sections. Photo-oxidation with the EITC labelled PLP/DM20 failed to reveal any recognisable reaction product during electron microscopic observation in contrast stained sections. A reaction product was only detectable in

sections where contrast staining was omitted and micrographs computer enhanced. Reasons for the faint PLP labelling could be the small amount of epitopes labelled in a thin section i.e. 70nm in an EM section compared to a section labelled for fluorescence microscopy of greater than 10µm.

The avidin-biotin complex technique was used, prior to investigating unstained photo-oxidised sections, to try to establish the EM appearance of the DAB reaction product. Photo-oxidation and DAB produce the same reaction product although it is less specific with photo-oxidation. Again labelling at LM level was excellent but only astrocytes using anti-GFAP were visibly labelled at EM level. When labelling with the ABC technique was strong enough to be seen easily, the morphology of the tissue deteriorated. A possible explanation is that the reaction product becomes very hard compared to the rest of the tissue and is ripped out during sectioning (Buhl et al, 1993). The ABC technique confirmed that the antigen must be heavily labelled to provide a DAB precipitate that can be easily visualised in the EM. If the aim is to identify an antigen, preferably not a membrane bound molecule, and not as in our case to compare the differential labelling of two antibodies, the photo-oxidation or the ABC technique then might be worth pursuing.

The immunogold technique was chosen to evaluate if PLP/DM20 can be labelled at EM level because unlike the photo-oxidation technique the immunogold method produces specific and distinct reaction product. Most published immunogold methods directed at myelin proteins employ protocols which avoid or use very weak concentration of glutaraldehyde (i.e. 0.1%) as fixative together with specialist embedding medium (Gershon et al 1994; Scherer et al, 1995; Hirst et al, 2000; Tait et al, 2000), ultracryostat sectioning (Trapp et al, 1989; McLaurin et al, 1993; Sobel et al, 1994; Yin et al, 1998 and 2006) or freeze fracture replica immunogold labeling (FRIL) (Li et al, 2002; Nagy et al, 2004; Rash et al, 2004). These methods are very successful but they require specialist equipment or expertise which was not available to me. Conventional Durcupan™ embedding medium and glutaraldehyde concentration of 1% for immunogold labelling in CNS tissue are used successfully by Prof. D. Maxwell's group (Maxwell et al, 1995; Maxwell and Ridell, 1999) and he kindly allowed me to learn their method in his laboratory for the possibility of labelling PLP/DM20. One pre- and one post-embedding staining was carried out with the supervision and help of Mr Robert Kerr, a senior technician in Prof Maxwell's laboratory, who is an authority in immunogold techniques as confirmed by co-authorships in published papers (e.g. Maxwell et al, 1997; Pollock et al, 1997; Sutherland et al, 2002). The pre-embedding technique revealed no specific staining of PLP/DM20. The morphological preservation was unacceptable possibly due to the lengthy staining protocol and permeabilising treatment (Yi et al, 2001). Furthermore the risk of cutting away labelled tissue, after

embedding, left this method less attractive for the time being. The decision to concentrate on the post-embedding technique was taken because labelling of PLP/DM20 was present and morphology adequately preserved. Myelin in these first sections from the post-embedding method was labelled although background, non-specific, staining was also present. In order to improve specificity and morphology different approaches were attempted. The formvar coated slot grids used caused wrinkling of the tissue due to surface expansion of the formvar film when sections are picked up and contraction when drying out with sections attached. Uncoated 300 mesh grids were tested and showed improved immunogold labelling possibly because they were immersed during staining allowing solution access on both sides of the grid. The negative effect was that the tissue was prone to breakage in the electron beam possibly due to the comparatively long staining procedure thus being exposed to strenuous handling. The anatomical linear feature of longitudinally sectioned axons is also a weak physical aspect that renders tissue prone to breakage. I therefore decided to sacrifice some resolution and persevere with intermittent wrinkling of sections by using formvar coated slot grids.

Micro-filtering all solutions were also a prudent decision and eliminated some of the contamination. Filtering is practised by Mr R. Kerr during immunostaining but was omitted by me in the beginning due to the fact that normal EM staining does not require filtered solutions. Immunological sera tend to be “dirty” but used widely at LM level. Some potential labelling (at low magnification) could be eliminated as artefact by careful observation at high magnification due to the fact that gold particles are perfectly smooth, round and very dense in contrast to contamination debris which appears irregular, often translucent.

A critical appraisal of the importance of fixation for immunogold labelling was conducted. As mentioned previously, glutaraldehyde is necessary for reasonable preservation of myelin due to its high fat content although some antigenicity is lost (see Eldred et al, 1983). The glutaraldehyde (1%) / paraformaldehyde (1%) fixative, previously used for the photo-oxidation with EITC method, provided the best preservation with the least concentration of glutaraldehyde. Two additional fixatives to compare with the glutaraldehyde (1%) / paraformaldehyde (1%) were tested. Neither picric acid (15%) / glutaraldehyde (1%) / paraformaldehyde (1%) in phosphate buffer (0.1M) (Li et al, 2001), nor paraformaldehyde (4%) / glutaraldehyde (0.1%) in phosphate buffer (0.1M), (Tait et al, 2000) gave satisfactory morphological preservation. The decision to use the original fixative was taken because labelling of tissue using picric acid / glutaraldehyde / paraformaldehyde was only marginally better and the preservation definitely worse. The immunostaining technique after paraformaldehyde (4%) /

glutaraldehyde (0.1%) was very different to the other two approaches; specifically the buffers were different; tannic acid was used as a pre-embedding stain, aldehyde quenching with ammonium chloride was employed, post-immunostaining fixation was achieved with stronger glutaraldehyde and osmium tetroxide. The labelling with paraformaldehyde (4%) / glutaraldehyde (0.1%) was perhaps slightly less but background non-specific staining almost completely eliminated. The major disadvantage of paraformaldehyde (4%) / glutaraldehyde (0.1%) was the very poor preservation of myelin which made this option unacceptable.

Murine myelin production peaks at P20 (Verity and Campagnoni, 1988) and mice for the immunogold study were chosen after this age to ensure full myelination with abundant PLP protein. The disadvantage with mature compact myelin is the large amount of lipid consequently making sufficient fixation a major problem. I therefore decided to use younger animals between the ages P8 and P12. Myelination at this age is very active although myelin is not fully compacted (Mitchell et al, 1992) thus allowing improved fixation and perhaps greater access to the PLP/DM20 protein. These animals showed a clearer picture of immunogold labelling although considerably reduced and sometimes absent. The background staining was surprisingly also reduced. The reason for this is difficult to determine. Perhaps it is an effect of using detergent which is necessary to allow antibody penetration of membranes i.e. reactive membrane debris scattered around the myelin which would be increased in the mature animals where more compact myelin are available. To increase penetration, the detergent (Triton X-100) is commonly used in immunostaining. However the detergent "punches" holes in the membranes therefore destroying morphology. Triton X-100 was reduced to a concentration of 0.1% to facilitate some degree of penetration (Priestley, 1984). The use of medium (10nm) gold particles restrict penetration into the tissue therefore in order to increase labelling a smaller (2nm) gold particle was tested. There was no visible labelling when used by itself, neither on sections contrast stained with uranyl acetate and lead citrate nor unstained sections. Silver intensification of small gold particles has been used successfully for post-embedding staining (see Maxwell and many others) and allows visualisation at EM level. However I found the silver intensification technique very difficult to control. When silver intensification was used, particles became irregular and clumped together which then became difficult to differentiate from artefacts, or too large thus obscuring reaction sites. The smaller gold particle with silver enhancement confirmed that wild type PLP was labelled when compared with *Plp1* null tissue (see Fig.3.18). With more extensive investigations to establish reproducibility, this method could perhaps differentially label PLP and DM20.

When using older animals it was noted that particles often were more concentrated in broken up myelin suggesting that access to the PLP protein could be enhanced. Accessibility to membrane-bound antigens is a notorious problem and there are many different ways of dealing with it, the most common as mentioned before is to use a detergent. Another option is to use freeze substitution in order to avoid initial water based, chemical fixation and embedding procedure that causes epitopes, particularly hydrophobic transmembrane molecules, to curl in on themselves thus preventing antibodies gaining access. Water is substituted for acetone whilst tissue is still frozen leaving membranebound hydrofobic proteins immobile and unable to fold in on themselves during the dehydration. Freeze substitution provided the best immunogold labelling. Mature animals with maximum amount of myelin could be used and displayed intense labelling however neuropil surrounding and axonal tissue within compacted myelin was often disrupted. The reproducibility and difficulty in finding nodes of Ranvier made this method only suitable for identifying antigens and not for a statistical analysis.

### **Concluding comments and future work:**

There are disadvantages with all subcellular immunological techniques. There are numerous publications on the use of subcellular immunological techniques in the CNS though their application to myelin protein is more limited. This provides support for the view that this is a difficult area. It is clear that one has to establish the research objectives for each study and reach compromises in a range of areas such as tissue preservation, antigenic preservation, size of label, specificity of label and accessibility to the antigen. Neurological antigens situated in cell bodies and synapses are readily immunostained using simple immunological techniques. However myelin is an exceptional neurological component and as such require special considerations. These considerations included preservation of morphology without the destruction of antigenic epitopes of the protein of interest. The criteria for immunolabelling (I) The structure of tissue should be preserved (II) There should be differential labelling of myelin to non-myelin tissue were not met fully by any of the methods I looked at. Although I have shown that myelin protein PLP and DM20 can be labelled using simple immunological techniques, differential labelling requires a specific antibody to DM20 alone in order to successfully quantify such a study or the employment of a more sophisticated method i.e. ultracryomicroscopy.

At the outset, the rationale for this thesis was to establish an immunolocalisation technique which would allow the hypothesis to be tested that DM20 is expressed in non-compacted regions of the

myelinating oligodendrocyte, whilst PLP expression is confined to the compact myelin sheath. Thus the extracellular portion of DM20 may position at sites where the oligodendroglial cell is coming into close contact with other cells, specifically the axon, and consequently be involved in axon-glia interaction. There are many differences (mainly the temporal expression pattern and structure) between the two isoforms that lends itself to this theory. DM20 message is expressed prenatally whereas Plp 1 message has only been detected postnatally thus implicating different functions. The slight difference in structure of the two protein isoforms will perhaps affect how the protein behaves i.e. anchors to its specific site again implicating different functions. DM20 lacks exon 3B (encoding amino acid residues 117-129) which is predicted to contain anchoring sites leaving it with one instead of three such sites. Studies with DM20 only expressing animals have shown a breakup of the intraperiod line which might be explained by its weakened anchoring ability. This again suggests that the primary function for DM20 is not to uphold the compaction of myelin and would support the theory that DM20 solely might reside in the paranodal loops which are uncompacted. The paranodal loops play a strong role in axon/glia communication with specialisations such as sodium and potassium channels closely situated in the underlying axon making the paranodes a vital region of the myelin to study. PLP have been immunolocalised to compact myelin, in the CNS, by fluorescence microscopy technology and extracted CNS myelin has been shown to contain both isoforms. The likelihood that both isoforms positions in the compact myelin is generally accepted however without a specific antibody for DM20 alone this is just a hypothesis.

One conclusion from this thesis is the importance of fixation and the constraint imposed on photo-oxidation and immunogold labelling by the need to use high concentrations of gluteraldehyde to preserve integrity of myelin. Although the original hypothesis could not be adequately tested with these immunological techniques to continue investigations of immunogold labelling of myelin, I have obtained support to attend a workshop on the use of ultracryomicroscopy for immunogold at the Max Planck Institute of Experimental Medicine in Göttingen, Germany. Developing proficiency in ultracryomicroscopy (which has been used with success in ultrastructural analysis of myelin) would allow further exploration of differential labelling of PLP and DM20 without the constraints imposed by gluteraldehyde fixation.

While immunogold labelling of myelin in the present thesis met with limited success at the ultrastructural level, immunogold labelling may have other utility in exploring demyelinating diseases.

I am currently collaborating with Prof. Michel Brahic, Department of Microbiology, Stanford University, CA, on a project to label Theiler's murine encephalomyelitis virus (TMEV) using immunogold techniques. TMEV affect neurons in grey matter but more importantly cause persistent infection of white matter, if animals are genetically susceptible, resulting in demyelination. When injected into the eye the virus is transported in axons which are largely unaffected. In contrast to the membrane bound proteins investigated in the present thesis the antibody being used targets epitopes on the surface of the virus and are therefore anticipated to be easier to label.

# CHAPTER 5 APPENDICES

## 5.1 GENERAL SOLUTIONS

### 5.1.1 PHOSPHATE BUFFERED SALINE (PBS)

Sodium chloride	8g
Disodium hydrogen phosphate	1.44g
Potassium dihydrogen phosphate	0.24g
Potassium chloride	0.2g

All ingredients were dissolved in 1litreb of dH<sub>2</sub>O and adjusted to pH 7.4 with 1M HCl.

### 5.1.2 KARNOVSKY'S MODIFIED FIXATIVE

Paraformaldehyde 4%, glutaraldehyde 5%.

Preperation of 500 ml of the fixative:

8% Paraformaldehyde:

20 g of paraformaldehyde was added to 250 ml of dH<sub>2</sub>O and heated to 65°C. A few drops of 1M NaOH was added to clear and solution was allowed to cool.

0.08M Cacodylate buffer:

17.1224g sodium cacodylate was dissolved in a 1 litre of dH<sub>2</sub>O and adjusted to pH 7.2 with .

8% paraformaldehyde	250 ml
25% glutaraldehyde	100 ml
0.08M cacodylate buffer	150 ml
Calcium chloride	250 mg

Liquid ingredients were mixed, calcium choride added and dissolved. The solution was adjusted to pH 7.2, filtered and stored at 4°C.

### 5.1.3 DV BUFFER

0.1% Triton X-100	100 µl
0.2% pig skin gelatine	0.2g

Ingredients were dissolved in 75 ml PBS on a hotplate and made up with PBS to a final volume of 100ml.

### **5.1.4 ISOTONIC CACODYLATE BUFFER**

Sodium cacodylate	16.05g
Sodium chloride	3.8g
Calcium chloride	0.055g
Magnesium chloride	0.102g

All ingredients were dissolved in dH<sub>2</sub>O and made up to final volume of 1 litre and adjusted to pH 7.2.

### **5.1.5. ARALDITE RESIN**

1. Araldite CY212 (resin)	30g
2. Dodecanyl succinic anhydride (hardener)	25.2g
3. 2,4,6-tri-dimethylaminomethyl-phenol (accelerator)	1.2 ml
4. Di-butylphthalate (plasticizer)	0.75 ml

Ingredients 1 and 2 were placed in an oven at 65°C for 10 min. and mixed. Ingredients 3 and 4 were added and stirred until homogenised.

### **5.1.6 METHYLENE BLUE/ AZURE II**

Preparation of 500 ml staining solution

1% Borax:

5g of sodium borate was dissolved in dH<sub>2</sub>O and made up to final volume of 500ml.

5g of Methylene blue and 5g of Azur II was added to a flask, the volume was made up to 500ml with 1% Borax. Solution was stirred, the flask capped and stored at RT. Small amounts of the solution was filtered and used as necessary.

### **5.1.7 REYNOLD'S LEAD CITRATE**

Lead Nitrate 1.33g  
Sodium citrate 1.76g

Each ingredient was dissolved in 15 ml dH<sub>2</sub>O, then combined and shaken vigorously from time to time over a 30 min. period. The solution was cleared with 8ml of 1M NaOH and made up to a final volume of 50 ml with dH<sub>2</sub>O.

## 5.2 SOLUTIONS FOR PHOTO-OXIDATION

### 5.2.1 PHOTO-OXIDATION BUFFER

Triton X-100	0.1ml
Normal goat serum	2g
Bovine serum albumin (fraction V)	2g
Pig skin gelatine	0.2g

Each ingredient was heated and dissolved in 25 ml dH<sub>2</sub>O and combined. 0.3g glycine was added before the solution was further diluted to 200 ml with 0.2 M sodium cacodylate buffer, pH 7.4.

### 5.2.2 SDS-PAGE

12.5% Acrylamide resolver gel:

8.3 mls	acrylamide
5.0 mls	1.5 M Tris pH 8.8
200 µl	10% SDS
150 µl	10% ammonium persulphate
6.4 mls	dH <sub>2</sub> O
10 µl	N,N,N',N'-tetramethyl-ethylenediamine (Temed, Sigma)

4 % Acrylamide stacker gel:

880 µl	acrylamide
1.64 mls	0.5 M Tris pH 6.8
30 µl	10% SDS
75 µl	10 % ammonium persulphate
4 mls	dH <sub>2</sub> O
9 µl	Temed

3X SDS Denaturing Buffer:

187 mM	Tris pH 6.8
6%	SDS
10 %	Glycerol
120 mM	Dithiothreitol (DTT)

10X PAGE running buffer:

30.3 g Tris  
144 g Glycine  
10 g SDS  
Make up to 1 litre

### **5.2.3 POLYETHYLENEAMINE COATED PETRIDISHES**

Stock solution:  
0.1% polyethyleneamine in dH<sub>2</sub>O

A few drops of stock solution was added to the bottom of the specialised MatTek culture Petri dishes, swirled around to coat the whole cut-out circle and left for approximately two minutes before adding dH<sub>2</sub>O to rinse the dish which was then left to air dry for ~ 1 hour

### **5.2.4 DURCUPAN RESIN**

Durcupan ACM™, EMS Catalog # 14040.

Durcupan A:  
Epoxy resin           10 ml  
964 Hardener        10 ml  
964 Accelerator     0.3 – 0.4 ml  
Dibutyl phthalate (2) 0.1 – 0.2 ml

Durcupan B:  
Epoxy resin           10 ml  
964 Hardener        10 ml  
Dibutyl phthalate (2) 0.1 – 0.2 ml

The mixtures were heated to 50°C and stirred on a magnetic stirrer for a minimum of 30 minutes.

## **5.3 SOLUTIONS FOR IMMUNOGOLD**

### **5.3.1 PHOSPHATE BUFFER (PB)**

Stock solutions:  
A. Sodium dihydrogen phosphate (NaH<sub>2</sub>PO<sub>4</sub> · 2H<sub>2</sub>O)       37.44 g/1200 ml

B. Disodium hydrogen ( $\text{Na}_2\text{HPO}_4$  anhydrous) 84.9 g/3000 ml

0.2 M buffer:

Solution A 1120 ml  
Solution B 2880 ml

The solutions were combined and adjusted pH 7.4

The buffer was diluted with other solutions as necessary to 1:1 for a final concentration at 0.1 M.

### **5.3.2 MALEATE BUFFER**

Stock solution 0.2 M:

Maleic acid (Sodium hydrogen maleate) 23.2 g  
Made up to 2 litres with  $\text{dH}_2\text{O}$  and pH to 6.2 with 0.1 M NaOH.

Stock solution was diluted as necessary with other solutions to a final concentration at 0.1 M.

### **5.3.3 FORMVAR COATED GRIDS**

1% stock solution of formvar:

1g of formvar was dissolved in 100ml chloroform and stored in a dark glass bottle at RT in a fume cupboard.

To coat grids:

1. Stock solution was diluted 1:5 or 1:6 with chloroform and filtered.
2. Cleaned glass slides were dipped in the solution, removed slowly and dried vertically.
3. The edges of the slide was scraped with a razor blade and the formvar film floated on to a water surface ( $\text{dH}_2\text{O}$  in a 1000ml beaker). Films with interference colour silver or silver/grey was selected.
4. Slot or 200 mesh nickel grids, pre-cleaned in acetone, were gently placed on the film dull side down using a forceps.
5. The films, loaded with grids, were recovered by placing a piece of Nescofilm™ on top of the film and picked up with a forceps, air-dried and stored in a Petri dish.

### **5.3.4 PHOSPHATE BUFFERED SALINE with TRITON-X 100 (PBST).**

0.1 ml of Triton X-100 was added to 100 ml of PBS (see 5.1.1) and gently heated until dissolved.

### **5.3.5 TRIS BUFFERED SALINE with TRITON-X 100 (TBST)**

Stock solution 0.05M:

Tris(hydroxymehtyl)methylanine	6.05g
NaCl	8.5 g

The ingredients were measured out, combined and dissolved in 750 ml of dH<sub>2</sub>O, adjusted to pH 8.2 with 1 M HCl and kept at 4°C.

0.1 ml of Triton X-100 was added to 100 ml of stock solution and gently heated until dissolv

## **REFERENCES**

- AFZELIUS, B.A. and MAUNSBACH, A.B. Biological ultrastructure research; the first 50 years. *Tissue Cell*, 36, 83-94 (2004).
- AINGER, K., AVOSSA, D., MORGAN, F., HILL, S.J., BARRY, C., BARBARESE, E. and CARSON, J.H. Transport and localisation of exogenous myelin basic protein mRNA microinjected into oligodendrocytes. *J. Cell. Biol.*, 123, 431-441 (1993).
- AINGER, K., AVOSSA, D., DIANA, A.S., BARRY, C., BARBARESE, E. and CARSON, J.H. Transport and localisation elements in myelin basic protein mRNA. *J. Cell. Biol.*, 138, 1077-1087 (1997).
- AL-SAKTAWI, K., McLAUGHLIN, M., KLUGMANN, M., SCHNEIDER, A., BARRIE, J.A., McCULLOCH, M.C., MONTAGUE, P., KIRKHAM, D., NAVE, K.A. and GRIFFITHS, I.R. Genetic background determines phenotypic severity of the Plp rumpshaker mutation. *J. Neurosci. Res.* 72, 12-24 (2003).
- ARVANITIS, D., POLAK, P.E. and SZUCHET, S. Myelin palingenesis. 1. Electron microscopical localisation of myelin/oligodendrocyte proteins in multilamellar structures by the immunogold method. *Dev. Neurosci.*, 14, 313-317 (1992).
- BASCHONG, W., SUETTERLIN, R. and LAENG, R.H. Control of autofluorescence of archival formaldehyde-fixed, paraffin-embedded tissue in confocal laser scanning microscopy (CLSM). *J. Histochem. Cytochem.*, 49, 1565-1572 (2001).
- BAUMANN, N. and PHAM-DINH, D. Biology of oligodendrocyte and myelin in the mammalian central nervous system. *Physiol. Rev.*, 81, 871-927 (2001).
- BAXANDALL, J., PERLMANN, P. and AFZELIUS, B.A. A two-layer technique for detecting surface antigens in the sea urchin egg with ferritin-conjugated antibody. *J. Cell. Biol.*, 14, 144-151 (1962).
- BERRY, M., BUTT, A. M., WILKIN, G. and PERRY, V. H., Structure and function of glia in the central nervous system. In: *Greenfield's Neuropathology*, Eds. David I. Graham and Peter L. Lantos Vol 1, pp. 75-121, 2003
- BIGNAMI, A., ENG, L.F., DAHL, D. and UYEDA, C.T. Localisation of the glial fibrillary acidic protein in astrocytes by immunofluorescence. *Brain Res.*, 43, 429-435 (1972).
- BOISON, D., BÜSSOW, H., D'URSO, D., MÜLLER, H.W. and STOFFEL, W. Adhesive properties of proteolipid proteins are responsible for the compaction of CNS myelin sheaths. *J. Neurosci.*, 15, 5502-5513 (1995).
- BRIGHTMAN, M. W. and PALAY, S. C, The fine structure of ependyma in the brain, *J. Cell Biol.*, 415-439 (1963).
- BUHL, E. H. Intracellular injection in fixed slices in combination with neuroanatomical tracing techniques and electron microscopy to determine multisynaptic pathways in the brain. *Microsc. Res. Tech.*, 24, 15-30 (1993).

- CAMPAGNONI, A.T. Molecular biology of myelin proteins from the central nervous system. *J. Neurochem.*, 51, 1-14 (1988).
- CARNEGIE, P.R. Amino acid sequence of the encephalitogenic basic protein from human myelin. *Biochem. J.*, 123, 57-67 (1971).
- CHAN, W.Y., KOHSAKA, S. and REZAIE, P. The origin and cell lineage of microglia: new concepts. *Brain Res.Rev.*, 53, 344-354 (2007).
- CHOW, E., MOTTAHEDEH, J., PRINS, M., RIDDER, W., NUSINOWITZ, S. and BRONSTEIN, J.M. Disrupted compaction of CNS myelin in an OSP/Claudin-11 and PLP/DM20 double knockout mice. *Mol.Cell.Neurosci.*, 29, 405-413 (2005).
- DEERINCK, T.J., LEVINSON, S.R., BENNETT, G.V. and ELLISMAN, M.H. Clustering of voltage-sensitive sodium channels on axons is independent of direct Schwann cell contact in the dystrophic mouse. *J. Neurosci.*, 17, 5080-5089 (1997).
- DEERINCK, T.J., MARTONE, M.E., LEV-RAM, V., GREEN, D.P., TSIEN, T.Y., SPECTOR, D.L., HUANG, S. and ELLISMAN, M.H. Fluorescence photooxidation with eosin: a method for high resolution immunolocalisation and in situ hybridisation detection for light and electron microscopy. *J. Cell. Biol.*, 126, 901-910 (1994).
- DICKINSON, P.J., FANARRAGA, M.L., GRIFFITHS, I.R., BARRIE, J.M., KYRIAKIDES, E. and MONTAGUE, P. Oligodendrocyte progenitors in the embryonic spinal cord express DM-20. *Neuropathol. Appl. Neurobiol.*, 22, 188-198 (1996).
- DIEHL, J.H., SCHAICH, M., BUDZINSKI, R.M. and STOFFEL, W. Individual exons encode the integral membrane domains of human myelin proteolipid protein. *Proc. Natl. Acad. Sci. USA.*, 83, 9807-9811 (1986).
- EDGAR, J.M., ANDERSON, T.J., DICKINSON, P.J., BARRIE, J.A., McCULLOCH, M.C., NAVE, K.A. and GRIFFITHS, I.R. Survival of, and competition between, oligodendrocytes expressing different alleles of the Plp gene. *J. Cell. Biol.*, 158, 719-729 (2002).
- EDGAR, J.M., McLAUGHLIN, M., BARRIE, J.A., McCULLOCH, M.C., GARBERN, J. and GRIFFITHS, I.R. Age-related axonal and myelin changes in the rumpshaker mutation of the Plp gene. *Acta. Neuropathol.*, 107, 331-335 (2004).
- EDGAR, J.M., McCULLOCH, M.C., THOMSON, C.E. and GRIFFITHS, I.R. Distribution of mitochondria along small-diameter myelinated central nervous system axons. *J. Neurosci. Res.*, 86, 2250-2257 (2008).
- ELDRED, W.D., ZUCKER, C., KARTEN, H.J. and YAZULLA, S. Comparison of fixation and penetration enhancement techniques for use in Ultrastructural immunocytochemistry. *J. Histochem. Cytochem.*, 31, 285-292 (1983).
- ENG, L.F., VANDERHAEGHEN, J.J., BIGNAMI, A. and GERSTI, B. An acidic protein isolated from fibrous astrocytes. *Brain Res.*, 28, 351-354 (1971).

EYLAR, E.H., BROSTOFF, S., HASHIM, G., CACCAM, J. and BURNETT, P. Basic A1 protein of the myelin membrane. The complete amino acid sequence. *J. Biol. Chem.*, 246, 5770-5784 (1971).

FANARRAGA, M.L., GRIFFITHS, I.R., McCULLOCH, M.C., BARRIE, J.A., KENNEDY, P.G. and BROPHY, P.J. Rumpshaker: an X-linked mutation causing hypomyelination: development differences in myelination and glial cells between the optic nerve and spinal cord. *Glia*, 5, 161-170 (1992).

FANARRAGA, M.L., SOMMER, I.U., GRIFFITHS, I.R., MONTAGU, P., GROOME, N.P., NAVE, K.A., SCHNEIDER, A., BROPHY, P.J. and KENNEDY, P.G. Oligodendrocyte development and differentiation in the rumpshaker mutation. *Glia*, 9, 146-156 (1993).

FAULK, W.P. and TAYLOR, G.M. An immunocolloid method for the electron microscope. *Immunochemistry*, 8, 1081-1083 (1971).

FERNANDEZ-MORAN, H. and DAHL, A.O. Electron microscopy of ultrathin frozen sections of pollen grains. *Science*, 116, 465-467 (1952).

FOLCH, J. and LEES, M. Proteolipides, a new type of tissue lipoproteins; their isolation from brain. *J. Biol. Chem.*, 191, 807-817 (1951).

FRAIL, D.E., WEBSTER, H.D. and BRAUN, P.E. Developmental expression of the myelin-associated glycoprotein in the peripheral nervous system is different from that in the central nervous system. *J. Neurochem.*, 45, 1308-1310 (1985).

GARBERN, J., CAMBI, F., SHY, M. and KAMHOLZ, J. The molecular pathogenesis of Pelizaeus-Merzbacher disease. *Arch. Neurol.*, 56, 1210-1214 (1999).

GERSHON, A. A., SHERMAN, D. L., ZHU, Z., GABEL, C. A., AMBRON, R. T., GERSHON, M. D. Intracellular transport of newly synthesized varicella-zoster virus: final envelopment in the *trans*-Golgi network. *J. of Virology*, pp. 6372-6390 (1994).

GRIFFITHS, I.R., DUNCAN, I.D. and McCULLOCH, M. Shaking pups: a disorder of central myelination in the spaniel dog. II. Ultrastructural observations on the white matter of the cervical spinal point. *J. Neurocytol.*, 10, 847-858 (1981).

GRIFFITHS, I.R. and McCULLOCH, M.C. Nerve fibres in spinal cord impact injuries. Part 1. Changes in the myelin sheath during the initial 5 weeks. *J. Neurol. Sci.*, 58, 335-349 (1983).

GRIFFITHS, I.R., KLUGMANN, M., ANDERSON, T., YOOL, D., THOMSON, C., SCHWAB, M.H., SCHNEIDER, A., ZIMMERMAN, F., McCULLOCH, M., NADON, N. and NAVE, K.A. Axonal swellings and degeneration in mice lacking the major proteolipid of myelin. *Science*, 280, 1610-1613 (1998).

GRIFFITHS, I.R., McCULLOCH, M.C. and ABRAHAMS, S. Progressive axonopathy: an inherited neuropathy of boxer dogs. 3. The peripheral axon lesion with special reference to the nerve roots. *J. Neurocytol.*, 15, 109-120 (1986).

- GRIFFITHS, I.R., MONTAGUE, P. and DICKINSON, P. The proteolipid protein gene. *Neuropathol. Appl. Neurobiol.*, 21, 85-96 (1995).
- GRIFFITHS, I.R., SCHNEIDER, A., ANDERSON, J. and NAVE, K.A. Transgenic and natural mouse models of proteolipid protein (PLP)-related dysmyelination and demyelination. *Brain Pathol.*, 5, 275-281 (1995).
- GOW, A., FRIEDRICH, V.L. Jr. and LAZZARINI, R.A. Intracellular transport and sorting of the oligodendrocyte transmembrane proteolipid protein. *J. Neurosci. Res.*, 37, 563-573 (1994).
- HAM, A.W. *Histology Seventh Edition*. J.B. Lippincott Company, 23-64 (1974).
- HAYES, G. M., WOODROOFE, M. N. and CUZNER, M. L. Microglia are the major cell type expressing MHC class II in human white matter. *J. Neurol. Sci.* 80, 25-37 (1987).
- HIRANO, A. and DEMBITZER, H.M. Further studies on the transverse bands. *J. Neurocytol.*, 11, 861-866 (1982).
- HIRST, E. M., JOHNSON, T. C., LI, Y., RAISMAN, G. Improved post-embedding immunocytochemistry of myelinated nervous tissue for electron microscopy. *J. Neurosci. Methods* 95, 151-158 (2000).
- HONG, Y.I., LEUNISSEN, J.L.M., SHI, G-M., GUTEKUNST, C-A. and HERSCH, S.M. A novel procedure for pre embedding double immunogold-silver labelling at the Ultrastructural level. *J. Histochem. Cytochem.*, 49, 279-284 (2001).
- HSU, S.M., RAINE, L. and FANGER, H. The use of antiavidin antibody and avidin-biotin-peroxidase complex in immunoperoxidase technics. *Am. J. Clin. Pathol.*, 75, 816-821 (1981).
- HSU, S.M., RAINE, L. and FANGER, H. Use of avidin-biotin-peroxidase complex (ABC) in immunoperoxidase techniques: a comparison between ABC and unlabeled antibody (PAP) procedures. *J. Histochem. Cytochem.*, 29, 577-580 (1981).
- HUANG, S., DEERINCK, T.J., ELLISMAN, M. H. and SPECTOR, D.L. The dynamic organization of the perinucleolar compartment in the cell nucleus. *J. Cell Biol.* 137, 965-74 (1997).
- IP C. W., KRONER, A., BENDSZUS, M., LEDER, C., KOBAR, I., FISCHER, S., WIENDL, H., NAVE, K.A. and MARTINI, R. Immune cells contribute to myelin degeneration and axonopathic changes in mice overexpressing proteolipid protein in oligodendrocytes. *J. Neurosci.*, 26, 8206-8216 (2006).
- IP C. W., KRONER, A., CROCKER, P.R., NAVE, K.A. And MARTINI, R.S. Sialoadhesin deficiency ameliorates myelin degeneration and axonopathic changes in the CNS of PLP overexpressing mice. *Neurobiology of Disease*, 25, 105-111 (2006).
- JUNG, M., SOMMER, I., SCHACHNER, M. and NAVE, K.A. Monoclonal antibody O10 defines a conformationally sensitive cell-surface epitope of proteolipid protein (PLP): evidence that PLP misfolding underlies dysmyelination in mutant mice. *J. Neurosci.*, 16, 7920-7929 (1996).

- KARASEK, M., SWILTOSLAWSKI, J. and ZIELINISKA, A. Ultrastructure of the central nervous system: the basics. *Folia Neuropathol.*, 42, 1-9 (2004).
- KIRSCHNER, D.A. and BLAUROCK, A.E. Organisation, phylogenetic variations and dynamic transitions of myelin. In: *Myelin: Biology and Chemistry* (Ed. R.E. Martenson), Boca Raton, FL: CRC Press, pp. 413-448 (1991).
- KLUGMANN, M., SCHWAB, M.H., PÜHLHOFER, A., SCHNEIDER, A., ZIMMERMAN, F., GRIFFITHS, I.R. and NAVE, K.A. Assembly of CNS myelin in the absence of proteolipid protein. *Neuron*, 18, 59-70 (1997).
- LAPPE-SIEFKE, C., GOEBBELS, S., GRAVEL, M., NICKSCH, E., LEE, J., BRAIN, P.E., GRIFFITHS, I.R. and NAVE, K.A. Disruption of *Cnp1* uncouples oligodendroglial functions in axonal support and myelination. *Nat. Genet.*, 33, 327-328 (2003).
- LAWSON, L. J. Quantification of the mononuclear phagocyte response to Wallerian degeneration of the optic nerve. *J. Neurocytol.*, 23, 729-744 (1994).
- LAWSON, L.J., PERRY, V. H., DRI, P. and GORDON, S. H. Heterogeneity in the distribution and morphology of microglia in the normal adult mouse brain. *Neuroscience* 39, 151-17- (1990)
- LEES, M.B., CHAO, B.H., LIN, L.F., SAMIULLAH, M. and LAURSEN, R.A. Amino acid sequence of bovine white matter proteolipid. *Arch. Biochem. Biophys.*, 226, 643-656 (1983).
- LI, C., TROPAK, M.B., GERAL, R., CLAPOFF, S., ABRAMOW-NEWERLY, W., TRAPP, B., PETERSON, A. and RODER, J. Myelination in the absence of myelin-associated glycoprotein. *Nature*, 369, 747-750 (1994).
- LI, J-L, SHIGEMOTO, R., KULIK, A., CHEN, P., NOMURA, S., KANEKO T., and MIZUNO, N. Immunocytochemical localization of GABA $\beta$  receptors in mesencephalic trigeminal nucleus neurons in the rat. *Neuroscience Letters* 315, 93-97 (2001).
- LI, X., LYNN, B. D., OLSON, C., MEIER, C., DAVIDSON, K. G., YASUMURA, T., RASH, J.E., NAGY, J. I. Connexin29 expression, immunocytochemistry and freeze-fracture replica immunogold labelling (FRIL) in sciatic nerve. *Eur. J. Neurosci.*, 16, 795-806 (2002).
- MAXWELL, D.J., KERR, R., JANKOWSKA, E. and RIDDELL, J.S. Synaptic connections of dorsal horn group II spinal interneurons: synapses formed with the interneurons and by their axon collaterals. *J. Comp. Neurol.*, 380, 51-69 (1997).
- MAXWELL, D.J., OTTERSEN, O.P. and STORM-MATHISEN, J. Synaptic organisation of excitatory and inhibitory boutons associated with spinal neurons which project through the dorsal columns of the cat. *Brain Res.*, 676, 103-112 (1995).
- MAXWELL, D.J. and RIDDELL, J.S. Axoaxonic synapses on terminals of group II muscle spindle afferent axons in the spinal cord of the cat. *Eur. J. Neurosci.*, 11, 2151-2159 (1999).

- MACKLIN, W.B., CAMPAGNONI, C.W., DEININGER, P.L. and GARDINIER, M.V. Structure and expression of the mouse myelin proteolipid protein gene. *J. Neurosci. Res.*, 18, 383-394 (1987).
- McLAURIN, J., ACKERLEY, C.A. and MOSCARELLO, M.A. Localisation of basic proteins in human myelin. *J. Neurosci. Res.*, 35, 618-628 (1993).
- McMAHON, C.D., CHAPIN, L.T., LOOKINGLAND, K.J., RADCLIFF, R.P. and TUCKER, H.A. Feeding reduces activity of growth hormone-releasing hormone and somatostatin neurons. *Proc. Soc. Exp. Biol. Med.*, 223, 210-217 (2000).
- MITCHELL, L.S., GILLESPIE, S.C., McALLISTER, F., FANARRAGA, M.L., KIRKHAM, D., KELLY, B., BROPHY, P.J., GRIFFITHS, I.R., MONTAGUE, P. and KENNEDY, P.G. Developmental expression of major myelin protein genes in the CNS of X-linked hypomyelinating mutant rumpshaker. *J. Neurosci. Res.*, 33, 205-217 (1992).
- MITTELBRONN, M., DIETZ, K., SCHLUESENER, H.J. and MEYERMANN, R. Local distribution of microglia in the normal adult human central nervous system differs by up to one order of magnitude. *Acta Neuropathol.*, 101, 249-255 (2001).
- MONTAG, D., GIESE, K.P., BARTSCH, U., MARTINI, R., LANG, Y., BLÜTHMANN, H., KARTHIGASAN, J., KIRSCHNER, D.A., WINTERGERST, E.S., NAVE, K.A., ZIELASEK, J., TOYKA, K.V., LIPP, H.P. and SCHACHNER, M. Mice deficient for the myelin-associated glycoprotein show subtle abnormalities in myelin. *Neuron*, 13, 229-246 (1994).
- MORI, S. and LEBLOND, C.P. Identification of microglia in light and electron microscopy. *J. Comp. Neurol.* 135, 57-80 (1969).
- MORI, S. and LEBLOND, C.P. Electron microscopic identification of three classes of oligodendrocytes and a preliminary study of their proliferative activity in the corpus callosum of young rats. *J. Comp. Neurol.*, 139, 1-28 (1970).
- MUGNAINI, E. and WALBERG, F. Ultrastructure of neuroglia. *Ergeb. Anat. Entwicklungsgesch.* 37, 194-236 (1964).
- NAGY, J. I., DUDEK, F. E. and RASH, J.E. Update on connexins and gap junctions in neurons and glia in the mammalian nervous system. *Brain Res. Rev.*, 47, 191-215 (2004).
- NAVE, K.A., LAI, C., BLOOM, F.E. and MILNER, R.J. Splice site selection in the proteolipid protein (PLP) gene transcript and primary structure of the DM-20 protein of central nervous system myelin. *Proc. Natl. Acad. Sci. USA*, 84, 5665-5669 (1987).
- NAVE, K. A. and GRIFFITHS, I. R. Models of Pelizaeus-Merzbacher disease. *Myelin biology and disorders*, (Eds. R. A. Lazzarini, J. W. Griffin, H. Lassmann, K.-A. Nave, R. H. Miller, B. D. Trapp) Amsterdam: Elsevier, pp. 1125-1142 (2004).
- NAIT-OUMESMAR, B., PICARD-RIÉRA, N., KERNINON, C. and BARON-VAN EVERCOOREN, A. The role of SVZ-derived neural precursors in demyelinating diseases: from animal models to multiple sclerosis. *J. Neurol. Sci.*, 15, 26-31 (2008).

- OLAVE, M., PURI, N., KERR, R., MAXWELL, D. Myelinated and unmyelinated primary afferent axons form contacts with cholinergic interneurons in the spinal dorsal horn. *Exp. Brain Res.*, 145, 448-56. (2002).
- PEKNY, M. and NILSSON, M., Astrocyte activation and reactive gliosis. *Glia* 50, 427-434 (2005).
- PAN, B., FROMHOLT, S.E., HESS, E.J., CRAWFORD, T.O., GRIFFIN, J.W., SHEIKH, K.A. and SCHNAAR, R.L. Myelin-associated glycoprotein and complementary axonal ligands, gangliosides, mediate axon stability in the CNS and PNS: neuropathology and behavioural deficits in single- and double-null mice. *Exp. Neurol.*, 195, 208-217 (2005).
- PANNESE, E. *Neurocytology; Fine Structure of Neurons, Nerve Processes and Neuroglial Cells*, Thieme, 156-169, 1994.
- PEKNY, M. and NILSSON, M. Astrocyte activation and reactive gliosis. *Glia*, 50, 427-434 (2005).
- PERRY, V.H., BELL, M.D., BROWN, H. C. and MATYSZAK, M. K. Inflammation in the nervous system. *Curr. Opin. Neurobiol.*, 5, 636-641 (1995).
- PERRY, V. H., CUNNINGHAM, C. and HOLMES, C. Systemic infections and inflammation affect chronic neurodegeneration. *Nat. Rev. Immunol.*, 7, 161-167 (2007).
- PETERS, A. Morphology of axons of the CNS. In: *The Fine Structure of the Nervous System: The Neurons and Supporting Cells*, (Eds. Peters, A., Palay, S.L. and Webster, H.D.), W.B. Saunders, Philadelphia, pp.141-186 (1976).
- POLLOCK, R., KERR, R. and MAXWELL, D.J. An immunocytochemical investigation of the relationship between substance P and the neurokinin-1 receptor in the lateral horn of the rat thoracic spinal cord. *Brain Res.*, 777, 22-30 (1997).
- POPOT, J.L., PHAM DINH, D. and DAUTIGNY, A. Major myelin proteolipid: the 4-alpha-helix topology. *J. Membr. Biol.*, 120, 233-246 (1991).
- PRIESTLEY, J.V. Pre-embedding ultrastructural immunocytochemistry : immunoenzyme techniques. In: *Immunolabelling for Electron Microscopy*. Eds. Polak/Varndell, pp.37-52 (1984).
- PRIVAT, A., GIMENEZ-RIBOTTA, M. and RIDET, J-L. Morphology of astrocytes. In: *Neuroglia*, (Eds. H. Kettenmann and B.R. Ransom), Oxford University Press, Oxford/New York, pp. 3-22 (1995).
- PRIVAT, A., JACQUE, C., BOURRE, J., DUPOUEY, P. and BAUMANN, N. Absence of the major dense line in myelin of the mutant mouse "shiverer". *Neurosci. Lett.*, 12, 107-112 (1979).
- RAFF, M.C., MILLER, R.H. and NOBLE, M. A glial progenitor cell that develops in vitro into an astrocyte or an oligodendrocyte depending on culture medium. *Nature*, 303, 390-396 (1983).
- RAINE, C.S. *Neurocellular Anatomy in Basic Neurochemistry*, 5<sup>th</sup> edition, (Eds. G.J. Siegel, B.W. Agranoff, R.W. Albers and P.B. Molinoff), Raven Press, New York, pp. 3-32 (1994).

- RASH, J.E., DAVIDSON, K.G., YASUMURA, T. and FURMAN, C.S. Freeze-fracture and immunogold analysis of aquaporin-4 (AQP4) square arrays, with models of AQP4 lattice assembly. *Neuroscience*, 129, 915-934 (2004).
- ROACH, A., TAKAHASHI, N., PRAVTCHEVA, D., RUDDLE, F. and HOOD, L. Chromosomal mapping of mouse myelin basic protein gene and structure and transcription of the partially deleted gene in shiverer mutant mice. *Cell*, 42, 149-155 (1985).
- ROMANKO, M. J., ROLA, R., FIKE, J. R., SZELE, F. G., DIZON, M. L., FELLING, R. J., BRAZEL, C. Y. and LEVISON, S. W. Roles of the mammalian subventricular zone in cell replacement after brain injury. *Prog. Neurobiol.*, 74, 77-99. (2004).
- ROSENBLUTH, J. A brief history of myelinated nerve fibers: one hundred and fifty years of controversy. *J. Neurocytol.*, 28, 251-262 (1999).
- SALZER, J.L., HOLMES, W.P. and COLMAN, D.R. The amino acid sequences of the myelin-associated glycoproteins: homology to the immunoglobulin gene superfamily. *J. Cell. Biol.*, 104, 957-965 (1987).
- SEKIRNJAK, C., MARTONE, M.E., WEISER, M., DEERINCK, T., BUENO, E., RUDY, B. and ELLISMAN, M. Subcellular localisation of the K<sup>+</sup> channel subunit Kv3.1b in selected rat CNS neurons. *Brain Res.*, 766, 173-187 (1997).
- SCHERER, S.S., XU, Y., BANNERMAN, P.G.C., SHERMAN, D.L. and BROPHY, P.J. Periaxin expression in myelinating Schwann cells: modulation by axon-glial interactions and polarized localization during development. *Development*, 121, 4265-4273 (1995).
- SCHERER, S. S., EDGARDO, J. A., PELES, E. Functional Organization of the Nodes of Ranvier. *Myelin Biology and Disorders*, Vol. 1, (Eds. R. A. Lazzarini.) Amsterdam: Elsevier), pp.89-115 (2004).
- SOBEL, R.A., GREER, J.M., ISAAC, J., FONDREN, G. and LEES, M.B. Immunolocalisation of proteolipid protein peptide 103-116 in myelin. *J. Neurosci. Res.*, 37, 36-43 (1994).
- SOBEL, R.A., GREER, J.M. and KUCKROO, V.K. Minireview: autoimmune responses to myelin proteolipid protein. *Neurochem. Res.*, 19, 915-921 (1994).
- SPASSKY, N., GOUJET-ZALC, C., PARMANTIER, E., OLIVIER, C., MARTINEZ, S., IVANOVA, A., IKENAKA, K., MACKLIN, W., CERRUTI, I., ZALC, B. and THOMAS, J.L. Multiple restricted origin of oligodendrocytes. *J. Neurosci.*, 18, 8331-8343 (1998).
- SPÖRKEL, O., USCHKUREIT, T., BÜSSOW, H. and STOGGEL, W. Oligodendrocytes expressing exclusively the DM20 isoform of the proteolipid protein gene: myelination and development. *Glia*, 37, 19-30 (2002).
- STECICA, B., SOUTHWOOD, C.M., GRAGEROV, A., KELLEY, K.A., FRIEDRICH, V.L. Jr. and GOW, A. The evolution of lipophilin genes from invertebrates to tetrapods: DM-20 cannot replace proteolipid protein in CNS myelin. *J. Neurosci.*, 20, 4002-4010 (2000).

- STENSAAS, L.J. and STENSAAS, S.S. Astrocytic neuroglial cells, oligodendrocytes and microgliaocytes in the spinal cord of the toad. I. Light microscopy. *Z. Zellforsch. Mikrosk. Anat.*, 84, 473-489 (1968a).
- STENSAAS, L.J. and STENSAAS, S.S. Astrocytic neuroglial cells, oligodendrocytes and microgliaocytes in the spinal cord of the toad. II. Electron microscopy. *Z. Zellforsch. Mikrosk. Anat.*, 86, 184-213 (1968b).
- STERNBERGER, L.A. and STERNBERGER, N.H. The unlabelled antibody method: comparison of peroxidase with avidin-biotin complex by a new method of quantification. *J. Histochem.*, 34, 599-605 (1986).
- STOFFEL, W., HILLEN, H., SCHRÖDER, W. and DEUTZMANN, R. The primary structure of bovine brain myelin lipophilin (proteolipid apoprotein). *Hoppe. Seylers. Z. Physio. Chem.*, 364, 1455-1466 (1983).
- STREIT, W.J. Microglia and the response to brain injury. *Ernst Schering Res. Found Workshop Review*, 39, 11-24 (2002).
- SUTHERLAND, F.I., BANNATYNE, B.A., KERR, R., RIDDELL, J.S. and MAXWELL, D.J. Inhibitory amino acid transmitters associated with axons in presynaptic apposition to cutaneous primary afferent axons in the cat spinal cord. *J. Compl. Neurol.*, 452, 154-162 (2002).
- SZUCHET, S. The morphology and ultrastructure of oligodendrocytes and their functional implications. In: *Neuroglia*, (Eds. H. Kettenmann and B.R. Ransom), Oxford University Press, Oxford/New York, pp. 23-43 (1995).
- SZUCHET, S., POLAK, P.E., YIM, S.H. and LANGE, Y. Plasma membrane of cultured oligodendrocytes: II. Possible structural and functional domains. *Glia*, 1, 54-63 (1988).
- SZUCHET, S., POLAK, P.E., YIM, S.H. and ARVANITIS, D. Plasma membrane of cultured oligodendrocytes: III. Relatedness to myelin. *Glia*, 1, 141-150 (1988).
- TAIT, S., GUNN-MOORE, F., COLLINSON, J.M., JUANG, J., LUBETZKI, C., PEDRAZA, L., SHERMAN, D.L., COLMAN, D.R. and BROPHY, P.J. An oligodendrocyte cell adhesion molecule at the site of assembly of the paranodal axo-glial junction. *J. Cell Biol.*, 150, 657-666 (2000).
- THOMSON, C.E., HUNTER, A.M., GRIFFITHS, I.R., EDGAR, J.M. and McCULLOCH, M.C. Murine spinal cord explants: a model for evaluating axonal growth and myelination in vitro. *J. Neurosci. Res.*, 84, 1703-1715 (2006).
- THOMSON, C.E., MOTAGUE, P., JUNG, M., NAVE, K.A. and GRIFFITHS, I.R. Phenotypic severity of murine Plp mutants reflects in vivo and in vitro variations in transport of PLP isoproteins. *Glia*, 20, 322-332 (1997).
- TIMSIT, S.G., BALLY-CUIF, L., COLMAN, D.R. and ZALC, B. DM-20 mRNA is expressed during the embryonic development of the nervous system of the mouse. *J. Neurochem.*, 58, 1172-1175 (1992).

- TOKUYASU, K.T. A technique for ultracryotomy of cell suspensions and tissues. *J. Cell. Biol.*, 57, 551-565 (1973).
- TRAPP, B.D., ANDREWS, S.B., COOTAUCO, C. and QUARIES, R. The myelin-associated glycoprotein is enriched in multivesicular bodies and periaxonal membranes of actively myelinating oligodendrocytes. *J. Cell. Biol.*, 109, 2417-2426 (1989).
- TRAPP, B.D., ANDREWS, S.B., WONG, A., O'CONNELL, M. and GRIFFIN, J.W. Co-localisation of the myelin-associated glycoprotein and the microfilament components, F-actin and spectrin, in Schwann cells of myelinated nerve fibres. *J. Neurocytol.*, 18, 47-60 (1989).
- TRAPP, B.D., BERNIER, L., ANDREWS, S.B. and COLMAN, D.R. Cellular and subcellular distribution of 2',3'-cyclic nucleotide 3'-phosphodiesterase and its mRNA in the rat central nervous system. *J. Neurochem.*, 51, 859-868 (1988).
- TRIFILIEFF, E., SKALIDIS, G., HĚLYNEK, G., LEPAGE, P., SOROKINE, O., VAN DORSSELAER, A. and LUU, B. Structural data on the myelin proteolipid of apparent molecular weight 20kDa (DM-20). *C R Acad Sci*, 300, 241-246 (1985).
- TRIFILIEFF, E., LUU, B., NUSSBAUM, J.L., ROUSSEL, G., ESPINOSA dell os MONTEROS, A., SABATIER, J.M. and Van RIETSCHOTEN, J. A specific immunological probe for the major myelin proteolipid. *FEBS Letts.*, 198, 235-239 (1986).
- VAUGHN, J.E. and PETERS, A. A third neuroglial cell type. An electron microscopic study. *J. Comp. Neurol.*, 133, 269-288 (1968).
- VERITY, A.N. and CAMPAGNONI, A.T. Regional expression of myelin protein genes in the developing mouse brain: in situ hybridisation studies. *J. Neurosci. Res.*, 21, 238-248 (1988).
- WEIMBS, T. and STOFFEL, W. Proteolipid protein (PLP) of CNS myelin: positions of free, disulfide-bonded, and fatty acid thioester-linked cysteine residues and implications for the membrane topology of PLP. *Biochemistry*, 31, 12289-12296 (1992).
- WESTERGAARD, E. The lateral cerebral ventricles and their ventricular walls. *Andelsborgtrykkerier, Odense*, 216 p. 1970
- WOLFGRAM, F. A new proteolipid fraction of the nervous system. I. Isolation and amino acid analyses. *J. Neurochem.*, 13, 461-470 (1966).
- YAMADA, M., IVANOVA, A., YAMAGUCHI, Y., LEES, M.B. and IKENAKA, K. Proteolipid protein gene product can be secreted and exhibit biological activity during early development. *J. Neurosci.*, 15, 2143-2151 (1999).
- YIN, X., BAEK, R.C., KIRSCHNER, D.A., PETERSON, A., FUJII, Y., NAVE, K.A., MACKLIN, W.B. and TRAPP, B.D. Evolution of a neuroprotective function of central nervous system myelin. *J. Cell. Biol.*, 172, 469-478 (2006).

YIN, X., CRAWFORD, T.O., GRIFFIN, J.W., TU, P., LEE, V.M., LI, C., RODER, J. and TRAPP, B.D. Myelin-associated glycoprotein is a myelin signal that modulates the calibre of myelinated axons. *J. Neurosci.*, 18, 1953-1962 (1998).

YIN, X., PETERSON, J., GRAVEL, M., BRAUN, P.E. and TRAPP, B.D. CNP overexpression induces aberrant oligodendrocyte membranes and inhibits MP accumulation and myelin compaction. *J. Neurosci. Res.*, 50, 238-247 (1997).

YOOL, D., KLUGMANN, M., BARRIE, J.M., McCULLOCH, M.C., NAVE, K.A. and GRIFFITHS, I.R. Observations on the structure of myelin lacking the major proteolipid protein. *Neuropathol. Appl. Neurobiol.*, 28, 75-78 (2002).

YOOL, D., MONTAGUE, P., McLAUGHLIN, M., McCULLOCH, M.C., EDGAR, J.M., NAVE, K.A., DAVIES, R.W., GRIFFITHS, I.R. and McCALLION, A.S. Phenotypic analysis of mice deficient in the major myelin protein MOBP, and evidence for a novel Mobp isoform. *Glia*, 39, 256-267 (2002).

ZHANG, S.C., GOETZ, B.D., CARRÉ, J.L. and DUNCAN, I.D. Reactive microglia in dysmyelination and demyelination. *Glia*, 34, pp. 101-109 (2001).